Clinical and Molecular Genetic Studies in Mitochondrial Disease

Robert D.S. Pitceathly

A thesis submitted for the degree of Doctor of Philosophy
in the University College London

MRC Centre for Neuromuscular Diseases
UCL Institute of Neurology and
National Hospital for Neurology and Neurosurgery
Queen Square
London
WC1N 3BG

May 2014

I, Robert D.S. Pitceathly, confirm that the work presented in this thesis is my own. Where information has been derived from other sources, I confirm that this has been indicated in the thesis.

Signed:

Abstract

Up to a third of adults attending the Queen Square UK NHS Specialised Service for Rare Mitochondrial Disease out-patient clinic remain genetically undetermined. This thesis describes research which aimed to establish the molecular basis of mitochondrial disease in these patients and evaluate genotype/phenotype correlations. Both novel clinical syndromes and molecular causes of disease were identified. Furthermore, new insights into the respiratory chain (RC) protein structure were elucidated.

***Novel clinical phenotypes*:** Three previously unrecognised mitochondrial disease phenotypes were characterised. First, m.9185T>C in *MT-ATP6*, encoding subunit 6 of ATP synthase (complex V), was detected in a pedigree exhibiting matrilineal inheritance. Presentation was with axonal Charcot-Marie-Tooth (CMT2) disease. Further screening of 270 patients with genetically unclassified CMT2 demonstrated three additional families harbouring the same mutation, thus proving a causal link between reduced complex V activity and impaired axonal function. Second, a severe distal myopathy was observed in two unrelated patients with *de novo* dominant *POLG* mutations. Finally, *COX10* mutations were linked to adult cytochrome *c* oxidase (COX) deficiency. Despite a complex multisystem phenotype comprising short stature, proximal myopathy, fatigue, sensorineural hearing loss, pigmentary maculopathy, renal Fanconi syndrome and premature ovarian failure, the patient's clinical severity was considerably milder than fatal *COX10*-related infantile disease.

***Nuclear gene mutations*:** Three major experimental strategies were employed to locate mutations in the nuclear genes of adults with clinically and/or biochemically suspected mitochondrial disease. First, a candidate gene approach identified *RRM2B* mutations in 2/33 patients with multiple mitochondrial DNA deletions. Second, whole-exome sequencing confirmed *COX10* mutations can cause adult mitochondrial disease. Finally, combined homozygosity mapping/whole-exome sequencing in a consanguineous family led to the discovery that *NDUFA4* mutations cause COX-deficient Leigh syndrome. This example of 'back-translation' led to the discovery that NDUFA4, previously considered to be a complex I subunit, is actually an important component of the COX enzyme complex.

Acknowledgments

I am indebted to my supervisors, Professor Michael Hanna and Dr Shamima Rahman, for their guidance and encouragement, to Dr Jan-Willem Taanman for his additional supervision and laboratory expertise, and to Professors Mary Reilly and Henry Houlden for their time, advice and support.

I would like to thank all the members of the UK NHS Specialised Service for Rare Mitochondrial Diseases of Adults and Children based at Queen Square, particularly Mary Sweeney, Cathy Woodward, Ese Mudanohwo, James Polke, Iain Hargreaves, Anu Chalasani, Rahul Phadke and Janice Holton.

I would also like to thank all our collaborators for their invaluable input: Brigitte Meunier for mutational modelling of *COX10* variants in yeast; Michael Sadowski for p53R2 and COX10 protein modelling work; Elisa Fassone for assistance with blue-native gel electrophoresis; Sinéad Murphy and Ellen Cottenie for help with Sanger sequencing of *MT-ATP6/8* and with restriction endonuclease analysis to quantitate the m.9185T>C mutant load; Yehani Wedatilake for Sanger sequencing of *NDUFA4*; Anna Sailer for assistance in interpreting homozygosity mapping data; and Francesco Muntoni and the UK10K Consortium for facilitating whole exome sequencing studies.

Finally, I want to thank Debbie for her unwavering patience, understanding and belief, and for tolerating the stresses and strains which invariably accompany any PhD thesis, and to Theo and Dalia for making it all worthwhile.

This work was supported by Medical Research Council grant number G0800674.

Publications arising from this Work

1. **Pitceathly RDS**, Fassone E, Taanman J-W, et al. Kearns-Sayre syndrome caused by defective R1/p53R2 assembly. *J. Med. Genet*. 2011;48(9):610-617.

2. Gorman GS, **Pitceathly RDS**, Turnbull DM, Taylor RW (2012). *RRM2B*-Related Mitochondrial Disease. In: Wong LC (Ed.). Mitochondrial disorders caused by nuclear genes. 1st ed. New York: Springer.

3. **Pitceathly RDS**, Murphy SM, Cottenie E, et al. Genetic dysfunction of *MT-ATP6* causes axonal Charcot-Marie-Tooth disease. *Neurology*. 2012 Sep 11;79(11):1145-54.

4. **Pitceathly RDS**, Smith C, Fratter C, et al. Adults with *RRM2B*-related mitochondrial disease have distinct clinical and molecular characteristics. *Brain.* 2012 Nov;135(Pt 11):3392-403.

5. **Pitceathly RDS**, Tomlinson SE, Hargreaves I, et al. Distal myopathy with cachexia: an unrecognised phenotype caused by dominantly-inherited mitochondrial polymerase γ mutations. *J. Neurol. Neurosurg. Psychiatr*. 2013 Jan;84(1):107-10.

6. **Pitceathly RDS**, Rahman S, Wedatilake Y, et al. *NDUFA4* mutations underlie dysfunction of a cytochrome *c* oxidase subunit linked to human neurological disease. *Cell Rep*. 2013 June;3(6):1795-1805.

7. **Pitceathly RDS**, Taanman J-W, Rahman S, et al. *COX10* Mutations Resulting in Complex Multisystem Mitochondrial Disease That Remains Stable Into Adulthood. *JAMA Neurol.* 2013 Dec;70(12):1556-61.

Table of Contents

List of Figures and Tables

Figures

CHAPTER 3

CHAPTER 4

Chapter 5

Chapter 6

Tables

CHAPTER 3

CHAPTER 4

CHAPTER 5

CHAPTER 6

CHAPTER 7

List of Abbreviations

ADP	adenosine diphosphate
adPEO	autosomal dominant PEO
ANS	ataxia neuropathy syndrome
APS	ammonium parsulphate
ATP	adenosine triphosphate
BCA	bicinchoninic acid
BG	basal ganglia
BN-PAGE	blue-native polyacrylamide gel electrophoresis
bp	base-pairs
BSA	bovine serum albumin
C10orf2	chromosome 10 open reading frame 2
cDNA	complementary deoxyribonucleic acid
CLA	congenital lactic acidosis
COX	cytochrome *c* oxidase
COX10	cytochrome *c* oxidase assembly homolog 10
CS	citrate synthase
CSF	cerebrospinal fluid
CT	computed tomography
DD	developmental delay
ddH_2O	double-distilled water
DDM	*n*-dodecyl-β-D-maltoside
ddNTP	dideoxyribonucleotide triphosphate
DNA	deoxyribonucleic acid
dNTP	deoxyribonucleotide triphosphate
ECG	electrocardiogram
ECHO	echocardiogram
EDTA	ethylene diamine tetra acetic acid, dipotassium salt
EEG	electroencephalography
EM	electron microscopy
EMG	electromyography
ESP	exome sequencing project
FAD	flavin adenine dinucleotide
FTT	failure to thrive
gDNA	genomic DNA
GTP	guanosine triphosphate
HCM	hypertrophic cardiomyopathy
IMM	inner mitochondrial membrane
Indel	insertion/deletion
kDa	kilodaltons
LD	learning difficulties
LOF	loss-of-function
LSP	light strand promoter
MEMSA	myoclonus, epilepsy, myopathy, sensory ataxia

MNGIE	mitochondrial neurogastrointestinal encephalomyopathy
MPTP	mitochondrial permeability transition pore
MRI	magnetic resonance imaging
mRNA	messenger RNA
MRS	magnetic resonance spectroscopy
MT-ATP6	mitochondrially encoded ATP synthase 6
mtDNA	mitochondrial DNA
MW	molecular weight
NAD	nicotinamide adenine dinucleotide
NCG	National Commissioning Group
NCS	nerve conduction studies
nDNA	nuclear DNA
NDUFA4	NADH dehydrogenase (ubiquinone) 1 alpha subcomplex, 4
NGS	next-generation sequencing
NHNN	National Hospital for Neurology and Neurosurgery
NSC	non-synonymous coding
OH	origin of heavy strand DNA replication
OL	origin of light strand DNA replication
OSCP	oligomycin sensitivity-conferring protein
OXPHOS	oxidative phosphorylation
PBS	phosphate buffered saline
PCR	polymerase chain reaction
PDH	pyruvate dehydrogenase
PEO	progressive external ophthalmoplegia
P_i	inorganic phosphate
POF	premature ovarian failure
POLG	mitochondrial DNA polymerase gamma
RC	respiratory chain
RITOLS	ribonucleotide incorporation throughout the lagging strand
RNA	ribonucleic acid
ROS	reactive oxygen species
RRF	ragged red fibre
RRM2B	ribonucleotide reductase M2 B (TP53 inducible)
rRNA	ribosomal RNA
SC	synonymous coding
SDH	succinate dehydrogenase
SNHL	sensorineural hearing loss
SNP	single nucleotide polymorphism
SNV	single nucleotide variant
SURF1	surfeit 1
TAS	termination-associated sequence
TEMED	tetramethylethylenediamine
tRNA	transfer RNA
UCLH	University College London Hospitals
UMN	upper motor neuron

CHAPTER 1

Introduction

CHAPTER 1

1. Introductory overview

Approximately 80% of children and 50% of adults with primary disorders of the mitochondrial respiratory chain (RC) harbour pathogenic mutations in nuclear genes encoding mitochondrial proteins (unpublished data). This is not surprising given that the majority of RC subunits and proteins involved with transcription and translation of mitochondrial DNA (mtDNA), assembly of the multimeric RC enzyme complexes, biosynthesis of mobile electron carriers within the inner mitochondrial membrane (IMM), import of solutes and proteins into the mitochondrion, regulation of mitochondrial membrane dynamics/composition, and mitochondrial fission and fusion are nuclear-encoded.

Over 120 nuclear genes are linked to mitochondrial disease (Vafai and Mootha, 2012). However, an estimated 1,500 nuclear-encoded proteins (5-10% of the genomic coding region) are targeted to mitochondria (Calvo et al., 2006). Defects in any of these genes can potentially cause a mitochondrial disorder. Deciphering the genetic basis for inheritable disease is essential in order to provide accurate genetic counselling and prenatal diagnostics and to attempt to predict the subsequent clinical course of the disorder. Fully characterising the clinical spectrum associated with mitochondrial dysfunction and advancing current understanding concerning the functional role of mitochondrial-related nuclear genes in both health and disease will help facilitate future development of treatment strategies for the benefit of patients. It is also likely that a genetic diagnosis will be an important inclusion criterion for future clinical treatment trials.

This thesis focuses on: 1) characterising novel clinical phenotypes associated with adult RC disease; and 2) identifying causative genetic mutations in the nuclear genes of patients with presumed but genetically undetermined mitochondrial disease and assessing the molecular pathogenesis of the variants. In keeping with these aims the introduction of this thesis focuses on the following: 1) mtDNA replication, both at the replication fork and via deoxyribonucleotide triphosphate (dNTP) metabolism, as dysfunction of these cellular processes can generate secondary

multiple mtDNA deletions as occurs with *POLG* and *RRM2B* mutations; and 2) cytochrome *c* oxidase (COX, complex IV) and complex V structure and function. Specific details of the individual genes discussed are included within the introduction of the relevant chapter headings. Finally, a general overview of next-generation sequencing (NGS) is outlined as this technology was utilised to identify the nuclear basis of mitochondrial disease in two unrelated families and forms an important component of the thesis.

1.1 The mitochondrion

The mitochondrion is a cellular organelle present in almost every eukaryotic cell and has a number of essential functions. The earliest recordings of mitochondria probably date back to the 1840s (Henle, 1841). However, it was not until 1890 that Richard Altmann recognised their universal cellular occurrence and labelled them 'bioblasts' (Altmann, 1890). The term 'mitochondrion,' derived from the Greek 'mitos' (thread) and 'chondros' (granule), was later coined by Carl Benda to describe their appearance during spermatogenesis, when they were likened to a collection of granules forming threads inside the cells (Benda, 1898).

Mitochondria are thought to have evolved up to two billion years ago from endosymbiotic prokaryotes (Grivell, 1983). Shared microbial characteristics (mitochondria contain multiple copies of a single circular genome which employs a variant genetic code) led to the suggestion that their ancestor was a Proteobacteria (Futuyma, 2005), possibly related to the Rickettsiales (Emelyanov, 2003), which was originally endocytosed by another species of prokaryote thereby becoming incorporated into its cytoplasm. The newly acquired ability of the symbiont bacteria to conduct cellular respiration in the host cell, which had previously relied solely on glycolysis and fermentation, enabled survival in much more diverse habitats and thus represented a considerable evolutionary advantage.

Under the electron microscope mitochondria appear as double membrane-bound structures in cross-section, with a diameter of approximately 0.5-1.0 μm and length of 2-5 μm. The inner mitochondrial membrane (IMM) is highly convoluted forming cristae which extend into a central matrix space (Palade, 1953). Many of the mitochondrion's enzymatic reactions occur on this expanded surface area. Although frequently depicted as discrete cylindrical structures, mitochondria are highly dynamic and move throughout the cell whilst constantly fusing and dividing (Bereiter-Hahn and Jendrach, 2010).

In the late 1940s the mitochondrion was recognised to be a major site of cellular energy production (Kennedy and Lehninger, 1949). It is now well-established that

oxidation decarboxylation of pyruvate, fatty acid β-oxidation and Krebs' citric acid cycle all occur within the mitochondrial central matrix space. The products of these metabolic pathways, specifically the reduced cofactors NADH (reduced nicotinamide dinucleotide) and $FADH_2$ (reduced flavin adenine dinucleotide), are subsequently used to generate cellular energy in the form of adenine triphosphate (ATP), from adenine diphosphate (ADP) and inorganic phosphate (P_i), via oxidative phosphorylation (OXPHOS).

Arguably the most important of the major functions of mitochondria, which includes cell signalling and the metabolism of amino acids, fatty acids, and cofactors, is the utilisation of molecular oxygen to convert the energy contained in food into ATP, the cellular energy currency. This process relies on the mitochondrial respiratory electron transport chain and OXPHOS system.

1.2 The mitochondrial respiratory chain and oxidative phosphorylation system

OXPHOS requires five multimeric enzyme complexes (complex I-IV, collectively termed the RC, and complex V) embedded in the IMM. The sequential transfer of electrons between each enzyme complex relies on specific electron carriers. These include flavins, iron-sulphur (FeS) complexes, quinones, and metals such as copper and the haem groups of cytochromes. Ubiquinone (Coenzyme Q10, CoQ10) and cytochrome *c* act as mobile carriers of electrons and move electrons from complexes I/II to III, and complexes III to IV respectively.

Complex I (NADH:ubiquinone oxidoreductase) comprises approximately 45 polypeptide subunits (at the time of writing, see Chapter 6), seven of which are encoded by mtDNA. Complex II (succinate-ubiquinone oxidoreductase) has four subunits, all of which are nuclear encoded. It also participates in Krebs cycle via one of its subunits, SDHA (succinate dehydrogenase complex, subunit A). SDHA contains a covalently attached FAD cofactor which catalyses oxidation of succinate to fumarate in step six of Krebs cycle. In doing so, FAD (reduced flavin adenine dinucleotide) is converted to $FADH_2$. Electrons are subsequently passed from $FADH_2$, via the other three complex II SDH subunits, to ubiquinone. Complex III (ubiquinol-cytochrome *c* oxidoreductase) consists of 11 subunits, one of which (cytochrome b) is mitochondrially encoded. Complex IV (cytochrome *c* oxidase) has long been considered (at the time of writing, see Chapter 6) to be composed of 13 subunits, three of which are encoded by mtDNA. Finally, complex V (ATP synthase, F_1F_o ATP synthase) has at least 16 subunits, of which two are mitochondrially encoded.

The process of ATP production is reliant on the presence of oxygen and the reducing equivalents NADH and $FADH_2$ which are generated by oxidation of: 1) pyruvate, produced in the cytosol during glycolysis and actively transported across the IMM; 2) fatty acids; and 3) acetyl-CoA in Krebs cycle. In the absence of oxygen, pyruvate remains in the cytosol and undergoes fermentation. NADH is oxidised to NAD to prevent build-up in the cytoplasm and NAD is subsequently re-used for glycolysis. The waste product of this reaction is lactic acid. When oxygen is abundant, pyruvate

is oxidised to acetyl-CoA and carbon dioxide by the pyruvate dehydrogenase complex within the mitochondrion. Acetyl-CoA subsequently enters Krebs cycle in the mitochondrial matrix and is oxidised during an eight-step process, which involves different enzymes and co-enzymes, to form carbon dioxide, the reducing equivalents NADH and $FADH_2$, and GTP (guanosine triphosphate).

NADH transfers electrons derived from oxidation of pyruvate and fatty acids to complex I, whilst $FADH_2$ transports electrons gained from oxidation of succinate to fumarate in Krebs cycle to complex II. Flavoproteins also transfer electrons from β-oxidation of fatty acids and other organic acids directly to ubiquinone. From complex I and II electrons are transferred to ubiquinone and then to complex III, and via cytochrome *c* to complex IV where they are accepted by oxygen to produce water (H_2O). The energy released during sequential transfer of electrons is used to generate the mitochondrial membrane potential ($\Delta\psi m$ ~150 mV) and pH gradient (ΔpHm) by translocating protons from the mitochondrial matrix to the intermembrane (IM) space. Proton pumping occurs at complexes I, III and IV. The resulting electrochemical gradient is harnessed by complex V which couples proton flow across the IMM back into the mitochondrial matrix with the synthesis of ATP from ADP and P_i. ATP is transported across the IMM by the mitochondrial carrier protein adenine nucleotide translocator (Ant). Although Ant was initially thought to function as a dimeric structure, recent evidence suggests it may be present in a monomeric form (Kunji and Crichton, 2010). Once in the cytoplasm, ATP is utilised by the cell as an energy source. Depending on the energy status of the cell, ATP synthase can either hydrolyse or synthesise ATP in humans.

1.3 Human mitochondrial genome structure and organisation

1.3.1 Human mitochondrial DNA

One unique property of mitochondria is that they contain DNA molecules separate to nuclear DNA (nDNA). The mitochondrial genome is organised into a double-stranded circle of DNA comprised of 16,569 base pairs (bp). Genes are located on both DNA strands which are termed the heavy (H) and light (L) strand due to their relative composition of either mainly purines (adenine and guanine) or pyrimidines (thymine and cytosine) respectively, with the former having greater molecular weight (MW) than the latter. It is highly compact with no introns and contains only one major non-coding region (NCR) known as the control region (comprising ~900 bp in mammals). The control region contains the origin of replication of one DNA strand, the origins of transcription for both DNA strands, and the Displacement loop (D-loop), a triple-stranded region whose third DNA strand (or 7S DNA) spans approximately 650 bp from nucleotide numbers 16,111 to 191 (Mao and Holt, 2009). In total mtDNA contains 37 genes encoding: 13 polypeptide OXPHOS subunits; 22 tRNAs; and two rRNAs, both of which are essential for mitochondrial protein synthesis.

MtDNA is susceptible to oxidative DNA damage due to its close proximity to reactive oxygen species (ROS) at the IMM, lack of protective histone proteins, and limited proof-reading and repair systems. As a result, mtDNA has a mutation rate 10-20 times that of nDNA (Lynch et al., 2006; Richter et al., 1988).

1.3.2 Mitochondrial nucleoid

In vivo, nDNA adopts a condensed structure associated with histones and other proteins (Kornberg, 1974; Olins and Olins, 1974) called nucleosomes which form the basic repeating units of eukaryotic chromatin. These protein-DNA complexes compact, order, and protect the DNA, and create a degree of regulatory control to ensure its correct expression. They also facilitate co-ordinated copying and segregation of DNA molecules.

MtDNA is also packaged into protein-DNA complexes known as nucleoids, which are believed to be the units of mtDNA transmission and inheritance (Holt et al., 2007; Malka et al., 2006). Early studies suggested a single mitochondrion, on average, contained 3.2 nucleoids and 4.6 mtDNA molecules (Satoh and Kuroiwa, 1991). Later work suggested that each nucleoid contained between 2-10 mtDNAs in rapidly dividing cells (Iborra et al., 2004; Legros et al., 2004). However, more recently next-generation imaging techniques have demonstrated nucleoids are smaller than previously thought, containing an average of 1.4 mtDNAs (i.e. either one or two mtDNA molecules per nucleoid) (Kukat et al., 2011).

1.4 Replication and maintenance of mitochondrial DNA

Since mtDNA encodes only 13 of the approximately 90 essential polypeptide OXPHOS subunits, the remaining subunits and proteins required for their transcription, translation, post-translational modification and assembly are all nuclear-encoded. The dependence on the nuclear genome extends to include the apparatus required for mtDNA maintenance and repair, the proteins for which are translated in the cytoplasm and imported into the mitochondria for mtDNA synthesis.

Accurate mtDNA replication is essential to maintain $\Delta\psi_m$, established across the inner mitochondrial membrane by respiration, and is necessary for energy production in the form of ATP. Despite the mtDNA replication machinery being nuclear encoded, it is completely separate from its nuclear counterpart consisting of just 5 basic enzyme components: 1) DNA polymerase gamma (POLγ) A and B; 2) DNA helicase Twinkle; 3) mitochondrial single-stranded DNA-binding protein (mtSSB); and 4) mitochondrial RNA polymerase (POLRMT). Unlike nDNA which replicates once during cell division, mtDNA continuously replicates throughout the cell cycle in replicating and post-mitotic cells.

1.4.1 Mitochondrial replication apparatus

1.4.1.1 DNA polymerase gamma A and B

POLγ is the only known DNA polymerase in animal mitochondria. It functions as a heterotrimer (Yakubovskaya et al., 2006) composed of one catalytic subunit (POLγA) encoded by *POLG*, and two accessory subunits (POLγB) encoded by *POLG2* (Ropp and Copeland, 1996). The catalytic subunit contains 3 functional domains; a 3' to 5' proofreading exonuclease domain; a linker domain; and a highly conserved carboxyl-terminal polymerase domain (Luo and Kaguni, 2005). The accessory subunits were first shown to confer high processivity in vitro by promoting formation of long stretches of DNA (Carrodeguas et al., 1999). This is achieved by both increasing binding affinity for DNA and enhancing replication rate (Lee et al., 2009, 2010; Lim et al., 1999; Yakubovskaya et al., 2007).

1.4.1.2 DNA helicase Twinkle

In 2001 Spelbrink et al. identified the mammalian replicative mtDNA helicase Twinkle (acronym for T7 gp4-like protein with intramitochondrial nucleoid localisation), encoded by *C10orf2*, with structural similarity to bacteriophage T7 gene 4 primase/helicase (T7 gp4) and other ring helicases required for DNA replication (Spelbrink et al., 2001a). This was achieved by searching for open reading frames (ORFs) in a region previously identified as being linked to autosomal dominant progressive external ophthalmoplegia (adPEO) on chromosome 10q24 (Li et al., 1999; Suomalainen et al., 1995). The C-terminal end of the Twinkle protein was found to have structural similarity with the C-terminal portion of T7 gp4 and other hexameric ring helicases, and is now known to be critical for maintenance of human mtDNA integrity. However, human Twinkle lacks the primase domain motifs found in the N-terminal primase region of T7 gp4 which confer primase activity. The authors screened *C10orf2* and identified 11 coding-region mutations co-segregating in 12 pedigrees with adPEO associated with multiple mtDNA deletions, thus confirming the importance of the protein in mtDNA maintenance. Expression of human and Drosophila Twinkle variants carrying mutations in the helicase motifs have since been shown to cause mtDNA depletion in cells (Matsushima et al., 2008; Wanrooij et al., 2007).

1.4.1.3 Mitochondrial single-stranded DNA-binding protein

MtSSB binds single-stranded DNA (ssDNA) as a homotetramer (Li and Williams, 1997). The ssDNA wraps around the tetrameric mtSSB protein through electropositive channels guided by flexible loop (Bochkarev et al., 1997; Yang et al., 1997) and prevents refolding and degradation of the nucleic acid. It also enhances primer recognition (Thömmes et al., 1995) and processivity of POLγ (Farr et al., 1999). In vitro, POLγ, DNA helicase Twinkle, and mtSSB can use double-stranded DNA (dsDNA) as a template to synthesise ssDNA molecules of over 16kb (Korhonen et al., 2004). In the absence of mtSSB protein, the ssDNA products are ~ 2kb. No mutations in the mtSSB gene have been associated with human mitochondrial disease.

1.4.1.4 Mitochondrial RNA polymerase

Mitochondrial RNA polymerase (POLRMT) is a nuclear encoded RNA polymerase involved in transcription of mtDNA and is distinct from other nuclear RNA polymerases. It was first discovered in yeast and found to be encoded by RPO41 (Greenleaf et al., 1986; Kelly et al., 1986), and later identified in human cells where significant homologies with sequences corresponding to mitochondrial RNA polymerases from lower eukaryotes, and to RNA polymerases from several bacteriophages was shown (Tiranti et al., 1997).

The basal transcription machinery of mitochondria consists of human POLRMT and mitochondrial transcription factor B2 (TFB2M) (Litonin et al., 2010; Shutt et al., 2010). They are activated by mitochondrial transcription factor A (TFAM), which also participates in mtDNA packaging and replication.

In addition to its role in transcribing mtDNA, POLRMT is essential during replication when it provides RNA primers used to initiate mtDNA synthesis at the origin of heavy strand DNA replication (OH) (Chang and Clayton, 1985; Chang et al., 1985; Wanrooij et al., 2008). Primer formation required for replication starts at the light strand promoter (LSP) in the D-loop, which is also the start point for polycistronic transcripts later processed to form the complex I subunit ND6 and 8 of the 22 tRNAs required for translation of the protein subunit encoding mRNAs. The primer extends from the LSP by ~100 bp from which leading strand DNA synthesis can start. Most H-strand replication initiation events are actually prematurely terminated around 600 bp from OH. The single stranded RNA-DNA (7S DNA) hybrid anneals to the parental DNA template forming a triple-stranded structure called the D-loop, so-called due to the displaced parental H-strand (Arnberg et al., 1971; ter Schegget et al., 1971).

The D-loop plays a critical role in controlling mtDNA replication and transcription (Anderson et al., 1981; Doda et al., 1981), and more recently evidence has highlighted its interaction with the mitochondrial nucleoid whose role includes mtDNA protection, repair, segregation and copy number control (He et al., 2007; Wang, 2006). The precise location of OH, and therefore the start of mtDNA H-strand replication, is debatable. Transition from RNA primer to DNA has been shown 5-10

bp downstream of a conserved DNA sequence known as conserved sequence box II (CSBII) (Kang et al., 1997; Pham et al., 2006), however, many believe OH to be further downstream from CSBII as evidenced by isolation of DNA replication intermediates, direct Sanger sequencing and primer extension analysis (Crews et al., 1979; Fish et al., 2004; Gillum and Clayton, 1978).

According to the asynchronous strand displacement model (see section 1.4.2.1), the replication machinery continues until two-thirds around the mitochondrial genome before reaching a 30 bp non-coding DNA region. Here, the replication machinery exposes the origin of light strand replication (OL) and displaces it into its single stranded form to allow lagging strand synthesis to be initiated (Kang et al., 1997; Martens and Clayton, 1979). The single-stranded OL region takes on a stem-loop conformation. Primer synthesis is initiated by POLRMT which acts as a lagging strand primase (Wanrooij et al., 2008) by recognising the origin sequence at the OL stem-loop structure, and extends for ~ 25 bp before being replaced by POLγ which initiates lagging strand DNA synthesis. These RNA-DNA transition points have been shown at the base of the double-stranded stem (Kang et al., 1997). RNA-DNA transition between POLRMT and POLγ can be mimicked in vitro (Fusté et al., 2010), unlike H-strand replication, suggesting OL dependent initiation is an unregulated event (Wanrooij and Falkenberg, 2010).

1.4.2 The mitochondrial replication process

Despite the replication apparatus being relatively well characterised over recent years, the precise mode of mtDNA replication has been intensely debated (Bogenhagen and Clayton, 2003a, 2003b; Holt and Jacobs, 2003). For many years mtDNA replication was thought to occur exclusively by a strand-displacement model, where a leading strand is synthesised from OH and a lagging strand from OL in an asymmetric and unidirectional pattern. In 2000, an alternative model was suggested which was further expanded in 2006 suggesting duplex replication intermediates were formed by coupled synchronous leading-lagging strand synthesis, and that the lagging strand is initially laid down as RNA before conversion to DNA (ribonucleotide incorporation throughout the lagging strand, so-called RITOLS model – see section 1.4.2.2) due to the observation that the intermediates were RNase

sensitive (Holt et al., 2000; Yasukawa et al., 2006). The main criticism of this proposal was the experimental use of the Brewer and Fangman 2D-agarose gel electrophoresis (2D-AGE) procedure, in which restriction enzyme-digested DNA is exposed to native gel electrophoresis in the absence of Ethidium Bromide in the first dimension, and in its presence in the second dimension (Brewer and Fangman, 1987). It has been suggested that when analysing mtDNA, interpreting 2D-AGE gel displays is challenging because the replication intermediates produced by the strand-displacement model are subject to branch migration when the DNA is cleaved by restriction endonucleases. Unlike fully duplex replicating structures, branch migration of triplex structures is unstable and liable to loss of the less stable nascent strands during electrophoresis. Many of the intermediates of the strand-displacement model would, therefore, be destabilised by 2D-AGE techniques, making rarer structures more abundant (Clayton, 2003). The proposed mechanisms for mtDNA replication are discussed in detail below.

1.4.2.1 Asynchronous strand displacement model

Leading strand replication is initiated from a POLRMT-synthesised primer at the LSP. The replication machinery (consisting of POLγA and B, Twinkle helicase and mtSSB) extends this primer, with the RNA-DNA transition point at CSBII. Replication will often cease prematurely at a 15 bp conserved sequence known as the termination-associated sequence (TAS) at the distal end of the control region, thus forming a stable triple-stranded structure known as the D-loop. The nascent strand of the D-loop is known as 7S DNA. It has been shown that productive replicative intermediates, in the process of elongation to full genomic size, have the same 5' ends as the nascent 7S DNA strand confirming their common origin (Kang et al., 1997; Tapper and Clayton, 1981). The D-loop is ~650 bp in humans (Clayton, 1982). The TAS may represent a regulation point for mtDNA synthesis. It has also been suggested the D-loop is critical for mitochondrial nucleoid regulation (see 1.2.2). When leading strand synthesis does proceed beyond the TAS it continues along the parental L-strand leaving behind ssDNA protected by mtSSB which also prevents primer formation of the lagging strand by non-specific binding of POLRMT to the lagging strand (Fusté et al., 2010).

Two-thirds of the way round the genome the replication machinery reaches OL which is exposed by Twinkle helicase in single stranded form when it takes on a stem-loop structure (Martens and Clayton, 1979; Tapper and Clayton, 1981). The stem structure prevents mtSSB binding thereby allowing POLRMT to initiate primer synthesis from a poly dT repeat in the loop region of OL (Fusté et al., 2010). POLγ replaces POLRMT and initiates lagging strand synthesis. To complete mtDNA replication, the two daughter molecules separate, RNA primers are removed from OH and OL by RNase H1, and gaps in the molecules are filled and ligated by mtDNA ligase (which is also involved with mtDNA repair). Finally superhelical turns are introduced into the covalently closed circular mtDNA by mitochondrial type II topoisomerase (Taanman, 1999). It is recognised that occasional use of secondary origins, particularly for lagging-strand initiation, may occur (Bogenhagen et al., 1979); however, human molecules lacking OH or OL do not appear to survive since both origins are present in almost all deleted forms of human mtDNA.

1.4.2.2 Coupled leading/lagging strand model and RITOLS model

In 2000, Holt et al. proposed the existence of a second replication model in which leading- and lagging-strand syntheses are coupled, on the basis of 2D-AGE which showed significant quantities of mtDNA formed duplex replication intermediates (Holt et al., 2000). Other replication intermediates were also present and thought to represent simultaneous stand-displacement replication. The strand-coupled mechanism is proposed to initiate in both directions from a broad zone, OriZ (Bowmaker et al., 2003). Later studies demonstrated some replication intermediates were RNase H-sensitive which led to the assumption they were derived from ribonucleotide-rich DNA synthesis initiated unidirectionally from the non-coding region (Yasukawa et al., 2005, 2006). According to this replication mode, referred to as ribonucleotide incorporation throughout the lagging strand (RITOLS) model, the lagging strand is initially laid down as RNA before being converted to DNA. In a similar manner to the strand displacement model, RITOLS predicts delayed lagging strand DNA synthesis, although the mtSSB is replaced by RNA. Short Okazaki-like fragments may also be used as primers that initiate lagging-strand DNA synthesis discontinuously (Yasukawa et al., 2006), although these have not yet been demonstrated *in-vitro*.

1.5 Deoxyribonucleotide synthesis and salvage

MtDNA synthesis is independent from nDNA replication and occurs continuously throughout the cell cycle. This means mitochondria require a constant supply of dNTPs, the building blocks of DNA, for mtDNA synthesis and maintenance (Bogenhagen and Clayton, 1976). Mitochondrial and cytosolic dNTP pools are separated by the mitochondrial inner membrane, which is impermeable to negatively charged nucleotides (Bestwick and Mathews, 1982). This means mitochondria must synthesise, salvage or import dNTPs. As mitochondria lack a functional *de novo* deoxyribonucleotide synthesis pathway, they rely on: 1) import of cytosolic dNTPs in replicating cells; and 2) mitochondrial nucleoside salvaging pathways in non-replicating cells. A number of cytosolic and mitochondrial enzymes are then involved in the dNTP salvage and synthesis process in both replicating and non-replicating cells, and are discussed below.

1.5.1 Replicating cells

The exchange of deoxyribonucleotides between the cytosol and mitochondria is mediated by the mitochondrial deoxynucleotide carrier (Dolce et al., 2001; Pontarin et al., 2003; Rosenberg et al., 2002). Mitochondria rely on *de novo* synthesis of cytosolic deoxyribonucleotides by ribonucleotide reductase (RNR), which catalyses the direct reduction of ribonucleotide diphosphates to their corresponding deoxyribonucleotides. They can also obtain them via cytosolic nucleoside salvage from direct phosphorylation of deoxyribonucleosides by deoxyribonucleoside kinases (dNK), nucleoside monophosphate kinase (NMPK), and nucleoside diphosphate kinase (NDPK).

The two major cytosolic dNKs are thymidine kinase (TK1) which phosphorylates deoxythymidine (dThy) and deoxyuridine (dUri), and deoxycytidine kinase (dCK) which phosphorylates deoxycytidine (dCyt), deoxyguanosine (dGua) and deoxyadenosine (dAdn). The latter can also be phosphorylated by adenosine kinase (ADK) (Arnér and Eriksson, 1995; Jones, 1980; Reichard, 1988; Van Rompay et al., 2000). RNR and TK1 are both regulated by S-phase and are, therefore, downregulated in post-mitotic cells.

1.5.2 Non-replicating cells

Until recently, mitochondrial nucleoside salvage was thought to be the only source of dNTPs in non-dividing cells. Recycled deoxynucleosides derived from within the mitochondria or cytoplasm, via the equilibrative nucleoside transporter 1 (hENT1) (LAI 2004), are phosphorylated by two dNKs: TK2 is specific for dThy, dCyt and dUri, deoxyguanosine kinase (DGUOK) for dGua, dAdn and deoxyinosine (dIno). Both are independent of the cell cycle (Eriksson et al., 2002; Wang et al., 1999; Zhu et al., 1998). Mitochondrial NMPK and NDPK perform the two further phosphorylation steps for dNTP formation.

In 2000 an R2 subunit homolog encoded by ribonucleotide reductase M2 B (*RRM2B*) was identified; termed p53R2 because its transcription is tightly regulated by the tumour suppressor protein p53 (Nakano et al., 2000; Tanaka et al., 2000). Unlike the cytoplasmic R2 subunit which is produced exclusively during S-phase in cycling cells, p53R2 is detectable at low levels throughout the cell cycle in both proliferating and post-mitotic cells. It is likely p53R2 has an essential role in supplementing the dNTPs produced by the mitochondrion's own deoxynucleotide salvage pathway by *de novo* synthesis of dNTPs in non-dividing cells.

1.5.3 Maintenance of deoxyribonucleotide triphosphate pools

NMPK and NDPK phosphorylation reactions are reversible, unlike phosphorylation of deoxynucelosides by dNKs. Dephosphorylation of dNMPs to their corresponding nucleosides can occur, however, by 5'-nucleotidases: dNT1 is located in the cytosol and counteracts TK1 and dCK; dNT2 is located in the mitochondrion and specific for thymidine monophosphate and deoxyuridine monophosphate and probably has an important role in regulating and protecting mtDNA from excess dTTP, accumulation of which can cause mitochondrial genetic disease (Gallinaro et al., 2002).

Cellular concentrations for all four dNTPs are tightly controlled via biosynthetic and degradation pathways (Reichard, 1988), with each dNTP maintained in proportion to its DNA concentration. Alterations in dNTP pools in cell cultures cause dysfunctional mtDNA replication and repair (Kunz et al., 1994; Martomo and Mathews, 2002), and mutations in functionally important dNTP synthesis and salvage genes are

associated with depletion and multiple deletions of mtDNA. The shortage and/or imbalance of the dNTP pool are thought to cause reduced efficiency and accuracy of mtDNA replication, with misincorporation of nucleotides. It may also interfere with replication by affecting synthesis of the RNA primers necessary for initiation of replication (Smits et al., 2010).

1.6 Cytochrome *c* oxidase (complex IV)

COX, a haem-containing oxidase (Calhoun et al., 1994), is the terminal enzyme complex (complex IV) of the mitochondrial respiratory chain. It is a large transmembrane protein with surfaces exposed to both the mitochondrial matrix and IM space, and exists within the IMM as either a monomer or a dimer, comprising two monomers connected by a cardiolipin molecule (Kadenbach et al., 2000; Tsukihara et al., 1995). The latter is considered the active form of the enzyme and catalyses the transfer of electrons from ferrocytochrome *c* to oxygen. In doing so, it receives one electron from four each of cytochrome *c* molecules and transfers them to one oxygen molecule to form two molecules of water. Four protons from the inner aqueous compartment are used to make H_2O and four protons are translocated across the IMM into the IM space, thereby establishing an electrochemical gradient utilised by complex V to drive generation of ATP. The overall reaction is represented as follows: 4 ferrocytochrome *c* + $8H^+_{(inside)}$ + $O_2 \rightarrow$ 4 ferricytochrome *c* + $4H^+_{(outside)}$ + $2H_2O$.

1.6.1 Cytochrome *c* oxidase structure

Mammalian COX was originally resolved into eight polypeptide components by gel filtration and sodium dodecyl sulphate gel electrophoresis (Steffens and Buse, 1976). However, later experiments using a high-resolution electrophoresis system identified 13 structural subunits (Kadenbach et al., 1983). The subsequent purification of bovine heart COX assigned all 13 subunits within the enzyme complex (Tsukihara et al., 1996). The three largest subunits (MTCO1-3) are mitochondrially encoded and form the catalytic core of the enzyme. The remaining ten nuclear-encoded subunits (IV, Va, Vb, VIa, VIb, VIc, VIIa, VIIb, VIIc, and VIII) surround the core and are thought to stabilise the enzyme, function in assembly of the enzyme complex, or regulate enzyme activity (Taanman, 1997a). Human subunits VIa and VIIa have heart and liver specific tissue isoforms coded for by different genes (Kadenbach et al., 1982; Yanamura et al., 1988), thus a total of 15 genes encode the structural COX subunits. COX has six prosthetic metal groups: two haem (*a*, *a3*); two copper (Cu_A, Cu_B); one zinc; and one magnesium (Capaldi, 1990). The two haem A and two copper moieties are involved in electron transfer, whilst the function of the zinc and magnesium groups is unknown.

Despite the historically accepted COX crystal structure, recent evidence from cell lines, including blue-native gel electrophoresis (BN-PAGE), proteomic analysis, short hair-pin (sh) RNA induced knock down/over expression studies, and evolutionary data, suggest that *NDUFA4*, previously assigned to encode an accessory subunit of complex I, is actually an additional complex IV subunit (Balsa et al., 2012a). The disassociation of NDUFA4 from the COX enzyme complex during routine purification is thought to account for previously failed attempts to identify it as a COX subunit during crystallisation studies. Misattribution to complex I was probably related to contamination, as it was previously only inconsistently detected in complex I preparations and its presence correlated with contamination by another COX subunit (VIb) (Hirst et al., 2003). As such, COX should now be considered to consist of 14 structural polypeptide subunits.

1.6.2 Cytochrome *c* oxidase assembly and dysfunction

COX biogenesis is thought to be a linear process in which addition of subunits and cofactors occurs in a sequential manner. This concept was first presented using data obtained from rat liver mitochondria in which the incorporation of subunits, labelled with radioactive methionine, into the COX enzyme complex was recorded (Wielburski and Nelson, 1983). Analysis of the human enzyme using Blue-native gel electrophoresis subsequently confirmed this model (Nijtmans et al., 1998). An assembly pathway characterised by at least three discrete assembly intermediates (so-called S1-3) forming around core subunit MTCO1 during synthesis of the holoenzyme, and probably representing rate-limiting steps in the process, was proposed. The three intermediates included: 1) S1 containing COXI; 2) S2 comprising COXI and IV; and 3) S3 consisting of all the COX subunits apart from COXVIa and VIIb, insertion of which concludes formation of the enzyme complex (Nijtmans et al., 1998; Williams et al., 2004a). A large number of accessory proteins (now known to number at least 46) required for COX assembly were subsequently identified by studying COX expression in yeast mutants defective in COX assembly (McEwen et al., 1986; Soto et al., 2012a). However, the mechanistic role of some of these is unclear.

At the time of writing, mutations in eleven human nuclear-encoded factors required for assembly of the enzyme complex (*SURF1*, *SCO1*, *SCO2*, *COX10*, *COX15*, *LRPPRC*, *TACO1*, *FASTKD2, C2orf64/COA5*, *C12orf62/COX14* and *FAM36A/COX20*) were linked to human COX deficiency, and typically cause severe neonatal/childhood onset presentations with an early fatal outcome (Soto et al., 2012b; Szklarczyk et al., 2013). Isolated COX deficiency is the second most common enzyme deficiency following complex I (5% of 1,406 fresh muscle samples examined in Nijmegen between 2005 and 2009) (Rodenburg, 2011). Mutations in the structural subunits are extremely rare (Hanna et al., 1998; Rahman et al., 1999) with only three nuclear-encoded COX subunits linked to human disease (Indrieri et al., 2012; Massa et al., 2008; Shteyer et al., 2009). To date, most cases of isolated COX deficiency are caused by mutations in nuclear-encoded proteins required for COX translation, maturation or assembly (Soto et al., 2012b) or secondary to mtDNA depletion. Furthermore, these reported nuclear gene mutations are typically associated with severe neonatal or childhood onset presentations and an early fatal outcome. However, many cases of COX deficiency remain undefined at the molecular level.

1.7 F_1F_o ATP synthase (complex V)

Human mitochondrial ATP synthase is the fifth multimeric enzyme complex (complex V) of OXPHOS.

Under physiological conditions, the ATP synthase utilises energy created by the proton electrochemical gradient to synthesise ATP from ADP and P_i in the mitochondrial matrix (Capaldi et al., 1994). The flux of protons which occurs down the proton gradient generated by electron transfer occurs from the protochemically positive (PP) to protochemically negative (PN) side of the IMM. The activity of the enzyme is reversible, so that ATP hydrolysis generates a protein gradient by reversal of this flux. Fermenting bacteria without an electron transport chain utilise this function in order to create a transmembrane proton gradient which is then used to transport nutrients into the cell, maintain ionic balance, and for flagella. The overall reaction can be represented as follows: $ADP + P_i + H^+_{(PP)} \leftrightarrow ATP + H^+_{(PN)}$

The enzyme complex is organised into dimers and oligomers (Wittig and Schägger, 2008) and consists of two distinct functional protein domains known as F_1 and F_o. The soluble F_1 portion contains the catalytic core of the enzyme complex and is situated within the mitochondrial matrix, whilst the F_o is bound to the IMM and contains the membrane proton channel. F_1 derives its name from 'Fraction 1,' whereas F_o is so-called as it binds and is subsequently inhibited by the antibiotic oligomycin. Both of the functional regions are comprised of multiple protein subunits which enable both 'rotatory catalysis' and oligomerisation to occur. The latter mediates mitochondrial and cristae morphology.

Recently, in addition to their ATP synthesising/hydrolysing capacity, dimers of mitochondrial ATP synthase have been suggested to form the mitochondrial permeability transition pore (MPTP) (Giorgio et al., 2013). The MPTP is a large conductance channel in the IMM whose opening causes an increase of permeability to solutes with molecular masses up to ~1.5kDa. This causes the mitochondrial permeability transition, which refers to the massive swelling and depolarisation of mitochondria that occurs under some conditions, most notably calcium overload and stress, with uncoupling of OXPHOS and subsequent cell death.

1.7.1 F_1F_o ATP synthase structure

F_1 comprises five polypeptide subunits: three α; three β; and one γ, δ, and ε. F_o contains a c-ring subunit, composed of eight copies (Watt et al., 2010), one copy of subunits a, b, d, F_6, and the oligomycin sensitivity-conferring protein (OSCP), and finally transmembrane accessory subunits e, f, g, and A6L. F_1 subunits γ, δ, and ε form the central stalk, and F_o subunits b, d, F_6, and OSCP the peripheral stalk of the enzyme. Subunits a and A6L are encoded by the mitochondrial genes *MT-ATP6* and *MT-ATP8* respectively. The remaining 14 subunits (including IF1) are nuclear-encoded. However, as the crystal structure for complex V is not complete it is possible additional subunits may still be characterised.

1.7.2 F_1F_o ATP synthase assembly and dysfunction

As with COX, research involving assembly-deficient yeast mutants has been extensively used to study ATP synthase assembly (Kucharczyk et al., 2009a, 2009b, 2009c, 2010, 2013). However, due to rapid turnover of F_o subunits and the stator in these yeast mutants (the latter formed of the peripheral stalk and subunit a, thereby linking the catalytic and membrane domains (Walker and Dickson, 2006), ATP synthase biogenesis is not easily analysed (Rak et al., 2009). Assembly of F_1, the stator, and the c-ring is thought to occur separately, although the sequence in which the individual subunits are inserted into each module is unclear. Mammalian ATP synthase is subsequently thought to proceed as follows: assembly of the c-ring followed by binding of F_1, the stator, and finally subunits a and A6L (Wittig et al., 2010). This process is dependent on numerous nuclear-encoded ancillary proteins.

Complex V deficiency is rare, and was the least frequent isolated RC enzyme defect seen in Nijmegen between the years 2005 and 2009 (1% of 1,406 fresh muscle samples examined) (Rodenburg, 2011). Mutations in only three structural ATP synthase-encoding subunits are described: 1) mitochondrial-encoded *MT-ATP6* (Holt et al., 1990) and 2) *MT-ATP-8* (Jonckheere et al., 2008); and 3) nuclear-encoded *ATP5E* (encoding the ε subunit of F_1) (Mayr et al., 2010). Two additional genes have been associated with complex V deficiency: *TMEM70*, which functions as an ancillary factor of complex V biogenesis (Cízková et al., 2008); and the F1 portion assembly factor *ATP12* (De Meirleir et al., 2004).

1.8 Whole exome sequencing

Until relatively recently, identification of causative pathogenic mutations in monogenic disorders was reliant upon two main strategies: 1) candidate gene analysis using automated Sanger sequencing, so-called ‘first-generation’ technology, of known genes reported, or having potential, to cause genetic disease; and 2) genetic linkage mapping studies, when families with multiple affected and unaffected relatives were available. The main disadvantage of the former is that prior knowledge is needed to enable selection of a suitable candidate gene(s) to be screened, whilst the latter depends on the availability of large multigenerational pedigrees with DNA required from numerous affected and unaffected relatives, and even when successful, a region of linkage rather than a single candidate gene is identified. Since 2005, ‘next-generation’ sequencing (NGS) platforms have been increasingly utilised to study rare variations in different diseases and to locate novel disease genes for both Mendelian disorders and complex traits (Metzker, 2005). Initially, NGS technology utilised three main platforms which relied on parallel, cyclic interrogation of sequences from spatially separated clonal amplicons, (oil-aqueous emulsion bead [Roche: pyrosequencing chemistry], clonal beads [SOLiD: sequencing by sequential ligation of oligonucleotide probes], or clonal bridges [Illumina: sequencing by reversible dye terminators]) (Pareek et al., 2011), although a number of additional platforms have since been developed. Whole exome sequencing uses NGS technology to couple targeted exon capture with massively parallel DNA sequencing (all NGS platforms perform both the sequencing reactions and data capture simultaneously, unlike automated Sanger sequencing where the sequencing reaction is performed separately to the read detection). This technique determines all the coding variations an individual harbours. Although limited to exons, which constitute only 1-2% of the human genome, most alleles known to underlie Mendelian disease disrupt these protein-coding sequences, thereby making it a powerful yet cost-effective model for the identification of mutant alleles (Stenson et al., 2009).

1.8.1 Next-generation sequencing workflow

Although a number of NGS platforms exist, they all share certain basic principles required to capture a whole or subset of the mammalian genome at a scale corresponding to massively parallel sequencing. These steps can be broadly grouped as: 1) template preparation; 2) sequencing and imaging; 3) sequence read alignment; and 4) variation detection. In the case of exome sequencing, an additional step is required in order to enrich the sample for protein-coding exons alone.

Genomic DNA (gDNA) is randomly fragmented to lengths of 300-400 bp. Several micrograms of DNA are then used to construct a shotgun library. The library fragment ends are repaired and ligated to adaptors (or linkers) containing universal priming sites which later allow individual fragments to be hybridised to a flowcell and subsequently amplified and sequenced using common PCR primers (Metzker, 2010). In the case of whole exome sequencing, the library is enriched for sequences corresponding to exons by hybridising the fragments to biotinylated probes (or baits) (RNA or DNA) complementing all known exons in the genome. Biotin-streptavidin based pulldown is then used to isolate the bound exome-containing fraction, followed by amplification and massively parallel sequencing of the enriched library. The sequences are then aligned with the reference sequence prior to variant detection.

1.8.2 Approaches to gene identification using whole exome sequencing

Whole exome sequencing has rapidly become the first-line molecular approach for identification of causative, rare (minor allele frequency [MAF] $\leq$ 1%) and novel, mutations in monogenic Mendelian disorders, due to the high throughput and relatively low expenditure of this technique in comparison with the available alternatives. The key challenge, however, is distinguishing disease-related alleles from the background of non-pathogenic polymorphisms and sequencing errors. Typically, exome sequencing identifies 20,000-30,000 single nucleotide variants (SNVs) to the reference exome in each individual (Bamshad et al., 2011). As such, it is important to adopt a clear bioinformatic approach prior to exome sequencing in order to maximise the likelihood of identifying the causal mutation(s). The following strategies can be utilised to aid identification of disease-causing alleles using whole

exome sequencing data: 1) filtering genes with rare or novel variants predicted to be pathogenic that are shared by multiple, unrelated, probands with identical clinical phenotypes; 2) sequencing the exomes of both parents and the affected child when spontaneous disease exists for *de novo* heterozygous mutations (so-called 'trio' analysis); and 3) linkage analysis (if sufficient affected individuals are available for study) prior to exome sequencing of the interval identified if access is limited to one or two small families or homozygosity mapping if parents of the proband are consanguineous.

Novelty is assessed by filtering the variants against recorded polymorphisms available in public databases, such as dbSNP and 1000 Genomes Project, and/or those found in a cohort of unaffected controls. This filtering step assumes that an allele found to harbour variants that occur in the filter set cannot be causative. This approach is powerful because only a small proportion (~2%) of the SNVs identified in any one individual is novel (Bamshad et al., 2011). However, there are limitations. First, dbSNP is known to be contaminated with pathogenic alleles. Second, as the number of sequenced exomes and genomes increases, filtering for observed variants independent of their MAF risks eliminating pathogenic alleles which occur in the general population at relatively high frequencies. This is of particular importance in recessive disorders in which the carrier does not exhibit a phenotype which would usually result in exclusion from a control database, for example the 1000 Genomes Project (Ng et al., 2010b). As such, searching for variants with a MAF of $\leq$ 1% in addition to novel variants, particularly in rare recessive disorders, is recommended.

Candidate alleles can be further divided according to their predicted pathogenicity. For instance, stop codons gained, frameshift, and missense mutations would be weighted more heavily than synonymous mutations. However, the risk is that variants which do not alter protein-coding sequences, such as splice site mutations, could be overlooked. The deleterious impact of the variant can also be quantitated using various algorithms. For example phyloP (Cooper et al., 2010), SIFT (Kumar et al., 2009), and Polymorphism Phenotyping v2 (Adzhubei et al., 2010) consider factors such as the sequence conservation of a particular genomic region, or the

physiochemical alterations that might be caused by an amino acid substitution and how these might affect protein function.

Finally, candidate genes can be identified using prior knowledge of their biological and functional characteristics which are shared with other genes or proteins, dysfunction of which is known to cause a similar clinical phenotype. In the case of mitochondrial disorders, filtering for an inventory of genes whose protein products are primarily localised to the mitochondria (the so-called mitochondrial proteome (Calvo and Mootha, 2010)) is a powerful albeit imperfect (in view of the extra-mitochondrial or double localisation of many gene products) tool to reduce the list of candidate alleles when a primary disorder of the RC is suspected. One such example of an inventory of mammalian mitochondrial genes is Mitocarta, a compendium of over 1000 human genes (compiled using mass spectrometry of mitochondria isolated from different tissue types, protein tagging/microscopy, and integration of other genome-scale datasets of mitochondrial localisation, using a Bayesian approach) with strong support of mitochondrial localisation (Pagliarini et al., 2008a).

1.8.3 Limitations of whole exome sequencing

Despite significant benefits to whole exome sequencing there are some limitations. Firstly, non-coding intronic regions are not interrogated and although most variants known to underlie Mendelian disorders are thought to disrupt protein-coding sequences (Stenson et al., 2009), the contribution of non-coding regions to disease has not yet been determined. Secondly, exome sequencing only captures what we currently know exists. Thirdly, not all known genes are properly captured and sequenced using exome sequencing. Examples include repetitive regions, sequences which are highly homologous for other locations in the genome, and AT- or GC-rich sequences. The first two examples make mapping the resulting reads back to the reference exome difficult, whilst GC and AT-rich target sequences may show PCR amplification bias in product yield during template preparation which results in their underrepresentation in exome alignments and assemblies (Dohm et al., 2008; Harismendy et al., 2009; Hillier et al., 2008; Metzker, 2010). Fourthly, in addition to the repeat expansion and intronic mutation mechanisms, copy number

variations (CNVs) are not detected. This is because PCR-based sample preparation methods are used, thus all targets eventually achieve similar concentrations.

1.9 Aims of thesis

The aims of this thesis were to: 1) characterise novel adult clinical phenotypes associated with primary dysfunction of the RC; and 2) identify causative genetic mutations in the nuclear genes of patients with presumed but genetically undetermined mitochondrial disease, and to assess their molecular pathogenesis.

CHAPTER 2

Materials and Methods

CHAPTER 2

2. Materials and Methods

Materials and methods shared amongst multiple chapters are outlined in detail below. Methods used only once are included under the relevant chapter headings within a separate methods section.

2.1 Histopathology and electron microscopy

Muscle and nerve biopsies were performed following informed consent. Muscle was snap frozen at the bedside and stored at -80°C until use. Standard histological and histochemical stains were used on cryostat sections as previously described (Rahman et al., 2000). The sural nerve was fixed in 3% glutaraldehyde with 0.1 M sodium cacodylate buffer, post fixed in 1% osmium tetraoxide and embedded in Araldite CY212 resin. One μm resin sections were cut and stained with methylene blue, azure II and basic fuchsin. Seventy nm resin sections of areas of interest were cut and contrasted with uranyl acetate and lead citrate for electron microscopy (EM). Teased fibres were prepared as previously described (Low et al., 1978).

Muscle and nerve histopathology and EM was performed in the University College London Hospitals (UCLH) National Hospital for Neurology and Neurosurgery (NHNN) National Commissioning Group (NCG) Neuropathology diagnostic laboratory and results were interpreted by Dr Janice Holton and Dr Rahul Phadke.

2.2 Cell culture methods

2.2.1 Cell incubation

Skin biopsies were performed following informed consent. Human fibroblasts were established from skin explants and cultured routinely in Dulbecco's modified Eagle's medium, 4.5 g/L D-(+)-glucose, Glutamax™-I (Life Technologies) supplemented with 10% fetal bovine serum, 110 μg/ml of sodium pyruvate, 50 U/ml of penicillin, 50 μg/ml of streptomycin and 50 μg/ml of uridine. Medium was changed every 4 days. The cell density was monitored by phase-contrast microscopy and cultures approaching 80-90% confluency were harvested and re-plated at a lower density.

Cells were grown routinely in plastic dishes at 37°C in a humidified atmosphere of 5% CO_2 in air, but cultured onto glass coverslips for 3 days prior to immunocytochemical investigations (Taanman et al., 2003). Cultures were checked for mycoplasma infection by 4',6-diamidino-2-phenylindole staining prior to all experiments.

Cell incubation was performed by Dr Jan-Willem Taanman at the Department of Clinical Neuroscience, University College London Institute of Neurology.

2.2.2 Harvesting cells

Fibroblasts were washed with sterile phosphate-buffered saline (PBS) and trypsinisation was then performed. Culture medium was added to the dislodged, trypsinised cells to stop further trypsin activity. The resulting fibroblast suspension was then collected, and was pelleted by centrifugation at 200 × *g* for 10 minutes in a Thermo Scientific Heraeus Megafuge 16 centrifuge. The cell pellet was subsequently resuspended with culture medium.

2.3 Biochemical methods

Spectrophotometric analysis of haem absorption spectra was performed using crude mitochondrial pellets from muscle tissue (see section 2.5.1). All other RC enzyme assays used mitochondria isolated from cultured skin fibroblasts by differential centrifugation (see section 2.5.2). The one exception to this was the RC enzyme assay performed on cultured skin fibroblasts grown on galactose-containing medium (Chapter 6) in which whole cell lysates were used (see section 2.5.3).

Spectrophotometric analyses of RC enzymes extracted from muscle tissue were performed in the UCLH NHNN NCG Neurometabolic diagnostic laboratory by Dr Iain Hargreaves.

2.3.1 Sample preparation

Whole cell lysates or mitochondrial fractions were used. For whole cell lysates, cultured skin fibroblasts, grown on galactose-containing medium (Chapter 6), were harvested. Pellets of harvested cells (see section 2.5.3) and mitochondrial fractions

(see sections 2.5.1 and 2.5.2) were resuspended in isolation medium (320 mM sucrose, 10 mM Tris, pH 7.4 and 1 mM EDTA) with three protease inhibitors (1 mM PMSF, 1 µg/ml leupeptin and 1 µg/ml pepstatin A). Snap-freezing was performed on samples for 3 cycles using liquid nitrogen to disrupt the cells and expose mitochondrial enzymes. A bicinchoninic acid (BCA) protein assay (see section 2.5.4) was then carried out on the samples (2 µl) in triplicate to determine the protein concentration and the remainder of the samples were used in spectrophotometric activity assays.

2.3.2 Spectrophotometric analysis

All measurements were made at 30°C using the HITACHI U-3310 spectrophotometer (apart from citrate synthase [CS] where a 96-well plate and a plate reader was used) and quadruplicated measurements were recorded. Complex I and complex IV were measured in the cultured skin fibroblasts of the adult patients with COX deficiency discussed in Chapter 5 and 6, whereas complex II+III was measured in the cultured skin fibroblasts of the adult patient with COX deficiency discussed in Chapter 5 only.

2.3.2.1 Complex I (NADH: ubiquinone reductase)

The oxidation of NADH was measured spectrophotometrically at 340 nm in 1 ml solution of 20 mM potassium phosphate (KP_i) buffer (pH 7.2), 8 mM $MgCl_2$, 150 µM NADH, 1 mM KCN, and 2.5 mg/ml bovine serum albumin (BSA) prewarmed at 30ºC. An additional 10 µl of H_2O was added to the reference cuvette, whereas 10 µl of mitochondrial extract was added to the sample cuvette. Approximately 30 seconds after initiating the measurement, ubiquinone-1 stock solution (~5 mM in ethanol) was added to a final concentration of 50 µM to start the reaction. When the time scale reached 380 seconds, 10 µl of 10 mM rotenone stock solution (in ethanol) was added to inhibit complex I. Measurement was continued for another 340 seconds to allow the evaluation of non-rotenone sensitive NADH dehydrogenase activity.

2.3.2.2 Complex II+III (succinate: cytochrome c reductase)

The succinate cytochrome *c* reductase assay measures the rate of reduction of cytochrome *c* and was performed as described by King (King, 1967) . The assay was

measured in 1 ml solution of 100 mM KP_i buffer (pH 7.4), 0.3 mM EDTA, 0.1 mM cytochrome *c*, 1 mM KCN, 20 mM Na^+ succinate, and 2.5 mg/ml BSA, at a wavelength of 550 nm. Two cuvettes with KP_i buffer, EDTA, cytochrome *c* and BSA were prewarmed at 30ºC, whilst 7.5 µl of mitochondrial extract was incubated with 40 µl of 500 mM Na^+ succinate and 10 µl of 100 mM KCN at 30°C for 5 min to activate the enzyme. After 4 min, both the reference and test cuvettes were loaded into the spectrophotometer. When the full 5 min had elapsed, the mitochondrial extract (along with Na^+ succinate and KCN) were added to the test cuvette, whilst 40 µl of 500 mM Na^+ succinate, 10 µl of 100 mM KCN and 7.5 µl of H_2O were added to the reference cuvette. Both cuvettes were mixed thoroughly and the absorbance at 550 nm was measured for 5 mins. After this time 10 µl of 2 mM antimycin A was added to the test cuvette and mixed and measurements continued for a further 4-5 mins. The antimycin A halts the reaction because cytochrome *c* reductase is antimycin A sensitive.

2.3.2.3 Complex IV (cytochrome c oxidase)

Spectrophotometric analysis was performed in 0.1 M KP_i (pH 7.0) prewarmed at 30ºC according to Wharton and Tzagoloff (Wharton and Tzagoloff, 1967). Two cuvettes (for reference and sample) were identically loaded with KP_i buffer. Cytochrome *c* was reduced by dithionite and added to a final concentration of 50 µM and a total volume of 1 ml. The cytochrome *c* in reference cuvette was then oxidised with 10 µl of 0.1 M potassium ferricyanide and 5 µl of mitochondrial sample was added to the sample cuvette 30 seconds after initiating the measurement by the spectrophotometer, which measured the absorbance difference at 550 nm between the reference and the sample. The entire measurement cycle lasted for 5 minutes and the absorbance values were recorded for every one-minute interval.

2.3.2.4 Citrate synthase

CS activity was measured using a previously described method (Coore et al., 1971). The activity of the mitochondrial citric acid cycle enzyme was used as an indication of the relative mitochondrial enrichment of the sample. CS catalyses the reaction between oxaloacetate (OAA), the substrate, and acetyl CoA resulting in the production of citrate and liberation of ‘free’ thiol groups (CoA-SH). DTNB (‘Ellman’s

reagent', 5,5'-dithio bis-2-nitrobenzoid acid) binds free thiol groups to produce DTNB-CoA which is yellow and absorbs at 412 nm. A master mix was made up as follows (for 1 sample to make a total volume of 1000 μl): 500 μl of 200 mM Tris; 20 μl of 10 mM acetyl-CoA; 20 μl of 10 mM DTNB ; 10 μl of 10% (w/v) Triton X-100; 10 μl of 10 mM oxaloacetate ; 430 μl of H_2O. The master mix was pre-warmed to 30°C. 10 μl of the sample was added to 990 μl of the mastermix and 240 μl was pipetted into 4 separate wells on the 96-well plate in order to perform the assay in quadruplicate, along with four blanks (replacing the sample with 10 μl of H_2O). The increase in absorbance at 440 nm was recorded over a 10 min period on a plate reader.

2.3.3 Respiratory chain enzyme activity calculations

The NADH dehydrogenase of complex I is the only rotenone-sensitive NADH dehydrogenase in the cell. To measure complex I activity the difference in absorbance change per minute before (activity of all NADH dehydrogenases) and after addition of rotenone (activity of all NADH dehydrogenases excluding complex I) was measured. The rotenone-sensitive activity of complex I can then be calculated via the Beer-Lambert Law with the ubiquinone extinction coefficient (=6.81 mM^{-1}). Likewise, the activities of Complex II + III and CS were calculated via the Beer-Lambert Law with the cytochrome *c* (19.2 mM^{-1}) and DTNB (13.6 mM^{-1}) extinction coefficients, respectively. The specific enzyme activities (nM/mg/min) were calculated by dividing the rate by the protein concentration obtained from the BCA protein assay.

For COX the rate constant (k) was calculated from a programmed spreadsheet by taking the logarithm of change in absorbance per min (Wharton and Tzagoloff, 1967). The specific COX activity (k/mg/min) was calculated by dividing the rate constant by the protein concentration obtained from the BCA protein assay.

2.4 Genetic methods

2.4.1 DNA extraction from whole blood and muscle tissue

DNA extraction was performed from whole blood using the Qiagen Flexigene DNA extraction kit and muscle tissue using the Promega Wizard Genomic kit according the manufacturer's instructions in the UCLH NHNN NCG Neurogenetics diagnostic laboratory by Ms Cathy Woodward.

2.4.2 DNA and RNA quantification

DNA and RNA quantification was carried out on a NanoDrop® ND-1000 spectrophotometer (NanoDrop). A 2 μl sample was loaded onto the machine. Nucleotides, RNA, single-stranded DNA, and double-stranded DNA all have an absorbance maximum at 260 nm, whereas proteins that may contaminate the sample have an absorbance maximum at 280 nm. The ratio of absorbance at 260 nm compared to that at 280 nm is therefore used to assess the purity of DNA and RNA. A ratio of approximately 1.8 is generally considered acceptable for DNA, whilst a ratio of approximately 2.0 is acceptable for RNA. All samples used in the experiments presented in this thesis were in the acceptable range of purity.

2.4.3 Polymerase chain reaction

DNA fragments were amplified using polymerase chain reaction (PCR) (Mullis et al., 1986; Saiki et al., 1988). The standard PCR mix per 1 μl DNA template (200 ng/μl) consisted of: 12.5 μl Amplitaq Gold 360 mastermix (Applied Biosystems); 9.5 μl nanopure H_2O; 1 μl of 10 pmol forward; and 1 μl of 10 pmol reverse primer, to make a total mastermix volume per well of 25 μl. The standard cycling conditions consisted of an initial denaturation step at 95°C for 10 min, followed by 30 cycles of denaturation at 95°C for 30 sec, annealing at 58°C for 30 sec, and extension at 72°C for 30 sec. The final extension step at 72°C was for 7 min. PCR products and RFLP fragments were separated on a 2% agarose gel that contained 0.25 μg/ml of ethidium bromide and then visualised under UV illumination. Five hundred ng of a 100 bp ladder (Invitrogen) was used as a size standard. To monitor for

contamination a negative control containing 1 μl of ddH_2O instead of template DNA was used for each reaction.

2.4.4 Automated Sanger sequencing

Sanger sequencing involves the selective incorporation of chain-terminating dideoxyribonucleotide triphosphates (ddNTPs) by DNA polymerase during *in vitro* DNA replication. The process requires a single-stranded DNA template, a DNA primer, a DNA polymerase, normal dNTPs and modified ddNTPs that terminate DNA strand elongation. Chain-terminating nucleotides lack the 3'-OH group necessary for formation of a phosphodiester bond between two nucleotides. As such, when ddNTPs are incorporated into the growing DNA chain they prevent DNA polymerase from any further extension. The ddNTPs may be radioactively or fluorescently labelled for detection in automated sequencing machines.

In this thesis, amplification of DNA fragments for sequencing was performed using specific overlapping primers (the oligonucleotide sequences for each primer are listed under the relevant chapter heading), and BigDye Terminator v.1.1 cycle sequencing kit (Applied Biosystems). The samples were run on a 3730xl DNA Analyzer, assembled and analysed using Seqscape v.2.5 software (Applied Biosystems) and were compared to the reference sequence.

2.4.5 Whole exome sequencing

Whole exome sequencing was performed within the UK10K project. DNA (1-3 μg) was sheared to 100-400 bp using a Covaris E210 or LE220 (Covaris, Woburn, MA, USA). Sheared DNA was subjected to Illumina paired-end DNA library preparation and enriched for target sequences (Agilent Technologies; Human All Exon 50 Mb - ELID S02972011) according to manufacturer's recommendations (Agilent Technologies; SureSelectXT Automated Target Enrichment for Illumina Paired-End Multiplexed Sequencing). Enriched libraries were sequenced using the HiSeq platform (Illumina) as paired-end 75 base reads according to the manufacturer's protocol. The mean coverage of the exomes was 74 times. The Burrows-Wheeler Aligner (BWA) (Li and Durbin, 2009) was used for alignment to the human reference genome build UCSC hg19 (Grch37). To improve raw alignment BAMs for single

nucleotide polymorphism (SNP) calling, we realigned around known (1000 Genomes pilot) indels, and recalibrated base quality scores using Genome Analysis Toolkit (GATK) (DePristo et al., 2011). BAQ tags were added using SAMtools calmd. BAMs for each sample were merged and duplicates marked using Picard. Variants (SNPs and Indels) were called on each sample individually with both SAMtools mpileup (0.1.17) (Li et al., 2009) and GATK UnifedGenotyper (1.3.21) (McKenna et al., 2010), restricted to exon bait regions plus or minus a 100 bp window. Various quality filters were applied to each of the callsets separately. Calls were then merged, giving preference to GATK information when possible. Calls were annotated with 1000 Genomes allele frequencies, dbSNP132 rsids and earliest appearance in dbSNP. Functional annotation was added using Ensembl Variant Effect Predictor v2.2 against Ensembl 64 and included coding consequence predictions, SIFT, PolyPhen and Condel annotations, and GERP and Grantham Matrix scores. Variant filtering of the single nucleotide variants and indels was done as previously described on the basis of autosomal recessive inheritance. The filtering of the variants was done very stringently, excluding variants in dbSNP132, 1000 Genomes, synonymous and other non-coding variants apart from essential splice site changes. Variants were also excluded if present in either the remaining UK10K rare disease cohort (823 exomes at the time of the analysis) or the NHLBI Exome Sequencing Project (ESP) database.

2.5 Protein methods

2.5.1 Isolation of mitochondria from muscle tissue using differential centrifugation

Frozen muscle tissue was ground in homogenisation buffer (320 mM sucrose, 1 mM EDTA, 10 mM Tris-HCl pH 7.4) in a glass homogenizer manually. Muscle homogenates were centrifuged at 600 × *g* for 10 min at 4°C. The supernatants were stored on ice and the pellets were resuspended in homogenising buffer, homogenised and centrifuged at 600 × *g* for 10 min at 4°C. Both the supernatants were pooled and centrifuged at 12000 × *g* for 10 min at 4°C. The mitochondrial enriched protein pellets were subsequently used for RC enzyme assays (performed in the Neurometabolic diagnostic laboratory by Dr Iain Hargreaves), haem-absorption spectra analysis, in-gel activity staining, and western blot analysis of sodium dodecyl sulphate (SDS)-denaturing and blue-native polyacrylamide gels. Protein concentrations were determined by BCA protein assay.

2.5.2 Isolation of mitochondria from cultured skin fibroblasts using differential centrifugation

Twenty 10 cm plates with confluent cultures of fibroblasts (~10 × 10^6 cells) were harvested by trypsinisation. Cell pellets were washed in 50 ml of PBS supplemented with 1 mM phenylmethysulfonyl (PMSF), 1 μg/ml of leupeptin, and 1 μg/ml pepstatin A (all Sigma). These protease inhibitors were added to the ice-cold buffer shortly before use. Cell pellets were frozen at -80°C. After storage at -80°C cell pellets were thawed and put on ice. All procedures (including centrifugations) were carried on ice or at 4°C. Each cell pellet was resuspended in 1 ml ice-cold homogenisation buffer (10 mM Tris-HCl pH 7.4, 1 mM sodium EDTA, 250 mM sucrose, 1 mM PMSF, 1 μg/ml leupeptin, 1 μg/ml pepstatin). Cells were pelleted by centrifugation at 4000 x *g* for 5 mins. The supernatant was discarded and the cell pellet resuspended in 2 ml ice-cold homogenisation buffer and transferred to an ice-cold, 2 ml Teflon® pestle PYREX® Potter-Elvehjem tissue homogeniser. Cells were homogenised (20 strokes at 1000 rpm) and the homogenate was transferred to a centrifuge tube. Nuclei, cell debris, and unbroken cells were pelleted by centrifugation at 1500 x *g* for 10 mins.

The supernatant was transferred to a new tube and kept on ice. The pellet was resuspended in 2 ml ice-cold homogenisation buffer and transferred to back to the glass tissue homogeniser. The pellet was homogenised, transferred to a centrifuge tube, and centrifuged at 1500 x *g* for 10 mins as before. The two supernatants were combined and centrifuged again at 1500 x *g* for 10 mins. The supernatant was transferred to a clear centrifuge tube and the mitochondria were pelleted by centrifugation at 11,500 x *g* for 12 mins. The supernatant was discarded and the mitochondrial pellet was resuspended in 100 μl homogenisation buffer. The resuspended mitochondria were stored at -80°C until use.

Mitochondria were isolated from all fibroblast cultures (apart from the cells grown on galactose-containing medium discussed in Chapter 6, where whole cell lysates were used for RC enzyme assay) using this previously described method of differential centrifugation (Rickwood et al., 1987). The isolated mitochondria were subsequently used for RC enzyme assays and western blot analysis of SDS-denaturing polyacrylamide gels. Protein concentrations were determined by BCA protein assay. As the mitochondrial enrichment by the differential centrifugation procedure may vary between samples, spectrophotometric assays of CS activity were performed (see section 2.3.2.4), so that the RC enzyme activities could be expressed relative to the mitochondrial marker enzyme CS and, thus, allow correction for different levels of mitochondrial enrichment of the samples.

2.5.3 Whole cell lysates

Two 10 cm plates with confluent cultures of fibroblasts (~10^6 cells) were harvested by trypsinisation. Cell pellets were washed in 5 ml of PBS supplemented with 1 mM PMSF, 1 μg/ml of leupeptin, and 1 μg/ml pepstatin A. Protease inhibitors were added to the ice-cold buffer shortly before use. Cell pellets were frozen and stored at -80°C. Cell pellets were thawed and put on ice. All procedures (including centrifugations) were carried on ice or at 4°C. The cell pellet was resuspended in 1 ml ice-cold homogenisation buffer and the cells were pelleted by centrifugation at 16,000 × *g* for 10 minutes at 4°C. The supernatant was removed and the cell pellet resuspended in a volume of homogenisation buffer relative to the size of the pellet (75 μl for a small

size pellet, 150 μl for a medium size pellet, and 200 μl for a large size pellet). Protein concentrations were determined by BCA protein assay.

Whole cell lysates of fibroblasts grown on galactose-containing medium were used for RC enzyme assay of complexes I and IV in Chapter 6.

2.5.4 Bicinchoninic acid protein assay

The BCA protein assay was performed according to the instructions provided by the Thermo Scientific Pierce BCA Protein Assay Kit. A serial dilution was made of the bovine serum albumin (BSA) standard provided and resulted in a final BSA concentration ranging from 0 to 2000 µl/ml. To estimate the protein concentration 25 µl of the BSA solution at varying concentrations and 25 µl of diluted mitochondrial extracts were mixed with 200 µl of Working Reagent (50:1 ratio of BCA Reagent A to Reagent B) in wells of a 96-well plate. The 96-well plate was subsequently incubated at 37˚C for 30 minutes, followed by the detection of the absorbance at 562 nm of the BSA standard and samples. A linear plot of absorbance against concentration was constructed for BSA standard and the protein concentration of samples could then be interpolated from the plot.

2.5.5 SDS denaturing polyacrylamide gel electrophoresis

A 12.5% and 15% separating gel mix and a 3% stacking gel mix were made up using the reagents below for the western blots performed in Chapters 4 and 5. The gel mixtures were filtered at 0.2 μm prior to addition of ammonium parsulphate (APS) and tetramethylethylenediamine (TEMED). After adding APS and TEMED the gel was poured between two glass plates separated by a 0.75 mm spacer (BIORAD mini PROTEAN II system) and overlaid with ddH_2O. Once polymerised, the ddH_2O was removed and APS and TEMED were added to the 3% stacking gel mix which was then poured on top of the separating gel. A comb was then inserted and the gel left to polymerise for 45 min.

	3% stack	12.5% separating	15% separating
3.75 M Tris-HCl (pH 8.6)	-	920 μl	920 μl
0.5 M Tris-HCl (pH 6.5)	500 μl	-	-
40% acrylamide/bis (37.5:1)	450 μl	3.1 ml	3.7 ml
20% SDS	25 μl	46 μl	46 μl
Urea	1.8 g	3.25 g	-
ddH_2O	3.25 ml	3.5 ml	2.9 ml
10% ammonium persulphate	25 μl	44 μl	44 μl
TEMED	3 μl	6 μl	6 μl

In Chapter 6, a 4-20% Tris-Glycine gel (Thermo scientific) pre-cast gel was used. Based on the BCA protein assay results, samples were diluted to the same concentration using PBS and 2x Dissociation Buffer (2x DB – 100 mM Tris-HCl, pH 6.5, 24% [v/v] glycerol, 8% [w/v] SDS, 4% [v/v] β-mercaptoethanol, 0.02% [w/v] bromophenol blue). Additional volumes of 1x DB were added to the samples (including blanks) to ensure each lane contained equal volumes of DB. Samples were incubated at 37°C for 30 mins and then centrifuged at 16,000 × *g*. The supernatant was transferred to a new tube prior to loading. Wells were rinsed and the samples loaded. Gels were run at 100 V for 15 min and then 200 V for further 45 min.

Western blotting was performed in a BIORAD Mini Trans-Blot® Electrophoretic Transfer Cell. Labelled polyvinylidene difluoride (PVDF) membranes (Millipore) were soaked in methanol then equilibrated in Towbin's buffer (TB 25 mM Tris-base, 192 mM Glycine, and 20% methanol). The transfer sandwich was made in the gel holder cassette and consisted of a sponge pad, followed by a sheet of Whatmann 3MM paper, the separating gel, the wet PVDF membrane, a second sheet of Whatmann 3MM paper and finally a second sponge pad. The transfer sandwich was assembled whilst submerged in TB, ensuring that there were no air bubbles between any of the different layers. The transfer sandwich was put in the transfer cell with the separating gel side facing the cathode and the PVDF membrane side facing the anode. An ice pack and a small magnetic stir bar were placed in the transfer cell which was then

filled with TB. The transfer was performed at 100 V for 75 min after which the sandwich was disassembled and the membranes left to dry overnight.

Once dried the membrane was briefly soaked in methanol and equilibrated in PBS. It was then blocked with 10% (w:v) milk powder in PBS. A falcon tube was also blocked with 5 ml of 10% milk powder. The milk was discarded and the blots and the falcon tube were washed briefly with PBS/Tween (1x PBS, 0.3% Tween 20) three times. The blots were then placed into the blocked falcon tubes with the protein side facing inwards. The primary antibody was added to 3 ml of PBS/Tween in the falcon tube and the blot was incubated for two hours on a roller mixer. Blots were then washed three times in PBS/Tween for 10 mins. The secondary antibody was then added and the blot incubated for one hour before being washed a further three times in PBS/Tween. The specific primary and secondary antibodies used for each experiment are included under the relevant chapter heading.

The Thermo Scientific Pierce ECL Western blotting substrate kit and Amersham Hyperfilm ECL was used to detect chemiluminscent signals with exposure times from 7 sec to 16 min.

2.5.6 Blue-native polyacrylamide gel electrophoresis

2.5.6.1 One-dimensional blue-native gel electrophoresis

Separating 8-16% acrylamide gradient gels with a 4% acrylamide stacking gel were used in Chapters 4 and 5, whereas a 3-12% acrylamide gel with a 3% acrylamide stacking gel was additionally used in Chapter 6. Acrylamide-bis (48% acrylamide, 1.5% bis), 3x gel buffer (1.5 M 6-aminocaproic acid, 150 mM bistris) , ddH_2O, glycerol, 10% APS, and TEMED were used to make the gels in the ratios listed below.

	High (16%)	**High (12%)**	**Low (8%)**	**Low (3%)**	**Stack (4%)**	**Stack (3%)**
Acrylamide/bis (37.5:1)	3.25 ml	2.44 ml	1.98 ml	0.744 ml	0.5 ml	0.38 ml
3x gel buffer	3.30 ml	3.3 ml	3.96 ml	3.96 ml	2 ml	2.0 ml
ddH_2O	1.70 ml	2.51 ml	5.86 ml	7.098 ml	3.5 ml	3.12 ml
Glycerol	1.98 g	1.98 g	-	-	-	-
10% ammonium persulphate	35 μl	35 μl	70 μl	70 μl	50 μl	50 μl
TEMED	3.5 μl	3.5 μl	7 μl	7 μl	5 μl	5 μl

The mixtures were filtered at 0.2 μm prior to addition of APS and TEMED. Once APS and TEMED had been added to the high and low percentage mixtures for the separating gel, 7 ml of each were pipetted into the wells of the gradient mixer. A peristaltic pump at a constant speed was used to pour four gels between two glass plates separated by a 0.75-mm spacer (BIORAD mini PROTEAN II system). The gradient gels were overlaid with H_2O-saturated butanol which was removed after the gels had polymerised. APS and TEMED were added to the stacking gel mix which was then poured on top of the separating gels. Combs were inserted and the gels were sealed with clingfilm and left overnight (or for up to one week) at 4°C.

The concentration of the mitochondrial enriched fraction of muscle tissues (~10 μg/μl of protein) was determined using a BCA protein assay and equalised by diluting by

adding homogenising buffer (320 mM sucrose, 1 mM EDTA, 10 mM Tris-HCl pH 7.4) with protease inhibitors. Ten μl of the samples with a protein concentration of 10 μg/μl were then suspended in 150 μl of protein solubilising solution (1 M ε-amino-*n*-caproic acid, 50 mM Bis-Tris [pH 7.0]) and 25 μl 20% *n*-dodecyl-β-D-maltoside (DDM). After incubation on ice for 30 minutes, the samples were centrifuged at 16,000 × *g* for 20 minutes at 4°C. To the supernatant 25 μl 1 M ε-amino-*n*-caproic acid, 5% Serva Blue G was added before loading 20 μl in each lane of the gradient polyacrylamide blue-native gel (Schägger, 1995; Williams et al., 2004b). Cathode buffer A (50 mM tricine, 15 mM bistris, 0.02% Serva blue G, pH 7.0) and anode buffer (50 mM bistris, pH 7.0) were added to the electrophoretic tank and electrophoresis was performed at 100 V for 20 min, then constant at 4 mA per gel. Electrophoresis was stopped 5 mins after the blue front had run off the bottom of the gel. If the gel was to be used for enzyme activity staining, the cathode buffer A was replaced with cathode buffer B (50 mM tricine, 15 mM bistris, 0.002% Serva blue G, pH 7.0) halfway through the run. Immunoblotting was performed as described in section 2.5.5 except that two additional washes of the PVDF membrane in methanol prior to blocking were performed in order to remove excess Serva blue G. The specific primary and secondary antibodies used for each experiment are included under the relevant chapter heading.

2.5.6.2 In-gel activity staining

In-gel enzyme activity staining of complex I and IV (Chapter 6) was performed as previously described (Zerbetto et al., 1997). The gel strips were first destained for a few minutes in anode buffer and rinsed in ddH_2O. The NADH:ubiquinone oxidoreductase (10 ml of 2 mM Tris·HCl pH 7.4, 25 mg nitroblue tetrazolium and 1 mg NADH) or the COX stain (1 ml 0.5 M NaP_i buffer pH 7.4, 5 mg diaminobenzidine, 10 mg cytochrome *c*, 10 μl catalase solution at 2 μg/ml and 9 ml ddH_2O) were added and the gel strips incubated overnight at 37°C. Gel strips were soaked in ddH_2O to halt the reactions. The staining intensity of each band was quantified using AlphaEase FC software from Alpha Innotech.

2.5.6.3 Two-dimensional blue-native gel electrophoresis

For two-dimensional blue-native gel electrophoresis (Chapter 6), lanes excised from the blue-native gel were soaked in 3 ml of reducing buffer (RB: 1% [v:v] β-mercaptoethanol, 1% [w:v] SDS) for 15 mins in a sealed tube under a fume hood as a denaturing step. The gel slices were then soaked in 3 ml of equilibrating buffer (EB: 50 mM tris, 1% [w:v] SDS, pH 6.8) twice for 10 min. Glass plates were assembled sandwiching the gel slice within the top third of the plates where the stacking gel is poured. Approximately 3-4 mm was left between the top of the gel slice and the top of the plates in order to completely seal the gel slice within the stacking gel. A 15% SDS-denaturing separating gel was poured with sufficient space between the top of the separating gel and the gel slice for the stacking gel. The separating gel was overlaid with ddH_2O. Once polymerised, the ddH_2O was removed and a 3% stacking gel was poured ensuring the gel strips were completely surrounded. A single toothed comb was inserted between the gel strip and the edge of the gel plate to enable a BioRad Precision plus Protein Standard to be used as a molecular size marker. The stacking gel was left 30 mins to polymerise and then electrophoresis was performed at 100 V. When the gel front had entered the separating gel the voltage was increased to 200 V (run at constant voltage) until the front reached the bottom of the gel. The gels were blotted and probed as described in section 2.5.5. The specific primary and secondary antibodies used are included in Chapter 6.

2.5.7 Immunocytochemistry

2.5.7.1 Polylysine Coating of Coverslips

Lyophilised poly-L-lysine (5 mg), purchased from Sigma, was resuspended in 5 ml of sterile 0.1 M sodium borate buffer, pH 8.1; and 200 µl of the polylysine mixture was incubated on the surface of 22-mm sterile coverslips for an hour, followed by two rinses with sterile H_2O.

2.5.7.2 Cell-seeding on coverslips

Polylysine coated coverslips were seeded with approximately 7.5×10^3 cultured skin fibroblasts in 500 µl medium at 37˚C, 5% CO_2 in wells of a 6-well plate. After 1 hour, 1.8 ml of medium was added to each well.

2.5.7.3 Immunofluorescence Staining of Cultured Cells

Cells were fixed by incubating with 4% w/v paraformaldehyde in PBS at room temperature for 20 min. The coverslips were subsequently incubated with methanol at -20˚C for 15 min for further fixation and membrane solubilisation. The coverslips were incubated with 300 µl of 10% normal goat serum (NGS) in PBS at 37˚C for 30 min to prevent non-specific antibody binding. Coverslips were probed with 80 µl of diluted primary antibody (anti-NDUFA4 and anti-MTCO1) and 2% NGS in PBS for 45 min at 37ºC. For secondary incubation, the coverslips were incubated with 80 µl of 100-fold diluted secondary antibody tagged with an Alexa fluorophore (Molecular Probes) and 2% NGS in PBS for 45 min at 37ºC. Prior to the paraformaldehyde fixation step, some samples were also counterstained with 5 µM MitoTracker Red CM-H_2XRos (Invitrogen) by incubation in the culture medium at 37˚C for 45 minutes, followed by a further 30 minutes of incubation at 37˚C in plain culture medium. The coverslips were mounted with Agar Scientific citifluor/PBS/glycerol supplemented with 1 µg/ml of 4',6-diamidino-2-phenylindole (DAPI) from Sigma and sealed with nail varnish. Fluorescent images were obtained with a Zeiss Axioplan confocal microscope. The optimal concentration of anti-NDUFA4/anti-MTCO1 used was determined by direct observation of fluorescent signal strength of diluted 1 mg/ml anti-NDUFA4/anti-MTCO1 (dilutions included 50^{-1}, 100^{-1}, 200^{-1}, 400^{-1} and 800^{-1}).

CHAPTER 3

m.9185T>C in *MT-ATP6* causes axonal Charcot-Marie-Tooth disease

CHAPTER 3

3. m.9185T>C in *MT-ATP6* causes axonal Charcot-Marie-Tooth disease

3.1 Introduction

Mitochondrial ATP generation by OXPHOS underpins key molecular processes that are essential for normal central and peripheral nervous system axonal function. Axonal peripheral neuropathies are a well-recognised complication of primary mtDNA mutations. However, the neuropathy is rarely the presenting or predominant clinical manifestation of the disease (Croft et al., 1977; Peyronnard et al., 1980; Gemignani et al., 1982; Yiannikas et al., 1986; Mizusawa et al., 1991; Schröder, 1993; Bouillot et al., 2002; Kärppä et al., 2003). In contrast, mutations in the nuclear-encoded mitochondrial genes *MFN2* (Chung et al., 2006) and *GDAP1* (Baxter et al., 2002), which encode outer mitochondrial membrane proteins, usually present with isolated peripheral neuropathy, and are now recognised to be important causes of both axonal and demyelinating forms of Charcot-Marie-Tooth (CMT) disease.

An extended family in which the index case presented with a pure motor neuropathy in childhood evolving into motor-predominant CMT2 in later life was investigated. Additional multi-system clinical features and a matrilineal inheritance pattern prompted mtDNA sequencing in one individual. The known pathogenic missense mutation m.9185T>C in *MT-ATP6* was identified and shown to segregate with disease in affected members of the pedigree. *MT-ATP6* encodes the ATP6 subunit of the mitochondrial ATP synthase (OXPHOS complex V). The ATP6 subunit is a component of F_o and involved in the translocation of protons across the IMM, a process which is coupled to ATP generation within the catalytic domain of F_1. In view of the striking neuropathic features observed in this family, a large cohort of 442 unrelated probands with genetically undefined CMT2 and dHMN was screened for mutations in *MT-ATP6* and *MT-ATP8*, encoding two components of complex V. Mitochondrial mutations that impair the function and stability of complex V are shown to be an important but previously unreported cause of CMT2.

3.2 Patient cohort

A cohort of patients from the Medical Research Council (MRC) Centre for Neuromuscular Diseases inherited neuropathy database was selected. These were patients presenting with a clinical phenotype compatible with either CMT2 (a progressive peripheral motor and sensory neuropathy, n=270) or dHMN (a progressive peripheral motor neuropathy without sensory involvement, n=172). Diagnosis was based on clinical and electrophysiological phenotypic evaluation. Patients were excluded from the study if inheritance was consistent with paternal transmission. All patients with CMT2 were negative for mutations in *MFN2*. The majority of patients with CMT2 were also screened for mutations in *MPZ*, *HSPB1*, *HSPB8, TRPV4* and *GJB1* where appropriate. Patients with dHMN were negative for mutations in *HSPB1*, *HSPB8*, *TRPV4*, and selected patients were negative for mutations in *BSCL2* and *GARS.* These genes were sequenced in the UCLH NHNN Neurogenetics diagnostic laboratory.

3.3 Methods

3.3.1 Automated Sanger sequencing of *MT-ATP6/8*

Amplification of DNA fragments for sequencing was performed using specific overlapping primers, Amplitaq Gold 360 mastermix (Applied Biosystems) and BigDye Terminator v.1.1 cycle sequencing kit (Applied Biosystems). The workload was shared with Sinéad Murphy and Ellen Cottenie (MRC Centre for Neuromuscular Diseases, UCL Institute of Neurology). The samples were run on a 3730xl DNA Analyzer, assembled and analysed using Seqscape v.2.5 software (Applied Biosystems) and were compared to the rCRS reference sequence (NCBI accession number NC_012920). Full mitochondrial genome sequencing was performed in one patient (Family 3.1, Patient III-6). Targeted sequencing of *MT-ATP6/8* was performed in all remaining patients (Table 3.1 for primer sequences).

Table 3.1: Primer sequences used for targeted analysis of *MT-ATP6/8*

Fragment	Forward primer Reverse primer	Length (nucleotides)	Nucleotide location
1	5'-ACAGTTTCATGCCCATCGTC-3' 3'-GTTCGTCCTTTAGTGTTGTG-5'	530	8196-8726
2	5'-CCGACTAATCACCACCCAAC-3' 3'-GGTTTTACTATATGATAGGC-5'	598	8646-9244
3	5'-ATCCAAGCCTACGTTTTCAC-3' 3'-CTGAGGCTTGTAGGAGGGTA-5'	593	9151-9744

3.3.2 Restriction endonuclease analysis to quantitate m.9185T>C mutant load

Restriction endonuclease analysis was used to quantitate mutant load in m.9185T>C positive cases. The workload was shared with Ellen Cottenie (MRC Centre for Neuromuscular Diseases, UCL Institute of Neurology). To introduce a BSP12OI restriction site (GGGCCC) into the mutant but not the wild-type mtDNA, a fragment of *MT-ATP6* containing the mutation site was amplified using the mismatch sense primer (9,161-9,184) ACGTTTTCACACTTCTAGT**GG**GCC and antisense primer (9,273–9,253) AGAGGGCCCCTGTTAGGGGTC. In order to calculate heteroplasmy, a FAM fluorophore (6-carboxyfluorescein) was used at the 5' end of the antisense primer. To amplify the fragment initially an annealing temperature of 58°C and 17 PCR cycles was used. The temperature, PCR cycle number and primer concentration was subsequently optimised so that sufficient PCR product was obtained. The PCR cycle number was then reduced to the lowest possible number to ensure that amplification occurred only in the linear phase to enable accurate quantitation of mutant load. The final PCR reaction was as follows: 1) initial denaturation (10 min, 95°C); 2) denaturation (30 sec, 95°C); 3) primer annealing (30 sec, 57°C); 4) elongation (30 sec, 72°C); 5) final elongation (7 min, 72°C). Steps two to four were repeated 18 times. The composition of the PCR reaction was as follows: Amplitaq Gold 360 Mastermix (12.5 μl); ddH_2O (5.5 μl); forward primer (3 μl, 10 pmol/μl); reverse primer (3 μl, 10 pmol/μl); DNA template (1 μl, 50ng/μl). Following the amplification phase, restriction enzyme digestion using 10 units of BSP12OI was

performed to cleave the 113 nucleotides mutant PCR product into 89 and 24 nucleotide fragments. The enzyme digest reaction mix was composed of: restriction enzyme (2 μl); restriction enzyme buffer (2 μl); and PCR product (16 μl). The reaction mix was subsequently incubated for two hours at 37°C. The PCR products were finally denatured by adding 12 μl of formamide to 1 μl of digested product. 0.3 μl of Liz 600 (ABI) was used a size standard. The resulting mixture was heated at 95°C for 3 min after which it was immediately put on ice before being loaded onto a 3730xl DNA analyser. The ratio of cut to uncut DNA was calculated with the GeneMapper (ABI) program. The experiment was performed in triplicate and the mean mutant mtDNA level calculated.

3.3.3 Clinical and electrophysiological characteristics for patients harbouring pathogenic m.9185T>C mutation in *MT-ATP6*

Detailed clinical assessment was performed for all patients harbouring the pathogenic m.9185T>C mutation in *MT-ATP6*. Data ascertained where possible included: age of symptom onset; clinical history and examination findings; CMT examination (CMTES2) and neuropathy (CMTNS2) scale, as an indicator of neuropathy severity (Murphy et al., 2011); nerve conduction studies (NCS) and electromyography (EMG).

3.3.4 Laboratory, imaging, histological and biochemical findings for patients harbouring pathogenic m.9185T>C mutation in *MT-ATP6*

Laboratory investigations, including plasma creatine kinase (CK) and plasma/cerebrospinal (CSF) lactate, brain magnetic resonance imaging (MRI) and muscle histological studies were performed for all patients found to harbour the pathogenic m.9185T>C mutation in *MT-ATP6* where possible. Spectrophotometric analysis of respiratory chain enzyme complexes I, II+III and IV and BN-PAGE of complex V were performed in the UCLH NHNN NCG Neurometabolic laboratory by Dr Annapurna Chalasani in cases where muscle tissue was available.

3.4 Results

3.4.1 Automated Sanger sequencing of *MT-ATP6/8*

Disease-causing m.9185T>C mutations were detected in three additional unrelated probands (Family 3.2, 3.3 and 3.4 discussed below) from the 270 CMT2 index cases analysed, representing a specific mutation frequency for this variant in *MT-ATP6* of 1.1%. No pathogenic *MT-ATP6* variants were found in patients with dHMN (172), and no pathogenic mutations in *MT-ATP8* were found in either the CMT2 or dHMN groups. All synonymous and non-synonymous single nucleotide variants (SNVs) detected in *MT-ATP6* and *MT-ATP8* are outlined in Table 3.2. Following removal of synonymous/non-coding SNVs and known polymorphisms, the potential pathogenicity of each variant was evaluated using control databases: mitowheel (http://mitowheel.org/mitowheel.html); mtDB (http://www.mtdb.igp.uu.se); and HmtDB (http://www.hmtdb.uniba.it:8080/hmdb). The following steps were used to exclude non-pathogenic variants: 1) SNVs detected in more than five control patients; 2) SNVs detected in less than five control patients but known to associate with specific haplotypes; 3) poorly conserved nucleotides (assessed using the mtSNP search tool: mtsnp.tmig.or.jp/mtsnp/search_mtSAP_evaluation_e.html). After applying this filtering strategy, one patient with CMT2 was found to harbour the novel variant m.8828A>G which causes a missense change from Asparagine to Serine at amino acid position 101 of the ATP6 protein (Asn101Ser). Unfortunately, there was no muscle tissue available from the patient for BN-PAGE, thus the potential pathogenic nature of this variant remains uncertain.

3.4.2 Restriction endonuclease analysis to quantitate m.9185T>C mutant load

Quantitation of the m.9185T>C mutant load showed segregation with disease severity and phenotype (Figure 3.1 and 3.3, Table 3.3), and allowed patients to be broadly classified into four clinical groups according to m.9185T>C mutant load: (Group 1) unaffected individuals (<64% mutant load); (Group 2) asymptomatic individuals with upper motor neuron (UMN) signs detectable on examination only (such as a spastic increase in tone, pyramidal pattern of muscle weakness, brisk reflexes and/or positive Babinski sign) (64-79% mutant load); (Group 3) affected individuals with clinical symptoms and signs of UMN involvement without neuropathy (80-91% mutant load); (Group 4) affected individuals with symptoms and signs of motor-predominant CMT2 (92-100% mutant load).

Table 3.2: Synonymous and non-synonymous *MT-ATP6* (nucleotide positions 8527-9207) and *MT-ATP8* (nucleotide positions 8366-8572) nucleotide variants detected in probands with CMT2 (n=270) and dHMN (n=172)

Synonymous variants	Non-synonymous variants
8545G>A: S-S (1)	8381A>G: T-A (1)
8572G>A: St-St (3)	8388T>C: V-A (1)
8598T>C: I-I (2)	8396A>G: T-A (1)
8679A>G: L-L (1)	8461C>A: N-K (1)
8740C>T: L-L (1)	8477T>G: S-A (2)
8754C>T: I-I (1)	8489A>C: M-L (1)
8769A>G: T-T (2)	8490T>C: M-T (2)
8772T>C: T-T (1)	8502A>G: N-S (1)
8805A>G: T-T (1)	8516T>C: W-R (1)
8820A>G: L-L (4)	8519G>A: E-L (1)
8889T>C: I-I (1)	8545G>A: A-T (1)
8925A>G: W-W (1)	8572G>A: A-T (3)
8940C>T: I-I (2)	8578C>T: P-S (1)
8955T>C: I-I (1)	8605C>T: P-S (2)
8958C>T: I-I (1)	8620C>T: P-S (1)
9006A>G: L-L (2)	8698A>G: M-V (1)
9015C>T: N-N (1)	8699T>C: M-T (1)
9042C>T: H-H (2)	8704A>C: M-L (2)
9060C>A: T-T (1)	8704A>G: M-V(1)
9061C>T: L-L (1)	8725A>G: T-A (1)
9075C>T: T-T (1)	8765C>T: A-V (1)
9078T>C: I-I (1)	8794C>T: H-Y (1)
9117T>C: I-I (3)	***8828A>G: N-S (1)***
9120A>G: L-L (2)	8836A>G: M-V (1)
9123G>A: L-L (5)	8839G>A: A-T (1)
9126T>C: T-T (1)	8864T>C: V-A (1)
9168C>T: F-F (1)	8875T>C: F-L (2)
	8887A>G: I-V (1)
	8950G>A: V-I (2)

	9025G>A: G-S (1) 9067A>G: M-V (1) 9101T>C: I-T (1) 9139G>A: A-T (1) **9185T>C: L-P (3)**

Abbreviations: Bold = known pathogenic variant; bold italics = novel variant; brackets = number of patients with variant.

3.4.3 Clinical and electrophysiological characteristics for index family harbouring m.9185T>C in *MT-ATP6*

Family 3.1 (Figure 3.1, Table 3.3): The index case (Patient III-8) presented with recurrent falls and foot drop aged 6 years following normal early development. Clinical examination aged 21 years showed distal muscle wasting of the legs, pes cavus, and clawing of the toes (Figure 3.2). Formal manual muscle strength testing (MRC graded) was normal in the upper limbs with mild proximal lower limb weakness (hip flexion 4+ bilaterally) and moderate distal lower limb weakness (ankle dorsiflexion 3, plantarflexion 4+, inversion 5, and eversion 2 bilaterally). Ankle jerks were absent. Plantar responses were extensor. Pin prick sensation was normal but vibration detection was reduced to the knees. Additional multi-system clinical findings in some family members and a matrilineal inheritance pattern prompted mtDNA sequencing in an older sibling (Figure 3.1, Family 3.1, Patient III-6). This revealed m.9185T>C (Haplogroup V), a homoplasmic (i.e. mutant load 100%) pathogenic mutation in *MT-ATP6*, causing a missense change from leucine to proline at amino acid position 220 of the ATP6 protein (Leu220Pro). Presence of the m.9185T>C mutation was confirmed in the index case and was shown to segregate with disease within the family. All affected individuals were homoplasmic, whilst the mutational load was present at much lower levels in an unaffected relative (Family 3.1, Figure 3.1, Patient II-4). Clinical features in addition to a pure motor/motor-predominant axonal neuropathy included: learning difficulties (Patients II-3, II-5, III-4, III-5, III-6, III-7, III-8, IV-1 and IV-2); sensorineural hearing loss (SNHL) (Patient III-7); and retinal degeneration (Patient III-8). Early proximal lower limb weakness was evident in three patients (with no evidence of myopathy either neurophysiologically or on muscle biopsy) despite a relatively mild neuropathy (patients III-6, III-7 and III-8). Two patients suffered rapid decompensation following a febrile illness (Patient III-5 and Patient IV-1). The available clinical data suggests a sudden onset Leigh-like illness in one patient (Patient III-5). Electrophysiologically the neuropathy was a pure motor neuropathy/neuronopathy in three individuals (Patients II-1, III-7 and III-8). However, sensory signs have since developed in one patient, making the diagnosis clinically compatible with motor-predominant CMT2 (Patient III-8). The neuropathy was particularly severe in two adults with wheelchair dependence in the third decade (Patient II-3 and Patient III-4).

Family 3.1

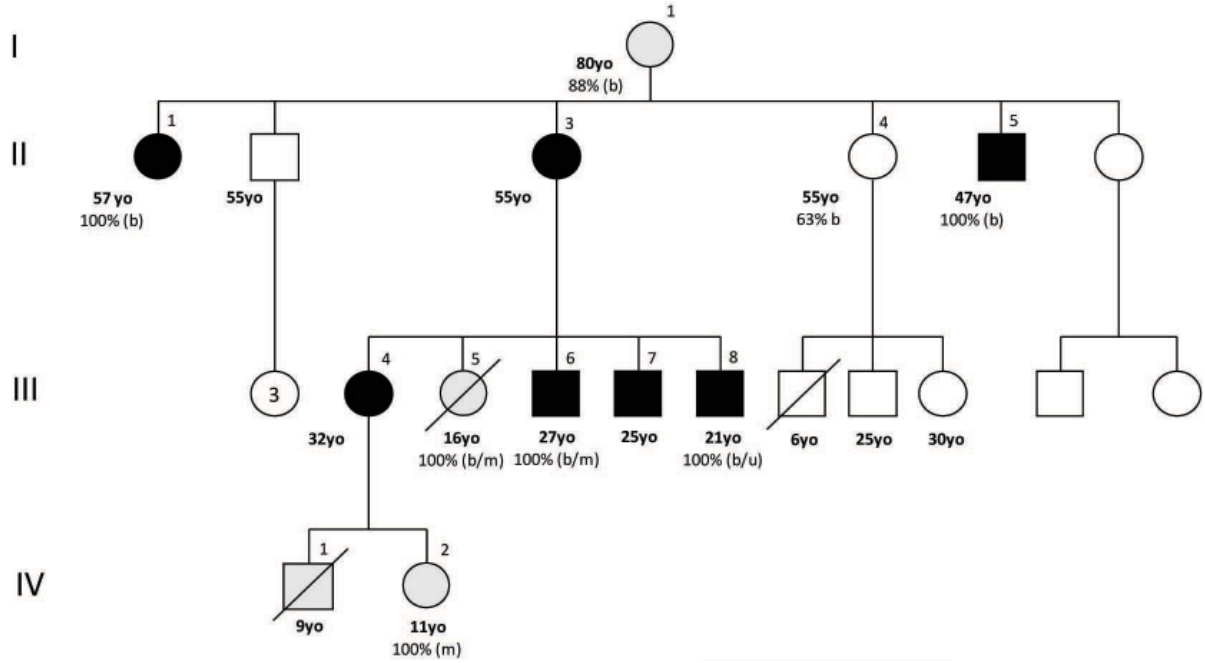

Figure 3.1: Pedigree of Family 3.1 (index family) harbouring the m.9185T>C mutation in *MT-ATP6*. Filled symbols indicate individuals with CMT2; light grey shaded symbols indicate individuals with unknown phenotype; square symbols indicate male gender; round symbols indicate female gender; numbers in symbols indicate multiple individuals; symbols with slashes indicate deceased. Abbreviations: (b) = blood; (u) = urine; (m) = muscle; yo = year old; % = percentage m.9185T>C mutant load detected in each patient.

Figure 3.2: Photograph demonstrating distal lower limb muscle wasting and pes cavus in a patient with the m.9185T>C mutation in *MT-ATP6* (Family 3.1, Patient III-8).

3.4.4 Clinical and electrophysiological characteristics for the three additional families harbouring m.9185T>C in *MT-ATP6*

Family 3.2 (Figure 3.3, Table 3.3): Patients with CMT2 (Patients II-8, III-6, and IV-3, all with 100% mutant load) presented in their first and second decades with typical features of inherited neuropathy. Patient III-6 had a pure motor neuropathy/neuronopathy electrophysiologically aged 29, although repeat studies aged 45 revealed reduced sensory nerve action potentials compatible with motor-predominant CMT2. Despite a gradually progressive clinical course, two patients suffered a rapid decline in mobility in their fifth and sixth decades with wheelchair dependence from unaided walking over a 5-year period (Patients II-8 and III-6). In these severe cases there was upper limb and proximal lower limb weakness without evidence of myopathy on EMG. However, early proximal lower limb weakness was also present in a mildly affected individual (Patient IV-3) without upper limb involvement.

Family 3.3 (Figure 3.3, Table 3.3): Symptom onset was in the first and second decades (Patients III-13 and IV-2, both with 100% mutant load). Electrophysiologically patients with homoplasmic mutant loads had a pure motor neuropathy/neuronopathy (Patient IV-2) or sensorimotor axonal neuropathy (Patient III-13). Those with lower mutant levels were asymptomatic (Patient III-5 with 75% mutant load and Patient IV-1 with 45% mutant load). Patient IV-2 had a severe neuropathic phenotype associated with learning difficulties, behavioural problems, and wheelchair dependence by early adulthood. Patient III-13 had motor-predominant CMT2 with pyramidal tract signs and proximal muscle weakness which developed in later life.

Family 3.4 (Figure 3.3, Table 3.3): Unlike Family 3.1, 3.2 and 3.3, Patient III-1 initially appeared to be a sporadic case of motor-predominant CMT2 (92% mutant load). He presented in the first decade with recurrent ankle sprains and falls and was diagnosed with CMT2 aged 11 years. NCS demonstrated a length-dependent sensorimotor axonal neuropathy and EMG showed proximal and distal lower limb denervation with no evidence of myopathy.

Family 3.2

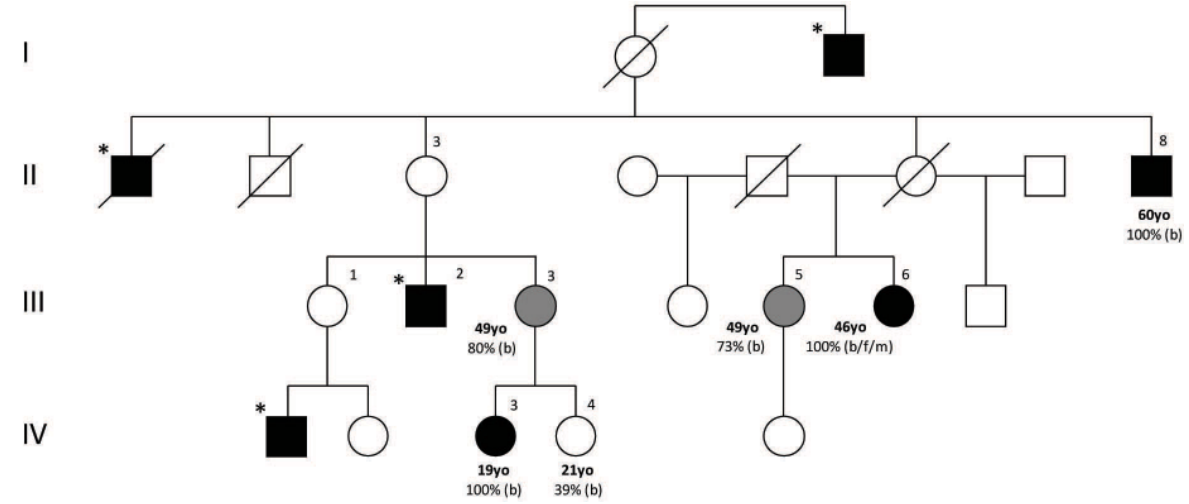

Family 3.3

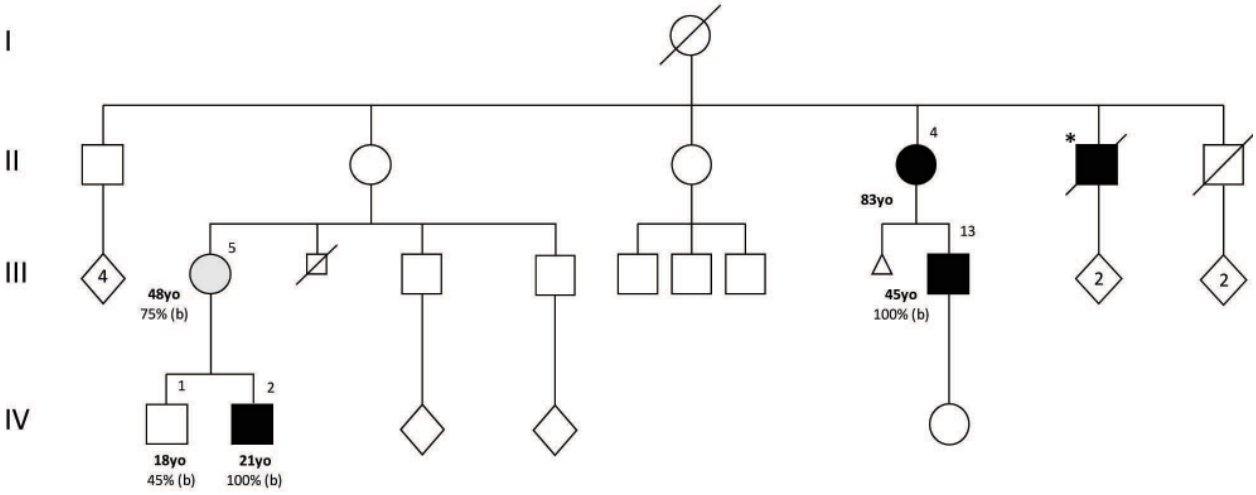

Family 3.4

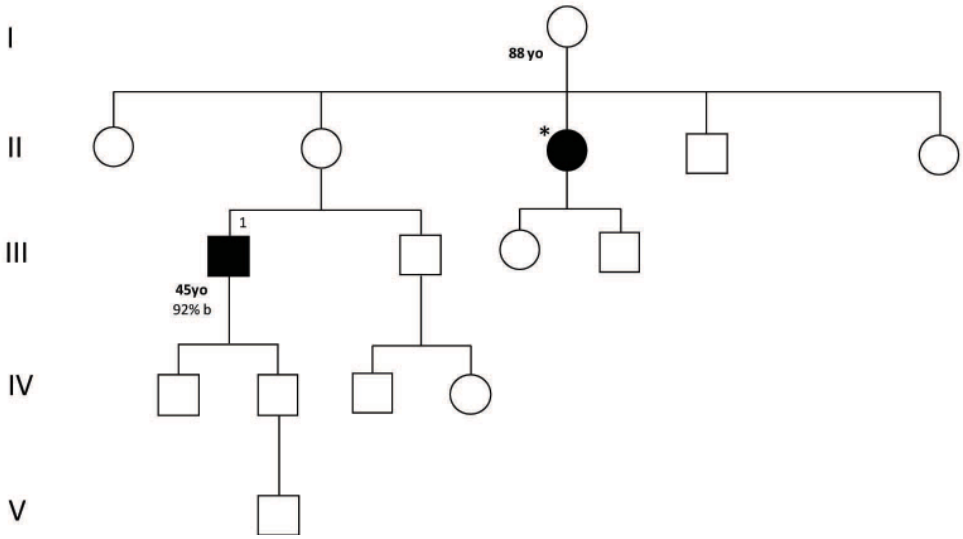

Figure 3.3: Pedigrees of three additional unrelated families harbouring the m.9185T>C mutation in *MT-ATP6*. Filled symbols indicate individuals with CMT2; dark grey shaded symbols indicate individuals with upper motor neuron signs only; light grey shaded symbols indicate individuals with unknown phenotype; square symbols indicate male gender; round symbols indicate female gender; diamond symbols indicate gender unknown; numbers in symbols indicate multiple individuals; symbols with slashes indicate deceased; a small square with a slash indicates still birth; a small triangle indicates miscarriage; asterisks indicate affected individuals not examined by authors. Abbreviations: (b) = blood; (u) = urine; (f) = fibroblasts; (m) = muscle; yo = year old; % = percentage m.9185T>C mutant load detected in each patient.

Table 3.3: Clinical and electrophysiological findings for patients with the m.9185T>C mutation in *MT-ATP6*

Family	Patient	Sex	Age onset (years)	Symptoms at onset	Age last exam (years)	Pes Cavus	Motor weakness	Sensory loss	UMN signs	Other features	Mobility	CMTES2(28)/ CMTNS2(36)	Summary of NCS/EMG/CMCT
3.1	II-1	F	2nd decade	Falls	42	Y	Distal LL	N	N	Blackouts	Unaided	ND	Pure motor neuropathy (no further data available)
	II-3	F	2nd decade	Unsteady	30	Y	Distal LL	N	N	Mild LD, ataxia	Wheelchair (3rd decade)	ND	ND
	II-4	F	Asymptomatic										
	II-5	M	1st decade	Late walker, falls	31	N	Distal LL	N	N	*Dysmorphic, LD	Unaided	ND	Axonal neuropathy (no further data available)
	III-4	F	U	Unsteady, falls	32	N	Distal UL and LL	N	N	Mild LD, migraine, ataxia	Wheelchair (3rd decade)	ND	Motor neuropathy/neuronopathy SAPs within normal limits
	III-5	F	16	Rapid decline following viral illness with Leigh-like syndrome. Died aged 16 years.	16	N	N	N	N	LD	Unaided	ND	ND
	III-6	M	11	Tripping	27	Y	Mild prox and mod distal LL	Knees	N	Mild LD, foot surgery	Unaided with ankle support	9(28)	Sensorimotor axonal neuropathy SAPs mildly reduced

	III-7	M	9	Unsteadiness, poor concentration	15	Y	Mild prox LL	N	N	Mod LD, SNHL, kyphoscoliosis,	Unaided	ND	Pure motor axonal neuropathy (no further data available)
	III-8	M	6	Falls, weak ankles	21	Y	Mild prox and mod distal LL	Knees	Extensor plantars	Mild LD, tapetoretinal degeneration, foot surgery	Unaided with leg irons	9(36)	Aged 18: Pure motor axonal neuropathy. SAPs within normal limits. Aged 21: Sensory involvement clinically
	IV-1	M	6	Deterioration in gait. Sudden death following viral illness aged 9 years.	8	N	N	N	Hyper-reflexia	LD	Unaided	ND	ND
	IV-2	F	10	Painful legs, tripping	10	N	N	N	N	Febrile seizure, mild LD	Unaided	ND	ND
3.2	II-3	F	Asymptomatic		54	N	None	None	N	None	Unaided	ND	ND
	II-8	M	2nd decade	Slow running	60	N	Mild prox and distal UL, severe prox and distal LL	Distal UL and LL	N	Late-onset DM	Wheelchair (6th decade)	21(28)	Aged 31: Pure motor axonal neuropathy SAPs within normal limits
	III-1	F	Asymptomatic										
	III-2	M	1-2nd decade	Foot drop	U	Hammer toes	U	U	U	None	Unaided	ND	ND

	III-3	F	5th decade	Leg cramps, reduced exercise tolerance, toes extend whilst walking	49	Y	Mild distal LL	N	Hyper-reflexia, clonus, extensor plantars	None		0(36)	Normal NCS/EMG/CMCT
	III-5	F	Asymptomatic		44	N	N	N	Hyper-reflexia, clonus, extensor plantars	Migraine	Unaided	ND	Normal NCS/EMG/CMCT
	III-6	F	2nd decade	Slow walking and flapping feet	40 45	N N	Mild distal LL Mild prox UL, mild prox and mod distal LL	None Distal UL/LL	N Extensor plantars	Migraine, late-onset DM	Unaided Wheelchair (5th decade)	20(28)/ 24(36)	Aged 29: Pure motor axonal neuropathy SAPs within normal limits Aged 45: Sensorimotor axonal neuropathy SAPs within normal limits
	IV-3	F	3	Falling, clumsy	19	Y	Mild prox and distal LL	Ankles	None	Kyphoscoliosis, focal seizures	Unaided	9(28)/ 11(36)	Sensorimotor axonal neuropathy SAPs mildly reduced
	IV-4	F	Asymptomatic		21	N	N	N	N	None	Unaided	ND	Normal
3.3	II-4	F	Asymptomatic		83	N	Mild distal LL	N	Y	Late onset SNHL	Rollator	ND	ND
	III-5	F	Asymptomatic		49	N	N	N	U	None	Unaided	ND	Sural SAPs mildly reduced

	III-13	M	17	Weak legs	43	Y	Mod prox and distal LL	N	Catch, hyper-reflexia and extensor plantars	None	Walking stick	ND	Aged 43: Sensorimotor axonal neuropathy SAPs mildly reduced
	IV-1	M	Asymptomatic										
	IV-2	M	4	Falls, delayed motor skills, toe walking	19	Y	Distal LL	Distal LL	N	Mild LD, ADHD, OCD	Wheelchair	ND	Motor axonal neuropathy SAPs within normal limits
3.4	II-1	M	1st decade	Recurrent ankle sprains, falls	45	N	Mild distal UL, mild prox and mod distal LL	Knees	Pout reflex	Foot surgery	Two sticks	15(28)/ 17(36)	Sensorimotor axonal neuropathy SAPs mildly reduced

Abbreviations: ADF = ankle dorsiflexion; ADHD = attention deficit hyperactivity disorder; BG = basal ganglia; CMCT = central motor conduction times; CMTES2 = Charcot-Marie-Tooth examination score 2 (total score 28); CMTNS2 = Charcot-Marie-Tooth neuropathy score 2 (total score 36, mild neuropathy: 0-10; moderate neuropathy: 11-20; severe neuropathy: >20); DM = diabetes mellitus; F = female; LD = learning difficulties; LL = lower limbs; M = male; mod = moderate; N = no; ND = not done; OCD = obsessive compulsive disorder; prox = proximal; SAPs = sensory nerve action potentials; SNHL = sensorineural hearing loss; U = unknown; UL = upper limbs; UMN = upper motor neuron; Y = yes. Asterisk (*) denotes not examined by author.

3.4.5 Laboratory, imaging, histological and biochemical findings for patients harbouring pathogenic m.9185T>C mutation in *MT-ATP6*

Laboratory investigations, brain MRI, muscle histological and biochemical studies for all four families harbouring the pathogenic m.9185T>C mutation in *MT-ATP6* are summarised in Table 3.4. BN-PAGE (Figure 3.4) was performed on four muscle samples and revealed both impaired assembly (demonstrated by multiple bands indicative of abnormal assembly intermediates) and/or activity (demonstrated by reduced band intensity) of complex V when patients were compared with control muscle tissue (Family 3.1, Patients III-5, III-6, IV-2 and Family 3.2, Patient III-6).

Table 3.4: Laboratory, imaging, muscle histological and biochemical findings for patients with the m.9185T>C mutation in *MT-ATP6*

Family	Patient	CK (<140IU/L)	Plasma lactate (<1.7mmol/L)	CSF lactate (<2.0mmol/L)	MRI	Muscle biopsy	RCEA	BN-PAGE V
3.1	I-1	ND	ND	ND	ND	ND	ND	ND
	II-1	ND	ND	ND	ND	ND	ND	ND
	II-4	ND	ND	ND	ND	ND	ND	ND
	II-5	U	U	ND	ND	ND	ND	ND
	III-4	U	U	ND	Brain: Cerebellar atrophy	ND	ND	ND
	III-5	U	U	ND	ND	LM: Mild increase lipid content. No RRF/COX-ves.	Normal	↓ assembly and activity
	III-6	U	U	Normal	Brain: Normal	LM: Neurogenic changes only	ND	↓ assembly
	III-7	U	1.2	2.4	Brain: High signal BG bilaterally	LM: Non-specific myopathic, neurogenic changes. No RRF/COX -ves. EM: Prominent subsarcolemmal aggregates	ND	ND
	III-8	168	0.9	2.1	Normal	U	ND	ND
	IV-1	Normal	ND	ND	Normal	Normal	ND	ND
	IV-2	ND	ND	ND	ND	Normal	Normal	↓ assembly
3.2	II-8	ND	ND	ND	ND	ND	ND	ND
	III-3	37	0.8	ND	ND	ND	ND	ND
	III-5	ND	ND	ND	Brain: Normal Spine: Normal	ND	ND	ND

	III-6	79	2.8	3.0	Brain: Mild cerebellar atrophy	LM: Neurogenic changes. Excess lipid content. No RRF/COX-ves.	Normal	↓ activity
	IV-3	99	1.51	ND	Normal	ND	ND	ND
	IV-4	60	0.8	ND	ND	ND	ND	ND
3.3	III-5	U	U	ND	ND	ND	ND	ND
	III-13	U	U	ND	ND	ND	ND	ND
	IV-1	ND	ND	ND	ND	ND	ND	ND
	IV-2	Normal	ND	ND	ND	LM and EM normal	ND	ND
3.4	II-1	132	1.3	ND	ND	ND	ND	ND

Abbreviations: ND = not done; U = unknown; CK = creatine kinase; CSF = cerebrospinal fluid; CMCT = central motor conduction times; MRI = magnetic resonance imaging; LM = light microscopy; EM = electron microscopy; BG = basal ganglia; b = blood; m = muscle; f = fibroblasts; u = urine; COX = cytochrome *c* oxidase; RRF = ragged red fibres; RCEA = respiratory chain enzyme analysis; BN-PAGE V = Blue-native polyacrylamide gel electrophoresis of complex V; normal reference ranges in our laboratory: CK < 140IU/L; plasma lactate <1.7mmol/L; and CSF lactate <2.0mmol/L.

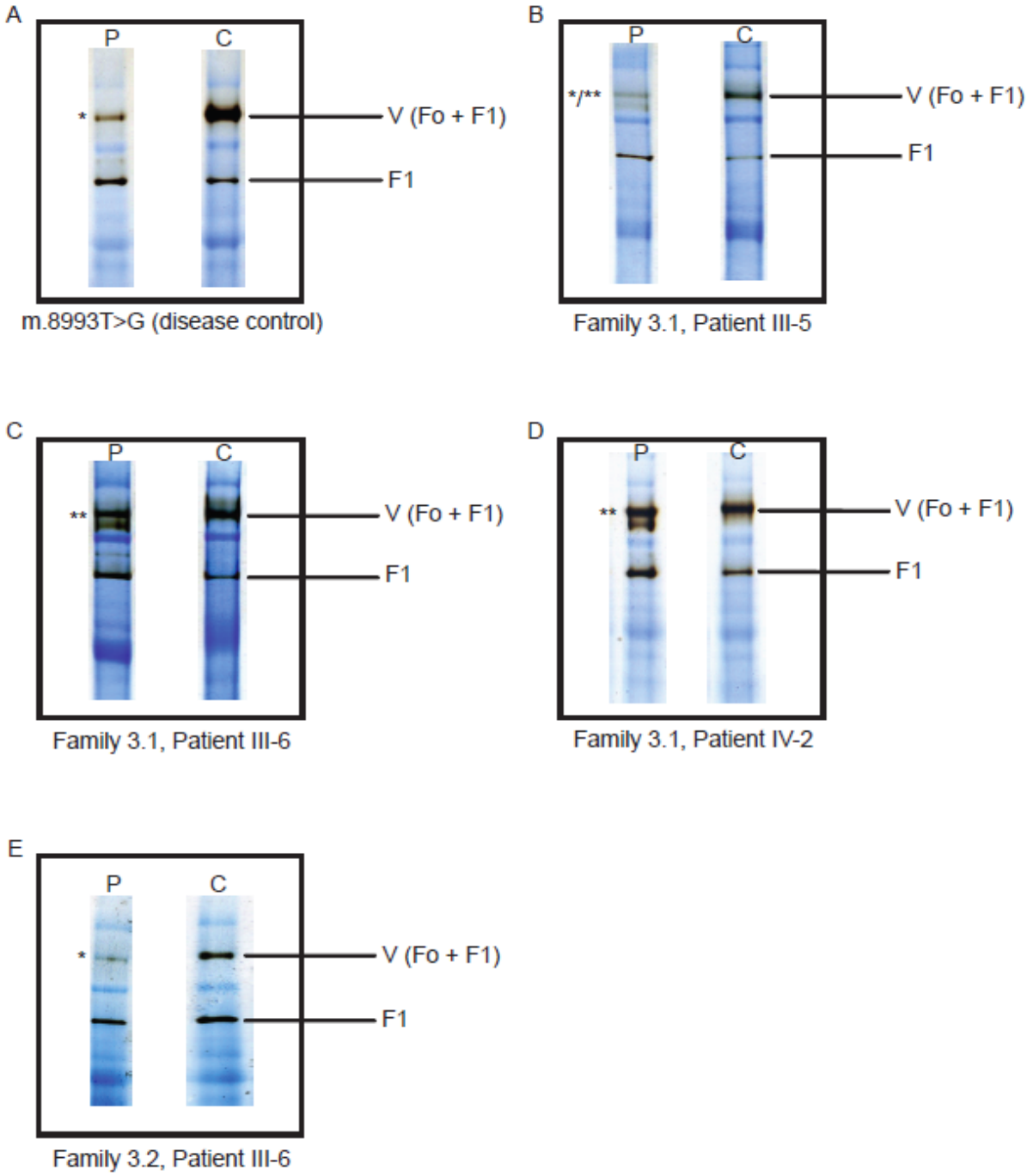

Figure 3.4: Blue-native polyacrylamide gel electrophoresis (BN-PAGE) using muscle tissue from patients with the m.9185T>C mutation compared with control muscle tissue. BN-PAGE was also performed in a patient with the m.8993T>G mutation as a positive control. Abbreviations: P = patient; C = control; V (F_o + F_1) = complex V holoenzyme; F_1 = F_1 catalytic site of complex V only; * indicates reduced complex V activity in patient compared to control muscle tissue (demonstrated by reduced band density); ** indicates impaired complex V assembly in patient compared to control

muscle tissue (demonstrated by multiple bands indicative of abnormal assembly intermediates); */** indicates both impaired complex V activity and assembly in patient compared to control muscle tissue (demonstrated by co-existence of reduced band density and multiple bands indicative of abnormal assembly intermediates). (A) Patient with the pathogenic mutation m.8993T>G (disease control). (B)-(D) Family 3.1, Patients III-5, III-6 and IV-2 respectively. (E) Family 3.2, Patient III-6.

3.5 Discussion

In this genetically undefined CMT2 cohort the disease-causing *MT-ATP6* m.9185T>C variant was identified in three unrelated probands, in addition to the index family in which the mutation was originally detected. Some affected family members were also classified as having dHMN. That 1.1% of this genetically undefined CMT2 cohort harboured the m.9185T>C mutation in *MT-ATP6* is important given that molecular defects are currently only detected in approximately 35% of patients with CMT2 and in 15% of patients with dHMN (Dierick et al., 2008; Reilly and Shy, 2009; Reilly et al., 2011; Saporta et al., 2011). Patient m.9185T>C mutant load correlated with disease severity within each pedigree.

Patients could be broadly divided into four clinical severity-related groups according to their m.9185T>C mutant load: (Group 1) unaffected individuals (<64% mutant load); (Group 2) asymptomatic individuals with UMN signs detectable on examination (64-79% mutant load); (Group 3) affected individuals with clinical symptoms and signs of UMN involvement without neuropathy (80-91% mutant load); (Group 4) affected individuals with symptoms and signs of motor-predominant CMT2 (92-100% mutant load).

BN-PAGE was used in muscle tissue to demonstrate the deleterious effects of the m.9185T>C; p.Leu220Pro mutation on complex V structure and function. The complex V assay measures the ATP synthase activity in the reverse direction. ATP is hydrolysed to produce ADP and P_i In the presence of P_i the lead ions used in the buffer (lead (II) nitrate) form a precipitate which correlates with the degree of ATP hydrolysis. This technique has not been used to assess complex V in patients with m.9185T>C previously. It has been shown that the m.8993T>G mutation associated with LS and NARP not only impairs assembly and stability of complex V, but also reduces intrinsic activity of the ATP synthase holoenzyme (Nijtmans et al., 2001). Impaired complex V assembly (Figure 3.4, Family 3.1, Patients III-6 and IV-2), reduced complex V activity (Figure 3.4, Family 3.2, Patient III-6) or both (Figure 3.4, Family 3.1, Patient III-5) was confirmed in patients who were homoplasmic for m.9185T>C. These data support the pathogenicity of m.9185T>C and indicate that this mutation impairs both complex V assembly and activity. In view of the previously

published data documenting impaired assembly and stability of complex V associated with the NARP m.8993T>G mutation (Nijtmans et al., 2001), the m.9185T>C mutation may also be expected to result in a poorly assembled and unstable complex V holoenzyme. The variation in both complex V activity and assembly observed on BN-PAGE for patients with identical m.9185T>C mutation loads may, therefore, be attributable to holoenzyme disassembly occurring during sample preparation. The muscle histology and histochemistry of patients with the m.9185T>C mutation were either normal or exhibited subtle non-specific mitochondrial abnormalities on EM as is frequently the case for mutations involving mtDNA protein encoding genes.

The findings reported here add to increasing evidence that mitochondrial dysfunction is an important cause of CMT2. Mutations in *MFN2*, a critical nuclear gene that regulates mitochondrial fusion, have been identified as the major cause of CMT2. Evidence is emerging that *MFN2* has a distinct role aside from mitochondrial fusion in mitochondrial axonal transport, and is an important component of the linker/adaptor complex between mitochondria and kinesin/microtubules (Misko et al., 2010). Disruption of this complex may explain the length-dependent nature of the neuropathy seen with *MFN2* mutations. More recently, a novel *MFN2* mutation causing optic atrophy, axonal neuropathy and mitochondrial myopathy was found to cause multiple mtDNA deletions in skeletal muscle. This finding was thought to result from mtDNA instability, caused by the variability of repair protein content across the mitochondrial population as a consequence of impaired mitochondrial fusion, and expands current knowledge of the pathogenic basis of *MFN2*-related neurological disease (Rouzier et al., 2012). It has also been shown that nerves expressing mutant forms of neurofilament (which causes CMT2E) can also alter mitochondrial dynamics, suggesting that dysfunctional axonal transport might precipitate axonal degeneration in a number of other CMT subtypes (Tradewell et al., 2009). These observations imply that impaired ATP dependant axonal transport is a candidate for axonal damage in other mitochondrial diseases.

MT-ATP6 should be considered in the molecular diagnostic evaluation of patients with CMT2, together with *MFN2*, *MPZ*, *RAB7*, *HSPB1*, *HSPB8*, *GDAP1*, *TRPV4*, *NEFL* and *GARS,* especially in pedigrees where there appears to be no paternal transmission (Reilly et al., 2011; Saporta et al., 2011). These findings have important clinical implications, particularly for genetic counselling. Diagnosis can be made in DNA extracted from blood, using restriction fragment length polymorphism genetic analysis, since m.9185T>C mutant load appears to be high in peripheral blood leucocytes in all affected cases reported to date. An invasive muscle biopsy is not required for diagnostic purposes, and histology is usually unhelpful. However, if muscle tissue is available BN-PAGE demonstrates both the structural and functional impairment caused by the effects of m.9185T>C; p.Leu220Pro on the ATP6 subunit.

The clinical and electrophysiological phenotype in these families was typical of CMT2/dHMN. However, the following features should be used to help prioritise *MT-ATP6* for mutation analysis in patients with neuropathy: (1) disease onset in the first or second decades; (2) variable clinical severity within a family with wheelchair dependence as early as 19 years; (3) an initial slowly progressive neuropathy, which may accelerate in the fifth and sixth decades from unaided walking to wheelchair dependence within a relatively short time frame; (4) an evolving clinical phenotype from a pure motor to a motor-predominant axonal neuropathy in the third and fourth decades; (5) early proximal lower limb muscle involvement despite mild distal weakness; (6) multi-system involvement in the patient or relatives; (7) UMN signs in affected or asymptomatic relatives; (8) rapid clinical decompensation in affected individuals following viral or septic illness.

CHAPTER 4

Novel *POLG* and *RRM2B*-related clinical phenotypes

CHAPTER 4

4. Novel *POLG* and *RRM2B*-related clinical phenotypes

4.1 Introduction

Mutations in nuclear genes encoding proteins involved in replication, maintenance and repair of mtDNA may cause sporadic, autosomal dominant and autosomal recessive mitochondrial disease associated with multiple large-scale deletions and/or depletion and/or point mutations in mtDNA (Cohen et al., 1993; Longley et al., 2005). To date, almost all known causative nuclear genes in this group fall into one of two categories: genes whose products function directly at the mtDNA replication fork, or genes encoding proteins important for supplying the mitochondria with deoxynucleotide triphosphate pools needed for DNA replication.

4.1.1 Polymerase gamma and mitochondrial DNA replication

DNA polymerase gamma is the only known DNA polymerase in animal mitochondria. It functions as a heterotrimer (Yakubovskaya et al., 2006) composed of one catalytic subunit polymerase gamma, encoded by *POLG*, and two accessory subunits, encoded by *POLG2* (Ropp and Copeland, 1996). The catalytic subunit contains 3 functional domains: a 3' to 5' proofreading exonuclease domain; a linker domain; and a highly conserved carboxyl-terminal polymerase domain (Luo and Kaguni, 2005). The accessory subunits confer high processivity on the protein complex by increasing binding affinity for DNA (Lim et al., 1999). Diseases caused by mutations in *POLG* are highly heterogeneous, and include: sporadic PEO; autosomal dominant or recessive PEO; cataracts; Alpers syndrome; mitochondrial neurogastrointestinal encephalomyopathy (MNGIE); premature menopause and ovarian failure; ataxia neuropathy spectrum (previously labelled as mitochondrial recessive ataxia syndrome, sensory ataxic neuropathy with dysarthria and ophthalmoplegia, and spinocerebellar ataxia epilepsy syndrome); and myoclonic epilepsy myopathy sensory ataxia syndromes (Cohen et al., 1993; Stumpf et al., 2013). More than 150 mutations have been reported in *POLG* (http://tools.niehs.nih.gov/polg/) since the first disease-causing mutations within the gene were identified in 2001 (Van Goethem et al., 2001a). The most common mutation in *POLG* is c.1399G>A, which

results in an alanine to threonine substitution at codon 467 (p.Ala467Thr) within the linker region of polymerase gamma, causes reduced DNA polymerase activity and inefficient interaction with the accessory subunit (Chan et al., 2005).

4.1.2 Ribonucleotide reductase and deoxyribonucleotide synthesis

There is increasing recognition that genetic disruption of the molecular processes that control the maintenance (replication and repair) of mtDNA, including those that regulate nucleotide pools, are an important cause of human mitochondrial disease. Approximately half of all adult mitochondrial disease results from genetic dysfunction of the nuclear-encoded mitochondrial genes. A significant number of these cases are due to disruption of genes involved in maintenance of mtDNA, leading to qualitative (accumulation of multiple mtDNA deletions) and/or quantitative (depletion of mtDNA copy number) downstream mitochondrial genomic effects. To date, almost all known nuclear maintenance genes fall into one of two categories: 1) genes whose protein products function directly at the mtDNA replication fork (Fratter et al., 2011; Longley et al., 2006; Spelbrink et al., 2001b); or 2) genes which encode proteins involved in supplying mitochondria with dNTP pools required for DNA replication (Bourdon et al., 2007a; Fratter et al., 2011; Kaukonen et al., 2000; Mandel et al., 2001; Nishino et al., 1999; Ostergaard et al., 2007; Saada et al., 2001). The most common presenting neurological feature seen in adults with mtDNA maintenance disorders is PEO and ptosis, although the clinical phenotype is not necessarily restricted to the extra-ocular muscles.

Ribonucleotide reductase M2B (TP53 inducible, *RRM2B*) encodes the p53-inducible small subunit of ribonucleotide reductase (RNR) known as p53R2. RNR is a heterotetrameric enzyme, comprised of two small (p53R2) and two large (R1) components, which catalyses the rate-limiting step in the *de novo* synthesis of dNTPs by direct reduction of ribonucleotide diphosphates to their corresponding deoxyribonucleotides. p53R2 is so-called because its transcription is tightly regulated by the tumour suppressor protein p53 (Nakano et al., 2000; Tanaka et al., 2000). It was initially suggested that p53R2 translocates to the nucleus during DNA damage-induced cellular arrest and was important for local DNA repair (Tanaka et al., 2000; Yamaguchi et al., 2001). However, the observation of constant low levels of both R1

and p53R2 in post-mitotic cells, and the clear correlations between depletion of mtDNA and functionally important mutations in the *RRM2B* have expanded the role of p53R2 beyond that of nDNA replication and repair to include an essential role in the supply of dNTPs for the synthesis of mtDNA. This process supplements the dNTPs produced by the mitochondrion's own deoxynucleotide salvage pathway.

Mutations in *RRM2B* are reported to cause severe mtDNA depletion in children with encephalomyopathy and lactic acidosis frequently associated with renal tubulopathy (Acham-Roschitz et al., 2009; Bornstein et al., 2008; Bourdon et al., 2007b; Kollberg et al., 2009). Patients with mtDNA depletion syndromes typically die in infancy or childhood (Rahman and Poulton, 2009). *RRM2B* mutations have also been shown to cause MNGIE with mtDNA depletion (Shaibani et al., 2009), and a heterozygous truncating mutation in *RRM2B* has been found to associate with adPEO with multiple mtDNA deletions (Tyynismaa et al., 2009). Depletion and deletions of mtDNA may result from unbalanced dNTP pools with subsequent misincorporation of nucleotides into mtDNA.

This chapter reports genetic investigations performed in a cohort of 50 adult patients with significant levels of multiple mtDNA deletions detectable in skeletal muscle tissue. Fourteen individuals were found to harbour *POLG* mutations, and a novel clinical phenotype exhibited by two of these patients was characterised. In addition, two patients with *RRM2B* mutations were identified, including one with Kearns-Sayre syndrome (KSS).

4.2 Patient cohort

Fifty unrelated adults with suspected mitochondrial disease and multiple mtDNA deletions detectable in skeletal muscle were identified using the UCLH NHNN NCG Neurogenetics diagnostic laboratory database. Multiple mtDNA deletions had previously been confirmed by the UCLH NHNN NCG Neurogenetics diagnostic laboratory using long-range PCR and/or Southern blot genetic analysis techniques. Sanger sequencing of *POLG* and targeted regions of *C10orf2* was initially performed by the Oxford NCG Neurogenetics diagnostic laboratory as mutations in both genes are known to be a common cause of multiple mtDNA deletion formation in adults. Fourteen of the 50 patients were found to harbour pathogenic mutations in *POLG*, whilst *C10orf2* mutations were detected in three patients.

Two unrelated patients (Patient 4.1 and Patient 4.2) with upper limb predominant distal myopathy caused by novel heterozygous missense mutations in *POLG* are reported here. One patient had marked cachexia. These findings expand the clinical phenotype associated with *POLG*-related adult mitochondrial disease with multiple mtDNA deletions, and indicate that *POLG* mutation analysis should be considered in cases of distal myopathy.

RRM2B was subsequently sequenced in the remaining 33 patients in whom the underlying nuclear gene defect had not been identified to determine the prevalence of *RRM2B* mutations in this adult population. Two patients (Patient 4.3 and Patient 4.4) were found to harbour pathogenic *RRM2B* mutations and are discussed in detail below.

4.3 Case histories

4.3.1 Patient 4.1

A 26 year old white European man was referred to the neurology clinic with longstanding progressive distal upper limb muscle wasting and weakness. Symptom onset was in early adolescence. Past medical history included rapid development of bilateral cataracts requiring removal aged 3 years. There was no family history of neuromuscular disease. At initial assessment he was ambulant but exhibited marked upper limb distal muscle wasting and weakness (Figure 4.1A).

Laboratory evaluation revealed raised serum creatine kinase of 373 to >1000 IU/L (reference range 38-204 IU/L). Thyroid function and plasma lactate levels were normal. Median, ulnar, sural and superficial peroneal sensory NCS and ulnar, common peroneal and posterior tibial motor NCS were normal with no electrophysiological evidence for a large fibre peripheral neuropathy. However, EMG revealed myopathic changes in all muscles sampled (deltoid, first dorsal interosseous, vastus medialis and tibialis anterior). Brain MRI was unremarkable. MRI of the thighs, calves, and forearms demonstrated severe fatty atrophy of both upper and lower limb musculature (Figure 4.2A-C). There was a distinct proximal-distal gradient with forearms and calves being more severely affected than the thighs. This pattern of distal predominant fatty infiltration was also apparent within partially affected muscles, such as tibialis posterior and vastus medialis. Striking selectivity existed between muscles, with some being severely affected whilst others, such as adductor magnus, showed normal signal intensity and even compensatory hypertrophy. A left quadriceps muscle biopsy of vastus lateralis aged 41 years revealed 3.7% ragged red fibres (RRF) on Gomori trichrome and SDH stains and 4.2% COX negative fibres (Figure 4.1C-F). Ultrastructural examination showed collections of abnormal mitochondria with ring forms and others containing type I paracrystalline inclusions (Figure 4.1G, H). Activity of respiratory chain complexes I, II+III and IV, expressed as a ratio to citrate synthase activity to correct for mitochondrial enrichment, were normal.

Most recent examination aged 49 years showed a high stepping gait and hyperlordosis resulting from anterior leg and axial muscle weakness (Figure 4.1B), bilateral aphakia and ptosis, PEO, and dysphonia. Formal manual muscle strength testing was MRC graded bilaterally as follows: shoulder abduction/adduction 5/5; elbow and wrist flexion/extension 2/5; finger flexion 2/5; finger extension 0/5; intrinsic hand muscles 2/5; hip and knee flexion/extension 5/5; ankle dorsiflexion/inversion/eversion 0/5; and ankle plantarflexion 3/4. Reflexes were normal and plantar responses down-going. Sensory examination was normal. The patient was markedly cachexic and had a static Body Mass Index (BMI) of 16.3 (normal male range 20-25). A formalised 3-day diet diary undertaken by a dietetic consultant confirmed adequate oral caloric intake (96.6% of predicted reference nutrient intake, CompEat© Nutrition Systems). Blood and urinary deoxyuridine and thymidine levels were undetectable and thymidine phosphorylase activity in white cells and platelets was normal, thereby excluding MNGIE.

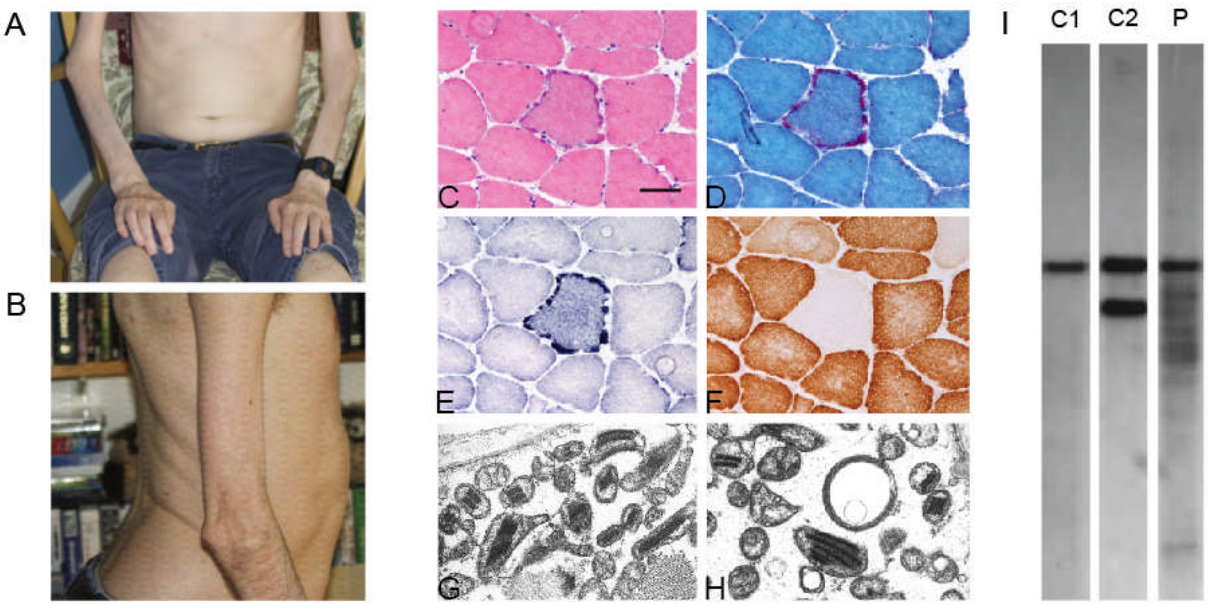

Figure 4.1: Clinical, muscle histological and Southern blot findings for Patient 4.1. Upper limb muscle wasting (A) and hyperlordosis secondary to axial muscle weakness (B). Ragged red fibres visualised in haematoxylin and eosin (C), Gomori trichrome (D) and succinate dehydrogenase (E) preparations. Histochemical staining for cytochrome *c* oxidase revealed significant numbers of fibres with deficient enzyme activity (F). Ultrastructural examination confirmed structurally abnormal mitochondria with type I paracrystalline inclusions (G) and ring forms (H). Bar in A represents 50μm in C – F and 500nm in G & H. Southern blot analysis of mitochondrial DNA (mtDNA) extracted from muscle tissue using PvuII restriction endonuclease showing normal control subject in lane 1 (C1); patient with single deletion of mtDNA in lane 2 (C2); and Patient 4.1 with multiple deletions of mtDNA in lane 3 (P) (I).

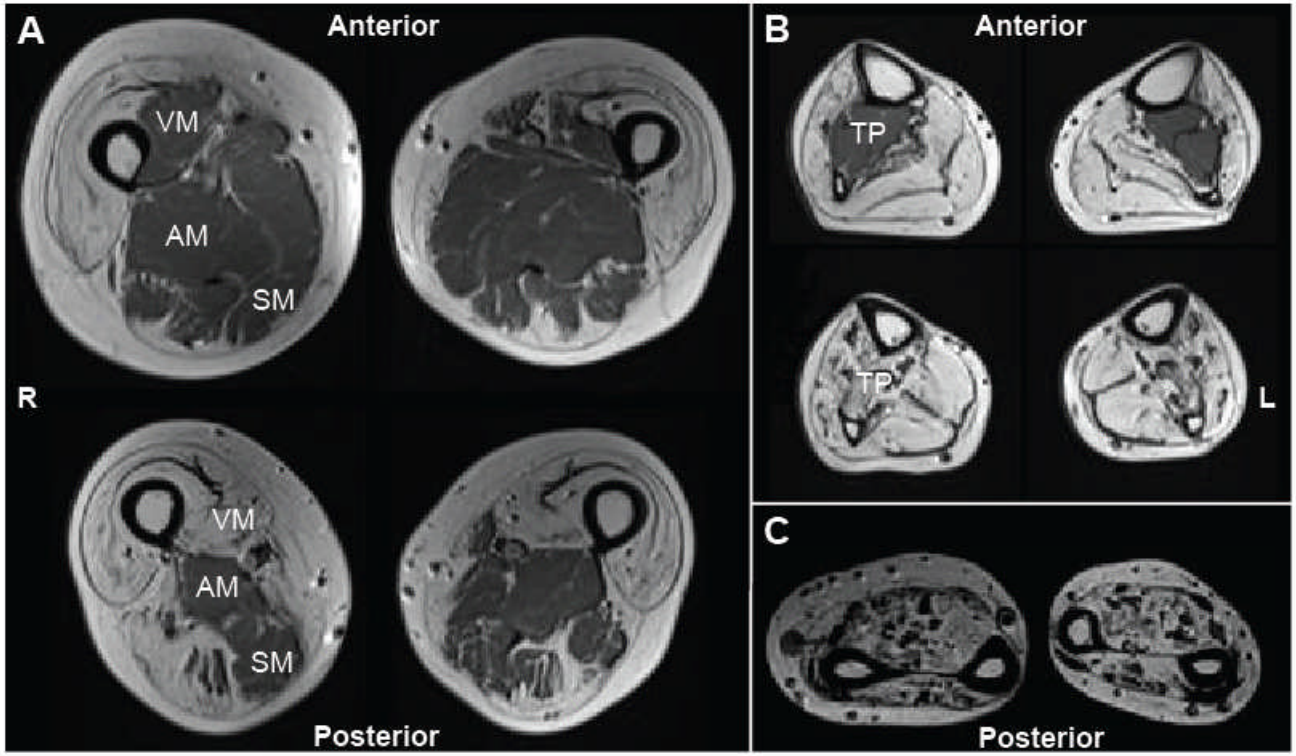

Figure 4.2: Axial T1 weighted MRI of thighs, calves and forearms of Patient 4.1. Proximal (top) and distal (bottom) thigh (A): severe fat infiltration and atrophy is seen in most muscles including quadriceps, gracilis and biceps femoris, with sparing of adductor magnus (AM) and semimembranosus (SM). A proximal-distal gradient is noted in muscles which are incompletely affected such as vastus medialis (VM). Proximal (top) and distal (bottom) calf (B): severe fatty atrophy of all muscles except tibialis posterior (TP) proximally. Mid-forearm (C): severe fatty atrophy of all muscles. R = right; L = left.

4.3.2 Patient 4.2

A 54 year old man of European descent presented to the adult neurology clinic with worsening dysarthria and dysphagia. He had developed progressive distal upper and, to a lesser extent, lower limb weakness in his early thirties and required bilateral frontalis slings for ptosis aged 43 years. Past medical history included surgical removal of bilateral cataracts during childhood. Skeletal muscle biopsy of vastus lateralis aged 40 years was compatible with a mitochondrial disorder; however, residual muscle tissue was unavailable for further molecular genetic testing. There was no reported family history of neuromuscular disease, but his daughter had congenital cataracts.

At initial assessment BMI was normal. Gait was high stepping due to bilateral foot drop. Cranial nerve examination revealed bilateral aphakia, ptosis, PEO, facial weakness, and neck flexor/extensor weakness (MRC grade 4/5). There was marked, predominantly upper limb, distal muscle wasting. MRC grading of muscle power was symmetrical and as follows: shoulder abduction/adduction 4/5; elbow flexion 2/5; elbow extension 4/5; wrist flexion/extension 0/5; finger flexion/extension 1/5; intrinsic hand muscles 0/5; hip flexion/extension 4/5; knee flexion 2/5; knee extension 4/5; ankle dorsiflexion/inversion/eversion 2/5; and ankle plantar flexion 5/4. Reflexes were all present and plantar responses flexor. Sensory examination was normal.

Laboratory tests, sensory NCS (median, ulnar, sural and superficial peroneal nerves tested), and motor NCS (median, ulnar and posterior tibial nerves tested) were normal. EMG confirmed evidence of a myopathy proximally (sternocleidomastoid, trapezius, deltoid and triceps) and distally (first dorsal interosseous) in the upper limbs. Lower limbs were affected to a lesser extent with some myopathic units evident proximally (iliopsoas and rectus femoris). Brain MRI was normal.

4.3.3 Patient 4.3

Patient 4.3 was born following normal pregnancy by assisted breech delivery to non-consanguineous parents of European descent. There were no neonatal problems and development was normal up to the age of four years when she developed bilateral SNHL. Over the next two years she developed PEO, proximal muscle weakness and poor weight gain, associated with malaise and tiredness. During adolescence the fatigue prevented her from keeping up with peers during exercise. She had short stature and delayed puberty. Parents are now in their late sixties and do not have PEO or clinical symptoms suggestive of mitochondrial disease, and there is no other relevant family history.

On examination aged 14 Patient 4.3 was found to have pigmentary retinopathy, sensorineural deafness, PEO and proximal fatiguable myopathy MRC grade 4/5. Serum CK was 281 IU/L. Blood lactate was normal (1.1 mmol/L) but CSF lactate was mildly elevated at 2.6 mmol/L and CSF protein was raised at 1.60 g/L. The combination of PEO and pigmentary retinopathy with onset before 20 years of age, in association with raised CSF protein and sensorineural deafness led to a clinical diagnosis of KSS.

Electrocardiogram did not reveal any conduction abnormalities. Echocardiogram (ECHO) showed increased thickness of the interventricular septum and left posterior ventricular wall with normal left ventricular function. She was found to have a right hydronephrosis but there was no suggestion of renal tubulopathy (tubular reabsorption of phosphate was normal at 98% at 15 years). Cranial MRI demonstrated abnormal high signal in the deep cerebral white matter, posterior limbs of the internal capsules and the region of the anterior commissure and diffuse changes in the lower half of the midbrain dorsally.

Continued enlargement of the kidney necessitated nephrectomy two years later. During the procedure a biopsy of the rectus abdominus was taken which showed fibre size variation and frequent necrotic fibres (Figure 4.3A). Numerous fibres showed enhanced SDH activity (Figure 4.3B) some of which showed classical morphology of RRF (7.8% of fibres) (Figure 4.3C-E). Most RRF and fibres with

enhanced SDH activity stained negatively for COX (10.3% of fibres) (Figure 4.3F). EM demonstrated mitochondrial aggregates, many with abnormal morphology including type I paracrystalline inclusions (Figure 4.3G). There were continuing problems with appetite and nutrition, and despite nutritional supplements body mass index aged 16 was 12.9 (weight 33.7 kg, height 161.5 cm). Patient 4.3 died aged 22 years following an episode of severe pneumonia.

4.3.4 Patient 4.4

Patient 4.4 presented aged 58 years with a 3-year history of diplopia on a background of longstanding fatigue, having been born to non-consanguineous parents of European descent. Birth history and early development were normal and there was no history of neurological or neuromuscular disease in her parents, two siblings or other relatives. Cranial nerve examination revealed mild bilateral ptosis, restricted extra-ocular movements and slowing of saccades with no evidence of retinopathy. Other than slight wasting of biceps there were no abnormal findings on motor and sensory assessment of limbs.

Investigation showed normal CK. MRI brain revealed areas of T2 high signal bilaterally in the pons and some further small foci in both frontal lobes in the anterior limb of the left internal capsule thought to be vascular in nature. NCS and EMG were normal. Muscle histology aged 58 years showed five RRF (0.6% of fibres) and frequent COX-deficient fibres (4.1% of fibres), compatible with a mitochondrial myopathy (Figure 4.3H). Similar to Patient 4.3, fibre necrosis was also observed with two necrotic fibres in the small biopsy available, a feature not usually reported in mitochondrial disease (Figure 4.3H, inset) (Shoffner and Shoubridge, 2001). She died aged 66 years of urinary sepsis.

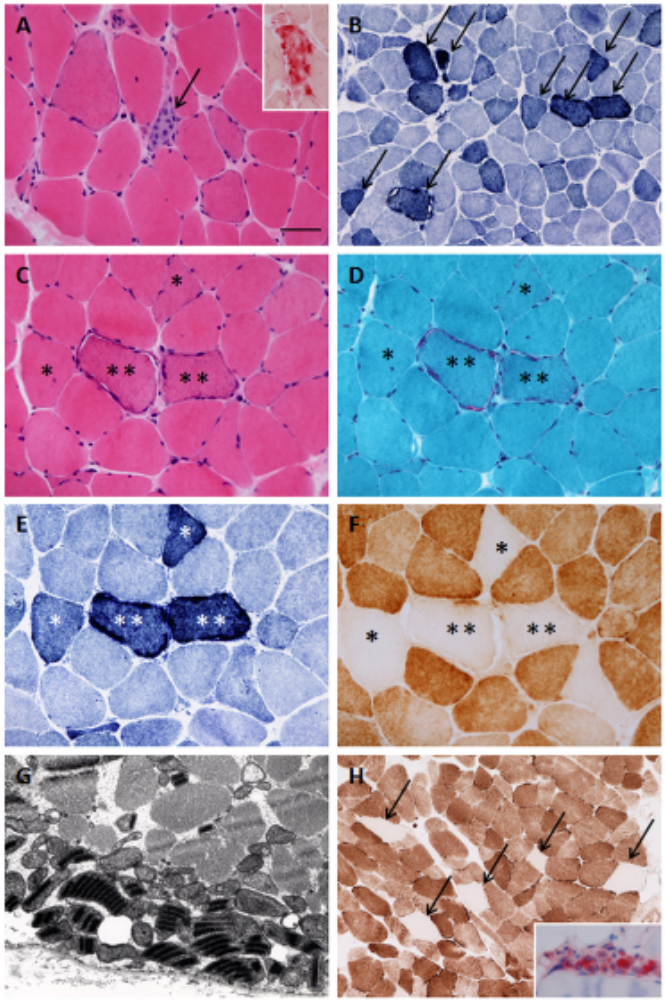

Figure 4.3: Muscle histopathology from Patient 4.3. The muscle biopsy showed increased variation in fibre diameter and fibre necrosis (A, arrow) confirmed by acid phosphatase histochemistry (A, inset). Frequent fibres showed increased succinate dehydrogenase (SDH) activity (B, arrows). Ragged red fibres were readily apparent (C & D, **) and these displayed an increase in SDH activity (E, **) with cytochrome *c* oxidase (COX) deficiency (F, **). Many of the fibres with a normal appearance in the haematoxylin and eosin (C, *) and Gomori trichrome (D, *) preparations showed enhanced SDH activity (E, *) and COX deficiency (F, *). Ultrastructural examination revealed abnormal mitochondria containing type I paracrystalline inclusions (G). Examination of the muscle biopsy from Patient 4.4 also showed increased numbers of COX deficient fibres (H, arrows) and a small number of necrotic fibres (H, inset). Bar in A represents 50μm in A, C-F and insets in A & H; 100 μm in B & H; 800 nm in G. A & C haematoxylin and eosin, B & E succinic dehydrogenase, D Gomori trichrome, F & H cytochrome oxidase, insets in A & H acid phosphatase.

4.4 Methods

4.4.1 Long-range polymerase chain reaction and Southern blot analysis of mitochondrial DNA

Multiple mtDNA deletions had previously been confirmed using long-range PCR and/or Southern blot genetic analysis techniques in all 50 patients by the UCLH NHNN NCG Neurogenetics diagnostic laboratory.

4.4.2 Automated Sanger sequencing of *POLG* and *RRM2B*

Sanger sequencing of the coding region and exon-intron boundaries of *POLG* and targeted regions of *C10orf2* to include nucleotides c.690-1592 (3' end of exon 1, exons 2 and 3) was performed by the Oxford NCG Neurogenetics diagnostic laboratory.

The nine exons and flanking intronic regions of *RRM2B* were amplified from total gDNA using specific primers (Table 4.1). PCR cycling conditions were: initial denaturation at 95°C for 10 min, followed by 30 cycles of 95°C for 30 sec, 58°C for 30 sec, and 72°C for 30 sec, and a final extension at 72°C for 7 min.

Table 4.1: Oligonucleotides used for *RRM2B* PCR amplification and sequence analysis

	Forward primers (5' to 3')	**Reverse primers (5' to 3')**
Exon 1	GGAGAAACCCTTAGGCCGC	CGCGGCGAATAACATTTCCTA
Exon 2	CAGGCTCTCAAACCAATGCC	GTAAAACAAGAAGGAACACTGC
Exon 3	GTGCTAACATCTTTCTTTTTCCA	AGACATCTTGTCTTTGGCTGAA
Exon 4	CCATAAGGTCTTTCTGACCTGTTT	TGCTCAGAAACTTCCATACTTGA
Exon 5	CTAGCTACTCGGGAGGCTGA	TTTGTACTCCTTTTCCATGCTG
Exon 6	TTTGGCCATGGCACTAACTT	AGCAAGCCATGATCGTGCC
Exon 7	ACCCCTCTTCCATTTTCCAG	TTGGTATTGTCAGGCTGACC
Exon 8	GGACATCATTTGCCACATTG	TTACCAGCCTCCTACTTCAGTT
Exon 9	CCTGACCTCTGTTTTGGTCA	GGTTTTGGATTTCCTTTTGAGC

4.4.3 Multiplex ligation-dependent probe analysis of *POLG* and *RRM2B*

Multiplex ligation-dependent probe analysis (MLPA) was used to exclude trans-acting large-scale genomic rearrangements when a monoallelic mutation alone was detected using automated Sanger sequencing. *POLG* MLPA was performed for Patient 4.1 and Patient 4.2 by the Oxford NCG Neurogenetics diagnostic laboratory.
The SALSA MLPA kit P089-A1 TK2 (MRC-Holland) was used in Patient 4.4 to exclude a large-scale genomic rearrangement in *RRM2B*. DNA was mixed with TE (10 mM Tris, 1 mM EDTA, pH 8) and denatured by heating to 98°C for 5 minutes, followed by incubation at 25°C for 1 min. The P089-A1 probe mix was added to the DNA and heated to 95°C for 1 min followed by incubation at 60°C for 16 h for hybridisation. Annealed probes were then ligated by adding Ligase-65 at 54°C for 15 min. Ligation products were amplified by PCR (35 cycles of 95°C for 30 sec, 60°C for 30 sec and 72°C for 1 min) with SALSA PCR primers (labelled with Cy4.0). The resulting PCR fragments were separated by capillary electrophoresis on an ABI 3730XL using 'GeneMapper Generic' protocol. Data were analysed using GeneMarker analysis software. Relative copy number was obtained after normalisation of peaks against controls with values between 0.75 and 1.25 considered to be within the normal range.

4.4.4 Quantitative real-time polymerase chain reaction

Assessment of mtDNA copy number in muscle tissue was performed using a quantitative real-time PCR assay using an ABI Step One real-time PCR system and power SYBR green PCR master mix (ABI, part no. 4367659). The following primers (Bai and Wong, 2005) were used: mtDNA D-loop (forward 5'-CATCTGGTTCCTACTTCAGGG, reverse 5'-TGAGTGGTTAATAGGGTGATAGA); single copy nuclear gene β2-Microglobulin (forward 5'-TGCTGTCTCCATGTTTGATGTATCT, reverse 5'-TCTCTGCTCCCCACCTCTAAGT).

Pipetting for amplification in one well (20 μl total volume) was as follows: 10 μl of master mix (2x); 7.4 μl of ddH_2O; 0.3 μl of 20 μM forward primer (either for mtDNA or

nDNA); 0.3 μl of 20 μM reverse primer (either for mtDNA or nDNA); and 2 μl of 4 ng/μl DNA.

Each DNA sample was analysed in quadruplicate. Eleven DNA samples from control subjects were included to reveal the normal range. DNA samples from age-matched rho^0 cells (cells whose mitochondria are depleted of mtDNA by prolonged incubation with ethidium bromide, a chemical which inhibits mtDNA replication) and a known mtDNA depletion patient were used as negative and patient control, respectively. PCR cycling was as follows: 1) enzyme activation step: 10 min, 95°C; 2) denaturing step: 15 sec, 95°C; 3) annealing and elongation step: 60 sec, 60°C; 4) repeat denaturing and annealing/elongation steps 45 times.

In addition to the DNA samples, a 10-fold serial dilution of the mtDNA amplicon (35 to 351809732 molecules) and the nDNA amplicon (26 to 257812896 molecules) were included in each experiment. The serial dilution was prepared from a very precisely known concentration of DNA (NanoDrop) so that the number of molecules per 2 μl could be calculated accurately. The 10-fold dilution series for both amplicons was 10^{-12} to 10^{-18} g per 2 μl.

The mtDNA amplicon is 104 bp and an average bp is 660 Da. Therefore, 1 mol = 68640 g = 6.022×10^{23} molecules (Avogadro's number). Thus, 20 ng amplicon DNA per μl = ($20x10^{-9}$ g/μl ÷ 68640 g) × $6.022 \cdot 10^{23}$ molecules = 1.755×10^{11} molecules per μl. The nDNA amplicon is 86 bp and an average base pair is 660 Da. Therefore, 1 mol = 56760 g = 6.022×10^{23} molecules.

The C_t values of the mtDNA and nDNA amplicon dilution series were used to construct standard curves (number of amplicons versus C_t value). The equations of the standard curves were used to calculate the number of amplicons in the DNA samples. The C_t values of the serial dilutions (Y-axis) were plotted against the number of original amplicons (X-axis) in Microsoft Excel. The logarithmic trend line and the equation and R^2 value of the trend line were displayed. The experiment was rejected when the R^2 of a standard curve was <0.98. The equations of the trend lines ($y = -a \ln(x) + b \Leftrightarrow x = e^{(y - b)/-a}$) and the C_t values of the DNA samples (y) were used

to calculate the number of mtDNA and nDNA molecules in 2 μl of DNA sample (x). The following equation was used to calculate the number of mtDNA molecules per diploid nuclear genome (i.e. per single cell) in the DNA samples:

(Number of mtDNA amplicons) / [(Number of nDNA amplicons) / 2]

4.4.5 Protein analysis

Western blot analysis was performed on 10 μg of muscle protein extracted from total cell lysate from Patients 4.3 and 4.4. The p53R2 and GAPDH proteins were detected using specific anti-p53R2 rabbit polyclonal (1:1,000, cat. no. ab8105) and anti-GAPDH mouse monoclonal (1:60,000) antibodies (Abcam) and visualised using secondary mouse anti-rabbit and goat anti-mouse antibodies conjugated to horseradish peroxidase (Dako).

Assembled heterotetrameric R1/p53R2 RNR protein complexes were detected using BN-PAGE, performed as previously described for respiratory chain complexes (see section 2.4.6), modified to examine total cell extracts (Williams et al., 2004c). Samples were obtained from the muscle biopsies of Patient 4.3 and two controls. No further muscle tissue was available from Patient 4.4 for BN-PAGE studies. Skeletal muscle tissue was pulverized in liquid nitrogen. After thawing, the powder was immediately mixed with 0.75 M 6-aminocaproic acid, 37.5 mM bistris (pH 7.0), 2.5% (w/v) n-dodecyl-beta-D-maltoside and protease inhibitors, followed by centrifugation at 16,000 g, 4°C for 20 min. The supernatant was transferred to a new tube and mixed with 0.1 volume of 1 M 6-aminocaproic acid and 5% (w/v) Serva blue G. The samples (15-20 μl) were then loaded, resolved on 4-12% polyacrylamide gels, electrotransferred to Hybond-P membrane (GE healthcare) and probed with specific polyclonal antibodies to p53R2 (1:1,000, Abcam, cat. no. ab8105). The secondary antibody was mouse anti-rabbit conjugated to horseradish peroxidise (Dako). A loading control was performed in parallel using SDHA, a major subunit of the nuclear-encoded Krebs cycle enzyme succinate dehydrogenase (SDH; also known as complex II).

4.4.6 Protein function prediction

The three mutations observed in these two patients were modelled by Dr Michael Sadowski, MRC National Institute for Medical Research (NIMR), using the published p53R2 crystal structure (pdb code 3hf1) (Smith et al., 2009), monomers A and B for the mono- and di-iron bound forms, respectively. Residues 1-29 and 318-351 were not observed in the crystal structure and these regions were therefore omitted from the model. Models were built using the automodel routine of the MODELLER software package (version 9v3) (DeLano, 2002) with no additional refinement.

4.5 Results

4.5.1 Long-range polymerase chain reaction and Southern blot analysis of mitochondrial DNA

Patient 4.1 (Figure 4.1I) and Patient 4.3 (Figure 4.4A, B) had multiple mtDNA deletions detectable in skeletal muscle tissue using both long-range PCR and Southern blot analysis techniques. Multiple deletions of mtDNA were detectable only by long range PCR in Patient 4.4 (Figure 4.4A and B).

4.5.2 Automated Sanger sequencing of *POLG* and *RRM2B*

Genetic analysis of *POLG* in Patient 4.1 revealed a novel heterozygous missense mutation c.2687T>G; p.Leu896Arg (Figure 4.5A) within the polymerase domain of the protein (Figure 4.5C). The mutation was absent in both parents, who are healthy; thus inheritance was considered *de novo* dominant. Since the clinical phenotype of Patient 4.2 strikingly resembled that of Patient 4.1, genetic sequence analysis of *POLG* in gDNA extracted from blood was performed without repeating the muscle biopsy to confirm whether multiple mtDNA deletions were present. This revealed a novel heterozygous missense mutation c.2851T>C; p.Tyr951His (Figure 4.5B) within the same functional polymerase domain of the polymerase gamma protein (Figure 4.5C).

Sanger sequencing of *RRM2B* revealed deleterious mutations in *RRM2B* in two of the 33 patients, whilst the remaining 31 patients were not shown to have pathogenic *RRM2B* variations. Patient 4.3 had two novel heterozygous missense mutations in

RRM2B: c.122G>A; p.Arg41Gln in exon 2 (Figure 4.6A) and c.391G>A; p.Glu131Lys in exon 4 (Figure 4.6B). The c.122G>A; p.Arg41Gln change in exon 2 segregated to the paternal allele (Figure 4.6C), and the c.391G>A; p.Glu131Lys in exon 4 to the maternal allele (Figure 4.6D). The c.122G>A; p.Arg41Gln change was not present in 332 ethnically matched control chromosomes and c.391G>A; p.Glu131Lys was not present in 308 ethnically matched control chromosomes.

Patient 4.4 had a heterozygous three base pair deletion in exon 3: c.253_255delGAG; p.Glu85del (Figure 4.6E). No DNA samples from other family members were available for study. The c.253_255delGAG; p.Glu85del mutation has previously been reported in compound heterozygous state with the missense mutation c.707G>T; p.Cys236Phe and also as a homozygous mutation (R. Van Coster et al., July 2010, Acta Myologica, abstract) in neonates with a very severe mtDNA depletion. This mutation has previously been shown to be absent from over 220 ethnically matched control chromosomes. These amino acid residues occur in highly conserved regions across species (Figure 4.7A-C).

4.5.3 Multiplex ligation-dependent probe analysis of *POLG* and *RRM2B*

Patient 4.1 and 4.2 were reported to have normal *POLG* MLPA by the Oxford NCG Neurogenetics diagnostic laboratory. Patient 4.4 had normal copy numbers for all 8 *RRM2B* MLPA probes at the default threshold level (0.75-1.25), excluding a large-scale rearrangement of this gene on the other allele in this patient.

4.5.4 Quantitative real-time polymerase chain reaction

Patients 4.3 and 4.4 had a normal mtDNA copy number compared to age-matched controls, measured by quantitative real-time PCR (Figure 4.4C).

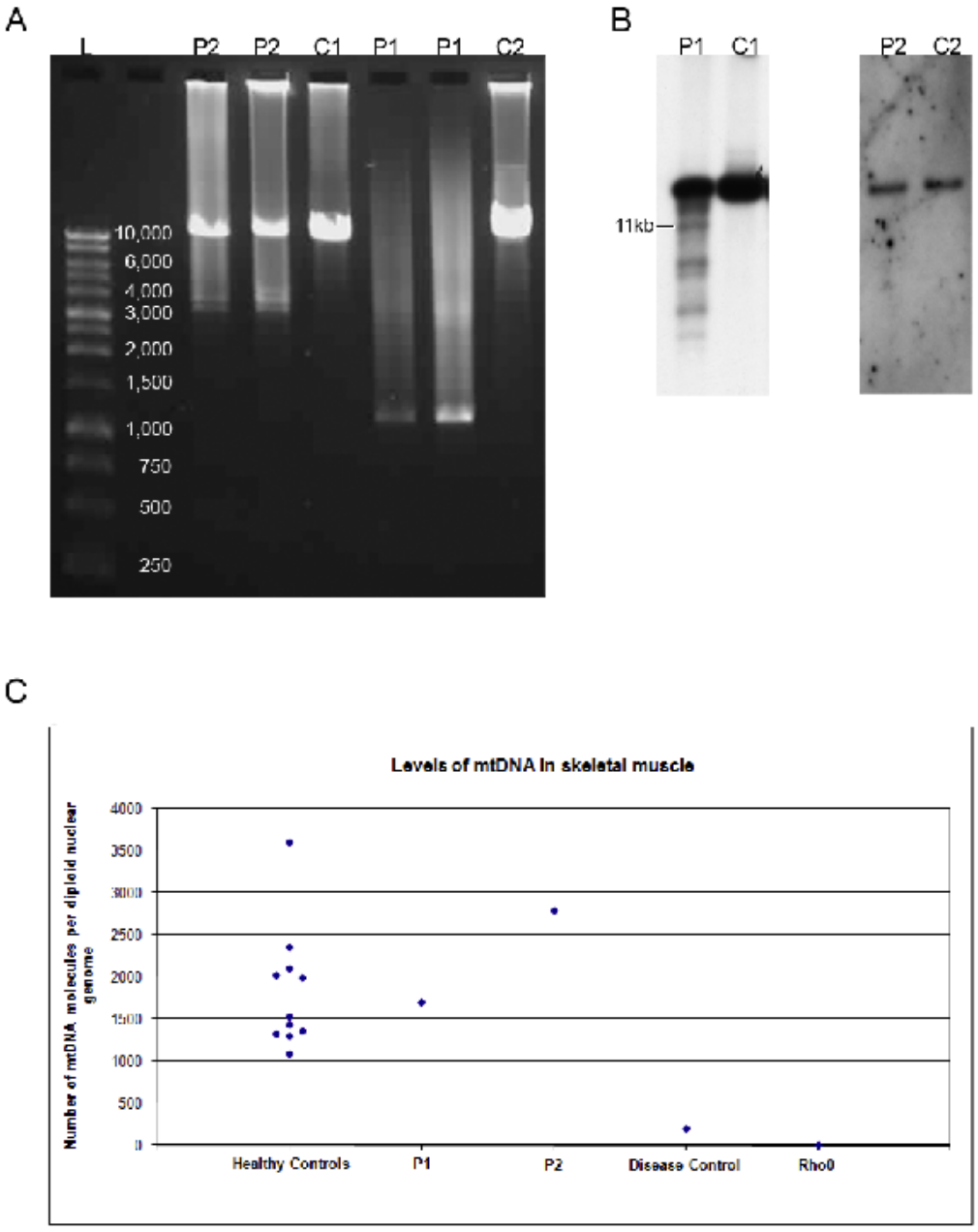

Figure 4.4: Long-range PCR, Southern blot and real-time PCR data for Patient 4.3 and 4.4. Long range PCR analysis showed multiple mtDNA deletions in muscle samples of Patients 4.3 and 4.4 (P1 and P2 respectively) compared with ladder (L) and normal control subjects (C1 and C2) (A). Southern blot analysis using PvuII restriction endonuclease shows multiple mtDNA deletions (with common 5kb mtDNA deletion annotated) in muscle sample of Patient 4.3 (P1) compared with control (C1) and only wild-type mtDNA band in muscle sample of Patient 4.4 (P2) compared with control (C2) (B). MtDNA copy number is normal in muscle samples of Patient 4.3 and Patient 4.4 compared to age-matched healthy controls, disease controls, and cells depleted of mtDNA (Rho^0) measured by quantitative real-time PCR (C).

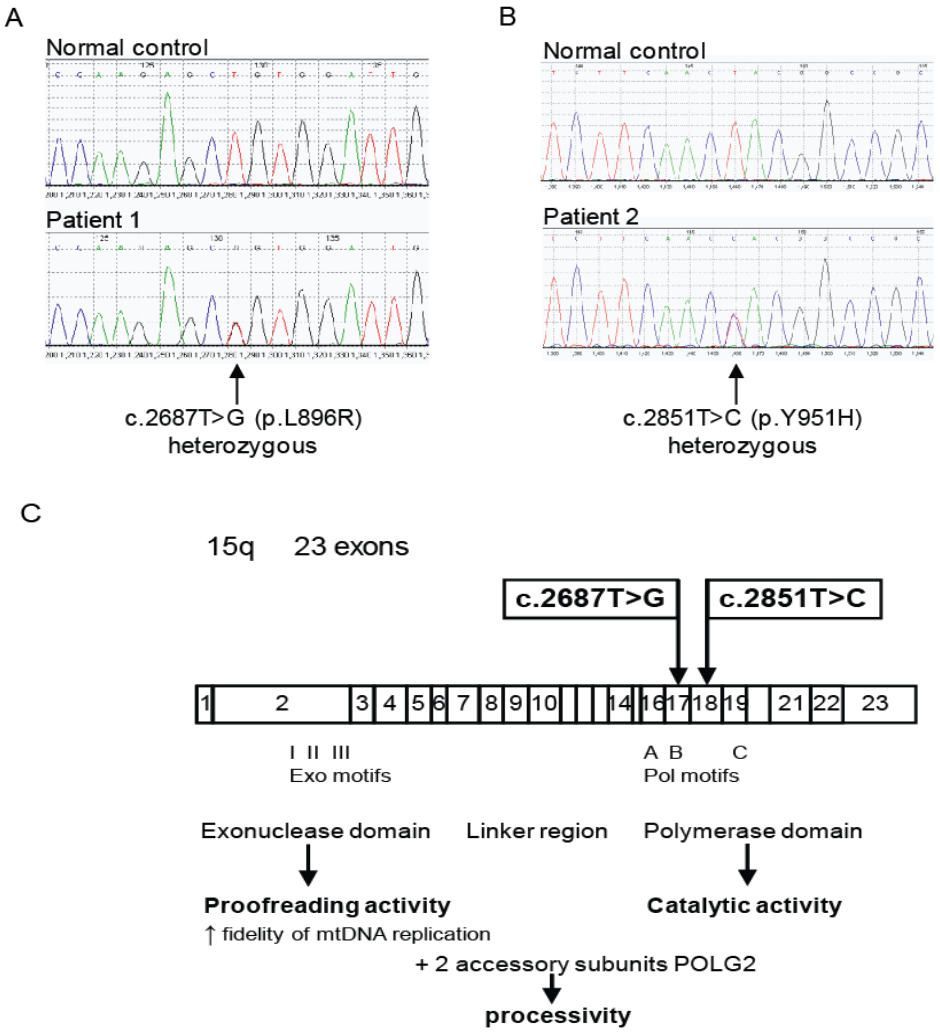

Figure 4.5: *POLG* sequencing data for Patient 4.1 (A) and Patient 4.2 (B) compared with control. Diagramatic representation of *POLG* transcript demonstrating novel heterozygous mutations c.2687T>G and c.2851T>C (C). Amino acid alignment of the human polymerase gamma catalytic subunit reference sequence versus sequences of various species with Leu896Arg and Tyr951His substitutions highlighted (D).

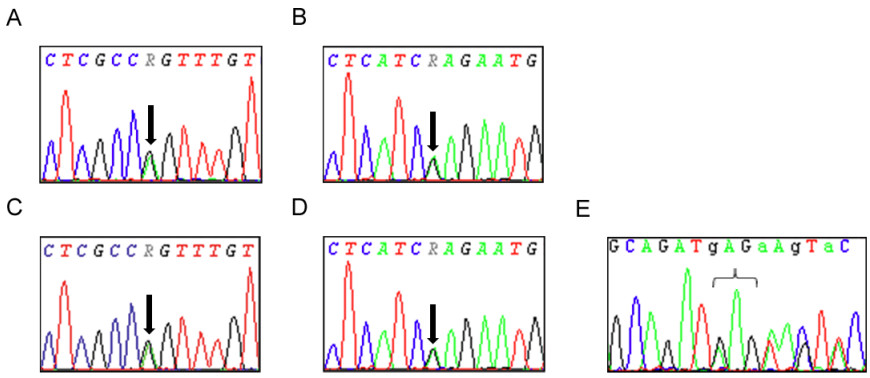

Figure 4.6: *RRM2B* sequencing data for Patient 4.3 showing: c.122G>A; p.Arg41Gln in exon 2 (A) segregating to the paternal allele (C), and c.391G>A; p.Glu131Lys in exon 4 (B) segregating to the maternal allele (D). *RRM2B* sequencing data for Patient 4.3 showing: c.253_255delGAG; p.Glu85del in exon 3 (E).

p53R2	33	34	35	36	37	38	39	40	**41**	42	43	44	45	46	47	48	49
Patient 4.3									**Q**								
Human	P	L	L	R	K	S	S	R	**R**	F	V	I	F	P	I	Q	Y
Chimp	P	L	L	R	K	S	S	R	**R**	F	V	I	F	P	I	Q	Y
Macaque	P	L	L	R	K	S	S	R	**R**	F	V	I	F	P	I	Q	Y
Mouse	P	L	L	R	K	S	S	R	**R**	F	V	I	F	P	I	Q	Y
Dog	P	L	L	R	K	S	S	R	**R**	F	V	I	F	P	I	Q	Y
Chicken	P	L	L	R	K	N	P	R	**R**	F	V	I	F	P	I	Q	H
Frog	P	F	L	R	K	N	P	Q	**R**	F	V	I	F	P	I	H	Y
Tetraodon	P	L	L	Q	E	N	P	R	**R**	F	V	I	F	P	I	Q	Y
C. Elegans	P	M	L	Q	D	L	D	N	**R**	F	V	I	F	P	I	K	H

p53R2	123	124	125	126	127	128	129	130	**131**	132	133	134	135	136	137	138	139
Patient 4.3									**K**								
Human	F	Y	G	F	Q	I	L	I	**E**	N	V	H	S	E	M	Y	S
Chimp	F	Y	G	F	Q	I	L	I	**E**	N	V	H	S	E	M	Y	S
Macaque	F	Y	G	F	Q	I	L	I	**E**	N	V	H	S	E	M	Y	S
Mouse	F	Y	G	F	Q	I	L	I	**E**	N	V	H	S	E	M	Y	S
Dog	F	Y	G	F	Q	I	L	I	**E**	N	V	H	S	E	M	Y	S
Chicken	F	Y	G	F	Q	I	L	I	**E**	N	V	H	S	E	M	Y	S
Frog	F	Y	G	F	Q	I	L	I	**E**	N	V	H	S	E	M	Y	S
Tetraodon	F	Y	S	Y	Q	V	L	I	**E**	S	V	H	S	E	M	Y	S
C. Elegans	F	Y	G	F	Q	I	A	I	**E**	N	I	H	S	E	M	Y	S

p53R2	37	78	79	80	81	82	83	84	**85**	86	87	88	89	90	91	92	93
Patient 4.4									**Q**								
Human	H	W	N	K	L	K	A	D	**E**	K	Y	F	I	S	H	I	L
Chimp	H	W	N	K	L	K	A	D	**E**	K	Y	F	I	S	H	I	L
Macaque	H	W	N	K	L	K	A	D	**E**	K	Y	F	I	S	H	I	L
Mouse	H	W	N	K	L	K	S	D	**E**	K	Y	F	I	S	H	I	L
Dog	H	W	N	K	L	K	S	D	**E**	K	Y	F	I	S	H	I	L
Chicken	H	W	N	K	L	K	A	D	**E**	K	Y	F	I	S	H	V	L
Frog	H	W	E	K	L	K	P	E	**E**	R	N	F	I	S	H	I	L
Tetraodon	H	W	D	S	L	K	P	E	**E**	K	H	F	I	S	H	V	L
C. Elegans	D	W	E	K	M	N	G	D	**E**	Q	Y	Y	I	S	R	I	L

Figure 4.7: Amino acid alignment of the human p53R2 enzyme reference sequence versus p53R2 enzyme sequences of various species for: (A) p.Arg41Gln in exon 2; (B) p.Glu131Lys in exon 4; and (C) p.Glu85del in exon 3.

4.5.5 Protein analysis

4.5.5.1 SDS-denaturing gel electrophoresis

Immunoblot analysis of both patients revealed normal steady state levels of p53R2, indicating that none of the three *RRM2B* mutations had any effect on p53R2 stability (Figure 4.8A, B).

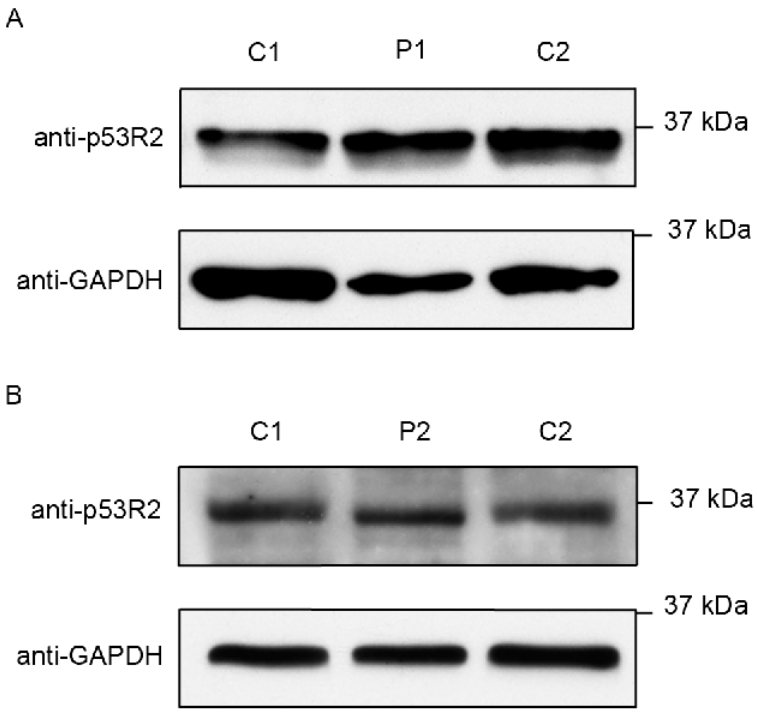

Figure 4.8: Western blot analysis of p53R2 and GAPDH proteins in muscle samples of Patient 4.3 (A, P1) and 4.4 (B, P2) shows normal p53R2 levels versus controls (C1 and C2).

4.5.5.2 Blue-native gel electrophoresis

BN-PAGE analysis demonstrated reduced levels of the heterotetramer R1p53R2 in the muscle sample from Patient 4.3 when compared with control muscle tissue (Figure 4.9A), suggesting impaired heterotetramer assembly despite the normal p53R2 levels seen on Western blot and BN-PAGE. BN-PAGE of Complex II in the muscle sample from Patient 4.3 when compared with control muscle tissue showed equal protein loading (Figure 4.9B).

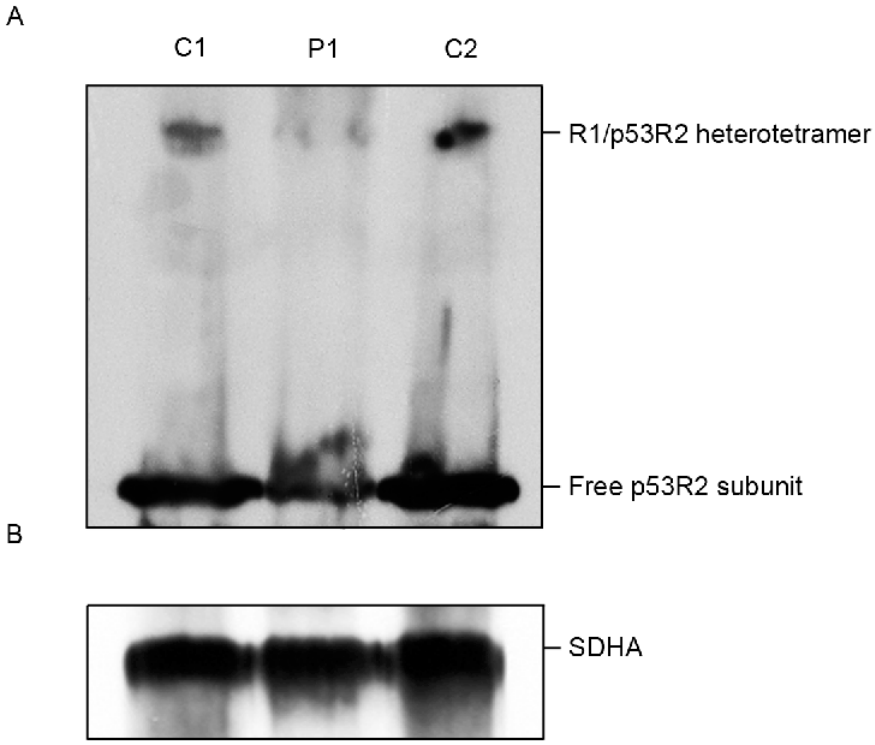

Figure 4.9: Blue-native polyacrylamide gel electrophoresis of p53R2 subunit, R1/p53R2 heterotetramer (A) and complex II (B) in muscle sample of Patient 4.3 (P1) shows reduced native R1/p53R2 levels despite normal p53R2 levels versus controls (C1 and C2).

4.5.6 Protein function prediction

All three *RRM2B* mutations were modelled on the previously published p53R2 crystal (Smith et al., 2009) (Figure 4.10A) in order to illustrate their structural implications. This enabled significant insight into the likely functional effects on RNR function, particularly as a result of an impaired interaction between the two p53R2 monomers within the heterotetrameric protein complex. Residue Arg41 is located within the N-terminal swivel region as defined by Smith *et al*. at the most N-terminal visible portion of the protein (Figure 4.10B). Conformational change of this region is associated with the formation of a salt-bridge between residues Arg41 and Glu119 and the stabilization of residues in helix B in the required conformation for formation of the di-iron bound monomer as a prerequisite for generation of the active tyrosyl-radical-bearing form of the subunit. Since glutamine would be unable to form a salt-bridge, the mutant would not be stable in the di-iron form and this would result in significant reduction of the active form of the enzyme. Glu131 is found in the centre of the iron-binding pocket (Figure 4.10C). In the wild-type p53R2 this residue bridges both ferric irons and is therefore required for binding one or possibly both ions. Mutation to the larger, positively-charged lysine would abolish di-iron binding completely and might prevent iron binding altogether. The effect of both mutations on RNR activity explains the clinical phenotype and is most likely the reason for the multiple mtDNA deletions observed in Patient 4.3.

Glu85 is located at the top of helix B at the opposite end to Glu119, the partner of Arg41 in the swivel mechanism (Figure 4.10D). It forms a salt bridge to Arg211 in helix D. Deletion of the Glu85 residue would preclude the formation of this salt-bridge and cause a significant loss of stability, of the order of a few Kcal mol-1, potentially reducing levels of correctly folded protein. Correctly folded proteins might also be functionally impaired: removal of the link might favour translocation of helix B over conformational change in helix D in response to movement of the swivel region, strongly destabilising the di-iron form and leading to a loss of native function; alternatively it may interfere with the adoption of the conformation of helix D required to form the channel leading to the iron-binding site. Since the mutant protein appears to exert a dominant effect, it is likely to compete with wild-type p53R2 to form the heterotetrameric R1/p53R2 RNR complex. The result of this competitive binding

would be a dominant-negative effect on R1/p53R2 function. The heterozygous nature of the defect is likely to account for the milder phenotype seen in our patient when compared to the two previously reported cases of the same mutation observed in compound heterozygous and homozygous (R. Van Coster et al., July 2010, Acta Myologica, abstract) states. The presence of the normal allele would be expected to partially compensate for impaired RNR activity.

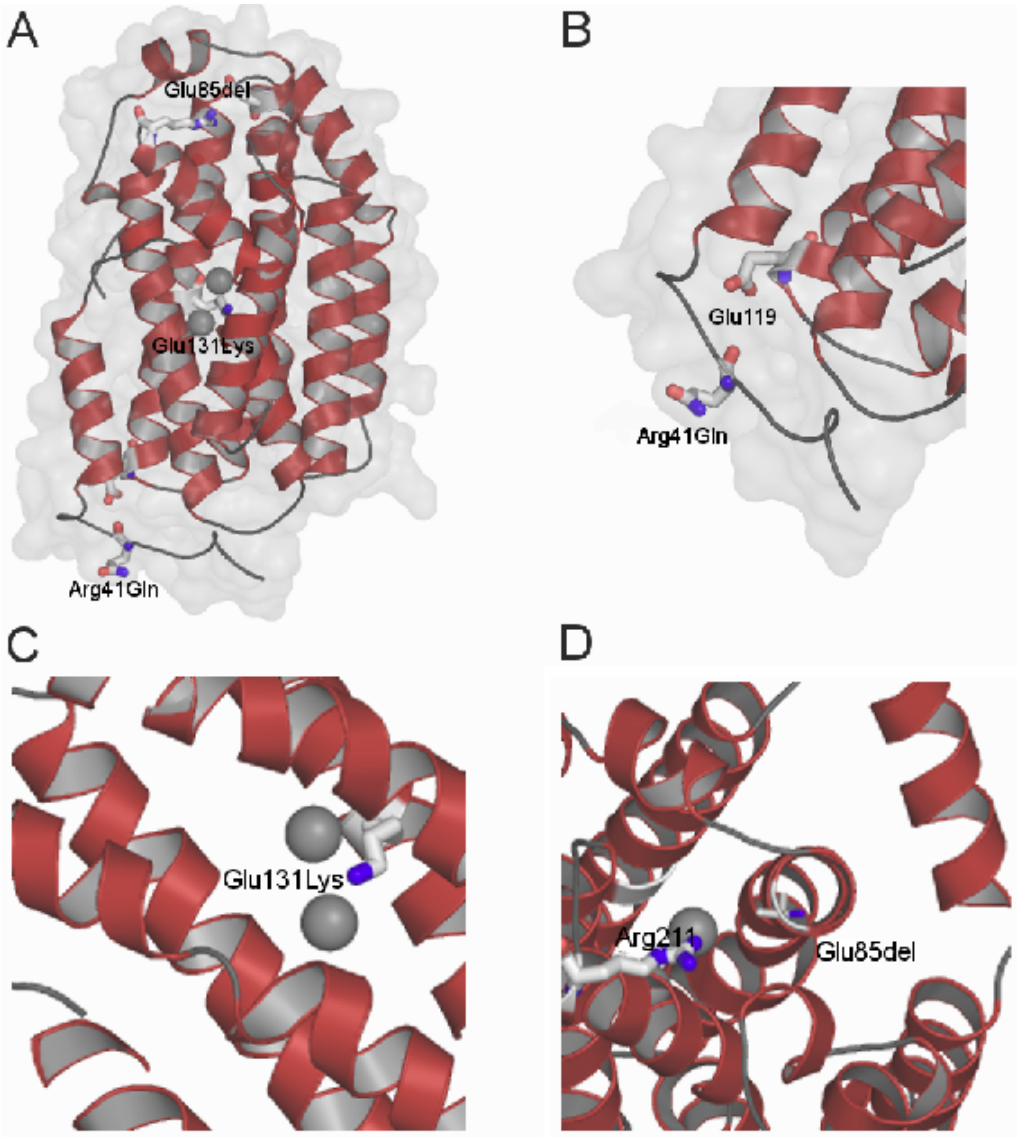

Figure 4.10: Mutations visualised on the p53R2 structure (PDB code 3hf1) showing details for all three mutations (A), Arg41Gln (B), Glu131Lys (C) and Glu85del (D) respectively.

4.6 Discussion

4.6.1 Distal myopathy caused by *de novo* dominant mitochondrial polymerase gamma mutations

Two unrelated patients with distal, predominantly upper limb, myopathy due to novel heterozygous missense mutations in *POLG* are described. Both mutations reside in the polymerase domain of the DNA polymerase catalytic subunit: c.2687T>G; p.Leu896Arg in Patient 4.1; and c.2851T>C; p.Tyr951His in Patient 4.2. Evolutionary conservation data confirmed that Leu896 and Tyr951 are invariant at these amino acid positions (Figure 4.5D). The Leu896Arg substitution occurs in the highly conserved motif A region of the polymerase domain, critical for nucleotide recognition and catalysis, and any alteration is highly likely to be pathogenic and cause impaired enzyme acitivity. Indeed, the majority of adPEO mutations in *POLG* are located in this region (Chan and Copeland, 2009). The mutation appears to be *de novo* dominant in Patient 4.1, since neither parent harboured the variant. A mutation involving the adjacent amino acid, c.2684A>G; p.Glu895Gly, has been associated with a neonatal-onset mtDNA depletion syndrome with 5% and 20% residual mtDNA in skeletal muscle and liver respectively (Spinazzola et al., 2009a). Tyr951 is one of three key amino acids, together with Tyr955 and Glu895, which form a hydrophobic pocket within the polymerase domain of polymerase gamma (Graziewicz et al., 2006). Tyr955Cys was the first reported mutation in *POLG*, causing adPEO in a Belgian pedigree (Van Goethem et al., 2001a). The heterozygous nature of the Tyr951His mutation, in the absence of any family history of neuromuscular disease, suggests this mutation is also *de novo*. Unfortunately, no other family members were available for genetic testing.

Patient 4.1 had an extremely low but static BMI despite normal dietary caloric intake. There was no evidence of malabsorption on laboratory testing and MNGIE was excluded. Gastrointestinal symptoms are not uncommon in patients with mitochondrial disease and include dysphagia, cachexia, weight loss, constipation, pseudo-obstruction, nausea and vomiting (Rahman, 2013). Weakness of the bulbar and facial muscles can cause significant swallowing difficulties, and this may be compounded by ataxia (Rahman and Hanna, 2009). In Patient 4.1, the degree of

weight loss was disproportionate to muscle wasting and dysphagia, and caloric intake adjusted for age and activity levels was normal. It is possible he has metabolic dysfunction as a direct consequence of his underlying mitochondrial disorder, such as uncoupling of oxidative phosphorylation. In Luft's first description of mitochondrial disease, the patient had a RRF myopathy with 'severe hypermetabolism of nonthyroid origin' and a BMI of 16.6 (normal female range 18.5-25) (Ernster et al., 1959; Luft et al., 1962). Disruption of the same biological pathway may account for the severe cachexia documented in Patient 4.1. Further work, such as measurement of the basal metabolic rate, would be required in order to clarify the underlying aetiology of the weight loss.

4.6.2 *RRM2B* mutations cause Kearns-Sayre syndrome

This is the first case of KSS to result from a nuclear genetic defect: two novel missense mutations in *RRM2B*. Single large scale deletions of mtDNA are normally found to be the cause of KSS and were first reported in this condition in 1988 (Zeviani et al., 1988). It was subsequently shown that the causative mtDNA deletions may differ considerably in size and location, although a 5kb 'common' deletion is present in approximately one third of patients (Moraes et al., 1989). The mechanism for the formation of deletions is poorly understood. An initial hypothesis proposed that slipped replication occurs between homologous base-pair repeat sequences within mtDNA (Shoffner et al., 1989), since most deletions appear to occur within the major arc between the two origins of mtDNA replication. The validity of this model has since been questioned (Krishnan et al., 2008). Irrespective of the mechanism, single large-scale deletions are generally considered sporadic events with a low inheritance risk. The present discovery suggests that KSS can also follow Mendelian inheritance patterns as a result of a nuclear gene mutation associated with multiple mtDNA deletions. This potentially has significant clinical implications, particularly during genetic counselling, and analysis of *RRM2B* should be a priority in KSS when multiple mtDNA deletions are present.

There are currently 60 adults from 41 families reported to harbour pathogenic mutations in *RRM2B* characterised by either autosomal-recessive mtDNA depletion syndrome (Shaibani et al., 2009) or recessively- and dominantly-inherited mutations

that cause accumulation of multiple mtDNA deletions (Tyynismaa et al., 2009; Fratter et al., 2011; Pitceathly et al., 2011a; Takata et al., 2011; Pitceathly et al., 2012). The data presented here indicates that *RRM2B* mutations are an important cause of multiple mtDNA deletions in adults (4% of this cohort of 50 adult patients with multiple mtDNA deletions). It is also important to note that a significant number of this cohort do not harbour mutations in *POLG*, *C10orf2* or *RRM2B*.

In mammalian cells RNR exists as a heterotetrameric enzyme consisting of one large homodimeric R1 subunit which contains the catalytic site, and one small homodimeric R2 subunit which supplies the tyrosyl free radical required for catalysis. The R2 subunit is produced exclusively during S-phase in cycling cells when RNR provides the nucleus with dNTPs required for DNA replication (Tanaka et al., 2000). The R2 homologue p53R2, however, is detectable at low levels throughout the cell cycle in both proliferating and post-mitotic cells. It is thought that it is the R1/p53R2 heterotetramer which is important in providing dNTPs for nDNA repair and/or mtDNA synthesis. A recent study localised p53R2 exclusively to the cytosol during both cell proliferation and DNA damage, suggesting that the RNR enzyme itself does not translocate into the nucleus or mitochondrion to effect DNA repair locally as was initially thought, but rather that dNTPs diffuse into the nucleus and mitochondria to provide building blocks for DNA repair/synthesis (Pontarin et al., 2008). The role of RNR in repair was also challenged since DNA damage does not lead to significant increases in dNTP pools (Håkansson et al., 2006) and induction of p53R2 by p53 peaks around 24 hours, yet repair of damaged DNA is complete in a much shorter time period (Nordlund and Reichard, 2006; Tanaka et al., 2000). It is possible that p53R2 increases flux through the dNTP pool, rather than the absolute size of the dNTP pool itself (Tyynismaa et al., 2009). Furthermore, posttranslational modification of p53R2 by phosphorylation at Ser72 by the ataxia telangiectasia mutated (ATM) protein kinase confers p53R2 protein stability and resistance to DNA damage within 30 minutes of genotoxic stress (Chang et al., 2008). This would allow rapid repair of DNA by activating existing pools of p53R2 protein without reliance on slow transcriptional induction of p53R2.

BN-PAGE was used to demonstrate the deleterious effects of *RRM2B* mutations on heterotetramer assembly. This is a technique previously used to assess intact mitochondrial respiratory chain complexes. Data is presented that not only expands the application of this method to include analysis of cytosolic multiprotein complexes, but that also provides greater understanding of mutational effects on protein complex assembly. Impaired R1/p53R2 heterotetramer assembly is a potential pathogenic mechanism by which mutations in *RRM2B* cause disease. It is important that further attempts are made to replicate this experiment in patients with *RRM2B* mutations to fully understand the frequency of impaired R1/p53R2 assembly in the pathogenesis of these disorders. BN-PAGE should also be considered to demonstrate native multiprotein complexes when impaired assembly is suspected.

The presence of necrotic fibres alongside the more typical histopathological features of mitochondrial disease in both patients with *RRM2B* mutations is intriguing, particularly since both patients exhibit this finding. They may be a consequence of impaired nDNA repair caused by the defective p53R2; it has been shown that p53R2-null mice demonstrate enhanced frequency of spontaneous mutations and activation of p53-dependent apoptotic pathways (Kimura et al., 2003). Identification of necrotic fibres in muscle could be a useful guide when prioritising which nuclear genes to sequence in patients with multiple mtDNA deletions.

In conclusion, this work shows that mutations in *RRM2B* are an important cause of multiple mtDNA deletions in adults, and reports the first case of KSS related to nuclear genomic dysfunction, as a result of two novel *RRM2B* mutations. The heterotetrameric structure of R1/p53R2 RNR means that disease may arise from heterozygous, homozygous or compound heterozygous mutations which reduce RNR activity, and from impaired assembly of the heterotetramer. In addition, there is a dosage effect, dependent on the presence or absence of wild-type p53R2. Finally, BN-PAGE is shown to be a valuable method in the structural analysis of native R1/p53R2 RNR, allowing mechanistic insight into the effect of dysfunctional *RRM2B* on R1/p53R2 RNR assembly.

CHAPTER 5

COX10 mutations link to severe adult cytochrome *c* oxidase deficiency

CHAPTER 5

5. *COX10* mutations link to severe adult cytochrome *c* oxidase deficiency

5.1 Introduction

The COX10 protein is required to farnesylate protohaem (haem B) to haem O in the haem A biosynthetic pathway (Moraes et al., 2004). Two haem A moieties (*a* and a_3) are essential prosthetic groups of the MTCO1 subunit of COX and are involved in electron transfer (Taanman, 1997b).

In this study, an adult patient with a complex clinical phenotype, marked reduction of COX activity in almost all muscle fibres on biopsy, and isolated biochemical COX deficiency was investigated. In contrast to most patients with such profound COX deficiency, disease progression was milder and the patient is clinically stable aged 37 years. The aim of this work was to elucidate the molecular genetic basis of this disease and understand the milder clinical phenotype exhibited by this patient compared with previous reports.

5.2 Case history

Patient 5.1 is a 37-year-old woman of European descent. She was born at term to non-consanguineous parents and presented aged 12 months with poor weight gain for which no cause was found. Aged 10 years short stature and mild exercise intolerance was present. By 21 years, proximal muscle weakness and fatigue were prominent features and at 25 years renal Fanconi syndrome and metabolic acidosis were detected. She subsequently developed premature ovarian failure (POF). There was no family history of neuromuscular disease (Figure 5.1). Currently, exercise tolerance is limited to 200 yards with a walking aid. Recent clinical examination showed short stature (height 4 ft 10 in) and a proximal myopathic gait, with upper and lower limb proximal muscle weakness (MRC grade 4/5) and absent tendon reflexes, but no other signs of neuropathy. There is an asymptomatic pigmentary maculopathy and mild right-sided SNHL.

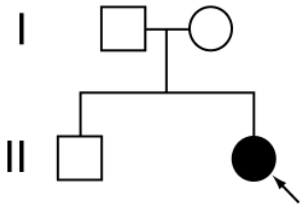

Figure 5.1: Pedigree of Patient 5.1

Laboratory evaluation demonstrated an elevated serum lactate of 3.8 mmol/L, with a normal CSF lactate. Brain MRI was normal at 12 years. Neurophysiology revealed slowing of motor and sensory nerve conduction (left median compound motor action potential [CMAP] at wrist 12.3 mV, motor conduction velocity [MCV] 30 m/s; left ulnar CMAP at wrist 8.3 mV, MCV 33 m/s; left ulnar sensory action potential 4 μV, sensory conduction velocity 43 m/s) and polyphasic units of brief duration in deltoid and iliopsoas, compatible with a demyelinating peripheral neuropathy and proximal myopathy.

Sural nerve biopsy showed moderate depletion of myelinated fibres with relative greater loss of small diameter axons. Many of the surviving myelinated fibres had inappropriately thin myelin sheaths for their diameter in the absence of regeneration clusters (Figure 5.2A, arrows). Morphometry confirmed a significant number of large calibre axons (≥ 8 μm diameter) had higher g-ratios compared to an age-matched control (45% versus 27% of axons had a g-ratio of ≥ 0.7; normal range for large calibre axons 0.55-0.65 age 10-60 years) (Jacobs and Love, 1985). Remyelination causes generation of a thinner myelin sheath. This phenomenon is demonstrated in the g-ratio (the ratio of axon to myelin circumference). Thus, remyelinated axons tend to have a g-ratio closer to one than those myelinated naturally. The difference in g-ratio between a normal and remyelinated nerve fibre is less apparent in small calibre axons.

EM confirmed frequent demyelination (Figure 5.2B, C). Membrane-bound 8-nm wide filament-containing inclusions were identified closely associated with and probably arising within the Golgi complex cisternae of some myelinated fibre Schwann cells

(Figure 5.2D, E). Redundant Schwannian cytoplasmic profiles were in keeping with myelinated fibre loss. Unmyelinated fibres were well preserved.

Teased fibres showed frequent segmental demyelination. Occasional larger mitochondria were noted in a few Schwann cells, but the cristae were of normal density and architecture, and no inclusions were seen.

Muscle biopsy revealed global reduction in COX histochemical staining but no RRF (Figure 5.2F).

Spectrophotometric activity assay confirmed severe COX deficiency in skeletal muscle (0.004 COX/CS; controls 0.014-0.034) but low-normal activity in cultured skin fibroblasts (0.015 COX/CS; controls 0.013-0.026). Mitochondrial respiratory chain complex I and complex II+III activities were normal. Polarographic studies demonstrated normal oxygen uptake of intact muscle mitochondria (Hargreaves et al., 2002).

Genetic analysis of *POLG*, performed because of POF (Duncan et al., 2012; Pagnamenta et al., 2006), was normal, as were sequences of the entire mitochondrial genome, *SURF1* (encoding the surfeit locus protein 1), *SCO1* (encoding protein SCO1 homolog), *SCO2* (encoding protein SCO2 homolog) and *TACO1* (encoding translational activator of cytochrome *c* oxidase 1).

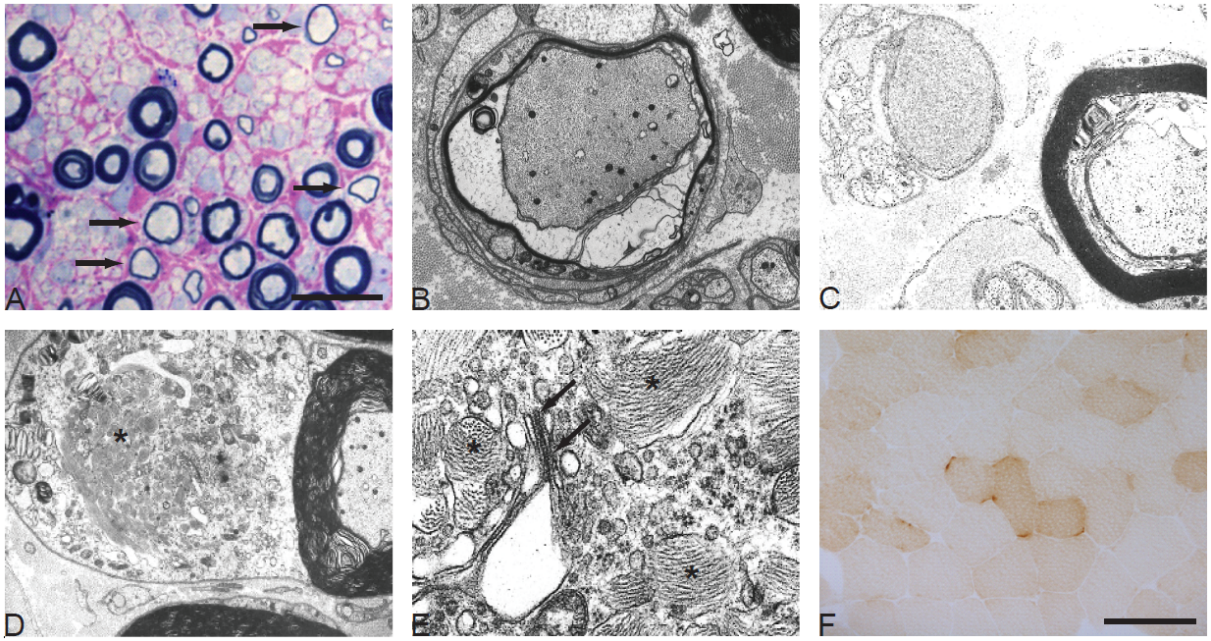

Figure 5.2: Sural nerve and muscle histopathology of Patient 5.1. Sural nerve biopsy: high magnification view of one fascicle (resin semi-thin section stained with methylene blue, azure II and basic fuchsin) shows moderate depletion of myelinated fibres with several large diameter axonal profiles displaying inappropriately thin myelin sheaths for their diameter, suggesting demyelination (A, arrows). Electron microscopy demonstrates two examples of demyelinating axons (B and C) and tightly packed inclusions within a myelinated fibre Schwann cell cytoplasm (D, star). Inspection at higher magnification shows membrane bound filamentous inclusions (stars) closely associated with the Golgi cisternae (E, arrows). Muscle biopsy: decreased cytochrome *c* oxidase staining in the majority of fibres (F). Ragged red fibres were not present. Bar in A and F represents 100 µm.

5.3 Methods

5.3.1 Spectrophotometric analysis

Complex I, complex II+III and complex IV were measured in the muscle tissue of Patient 5.1 in the UCLH NHNN NCG Neurometabolic diagnostic laboratory by Dr Iain Hargreaves and in cultured skin fibroblasts of Patient 5.1 as described in section 2.3.2.

5.3.2 Oxygen polarography

Polarographic studies were performed on a mitochondrial enrichment fraction isolated from the Vastus Lateralis muscle according to the method of Cooper *et al* (Cooper et al., 1992) in the UCLH NHNN NCG Neurometabolic diagnostic laboratory by Dr Iain Hargreaves. In these studies oxygen consumption rates were determined in the presence of the following substrates: glutamate/malate; pyruvate/malate; succinate and TMPD (N,N,N,N-tetramethyl-p-phenylenediamine)/ascorbate.

5.3.3 Whole exome sequencing

Genomic DNA (1-3 µg) was sheared to 100–400 bp using a Covaris E210 or LE220 (Covaris, Woburn, MA, USA). Sheared DNA was subjected to Illumina paired-end DNA library preparation and enriched for target sequences (Agilent Technologies; Human All Exon 50 Mb - ELID S02972011) according to manufacturer's recommendations (Agilent Technologies; SureSelectXT Automated Target Enrichment for Illumina Paired-End Multiplexed Sequencing). Enriched libraries were sequenced using the HiSeq platform (IIlumina, Inc., San Diego, CA, USA) as paired-end 75 base reads according to the manufacturer's protocol (see section 2.4.5).

5.3.4 Whole exome sequencing bioinformatic analysis

Autosomal recessive inheritance was assumed in view of the non-consanguineous lineage, because parents were unaffected, and because all reports of COX deficiency result from loss-of-function genetic defects. The filtering pathway searched for novel (absent from dbSNP132, 1000 Genomes Project, the UK10K rare disease cohort [823 exomes at the time of the analysis]), compound heterozygous, functional (non-synonymous coding [NSC] or loss-of-function [LOF] i.e. frame-shift coding, stop gained or splice site mutations) SNVs and/or coding indels in genes predicted to play a role in COX biogenesis. Across the entire exome no novel candidate SNVs/genes were identified. The stringency was therefore relaxed to include SNVs and coding indels reported to dbSNP132 and/or 1000genomes, still assuming recessive inheritance.

5.3.5 Automated Sanger sequencing of *COX10*

Confirmation and segregation of the mutations identified by whole exome sequencing analysis was assessed using standard dideoxynucleotide chain termination (see sections 2.4.3. and 2.4.4). Amplification of *COX10* fragments for sequencing was performed using specific primers: 5'-ATTCTTTGGAAATCTCTGGTGATGAC-3' (forward primer), and 5'-CTCGTACAACACCATTAAGACCT-3' (reverse primer), designed using Primer3 (http://frodo.wi.mit.edu/primer3/), Amplitaq Gold 360 mastermix (Applied Biosystems) and BigDye Terminator 246 v.1.1 cycle sequencing kit (Applied Biosystems). The samples were run on a 3730xl DNA Analyser, assembled and analysed using Seqscape v.205 software (Applied Biosystems).

5.3.6 Western blot analysis of SDS denaturing polyacrylamide gels and immunocytochemistry

Western blot analysis of SDS denaturing gels (see section 2.5.5) were performed on 10 µg of muscle protein extracted from muscle tissue and developed with specific mouse monoclonal antibodies (anti-SDHA and anti-MTCO1) from Abcam. The affinity purified rabbit anti-COX10 antibody was purchased from Proteintech Group Inc. (1:500, cat. no. 10611-1-AP). Proteins were visualised using secondary mouse

anti-rabbit and goat anti-mouse antibodies conjugated to horseradish peroxidase (Dako).

Immunocytochemistry of MTCO1/MitoTracker Red CM-H_2XRos (Life Technologies) stained cells was performed as described in section 2.5.7. Anti-MTCO1 (clone 1D6E11A8, Abcam) was detected with goat anti-mouse IgG Alexa Fluor 488 (Life Technologies) and nuclei were counterstained with 1 μg of 4',6-diamidino-2-phenylindole (Sigma) per ml of Citifluor-glycerol-PBS solution (Agar Scientific).

5.3.7 Western blot analysis of one-dimensional blue-native polyacrylamide gels

Western blot analysis of blue-native gels (see section 2.5.6) were performed on 10 μg of muscle protein extracted from muscle tissue and developed with specific mouse monoclonal antibodies (anti-SDHA, anti-MTCO1, anti-MTCO2, anti-COX4, and anti-UQCRC2) from Abcam. Proteins were visualised using secondary mouse anti-rabbit and goat anti-mouse antibodies conjugated to horseradish peroxidase (Dako).

5.3.8 Haem spectrophotometry

Air-oxidised versus sodium dithionite-reduced haem spectra of 1.5% DDM extracts of muscle mitochondrial fractions were recorded as described (Capaldi et al., 1995). The haem electron carriers of the respiratory chain give characteristic visible absorption spectra in their reduced state. Haem spectra can be used to identify COX and to assess its concentration in cell extracts or mitochondria. Spectral shifts or low absorbance indicate disturbances of the catalytic centre in the enzyme. Light scattering can be avoided by solubilising the respiratory chain complexes in 1.5% (w/v) dodecyl maltoside or 1% (v/v) Triton X-100.

The mitochondrial samples were incubated at a concentration of 0.5 to 5 mg protein/ml in 100 mM potassium phosphate buffer, pH 7.2, 25 mM NaCl, and 1.5% (w/v) DDM for 5 min on ice. Insoluble material was removed by centrifugation in a micro-centrifuge for 1 min. Air-oxidised versus sodium dithionite-reduced difference spectra was recorded between 400 and 650 nm in order to detect the α, β, and γ

bands. A few crystals of sodium dithionite in the cuvette were used to reduce the haems fully. Spectra were recorded using a double-beam spectrophotometer. Absorption maxima of the RC haems are shown in Table 5.1.

Table 5.1: Haem absorption maxima in air-oxidised versus sodium dithionite-reduced difference spectra, adapted from (Capaldi et al., 1995)

	Cytochrome *c* oxidase	**Cytochrome *c* reductase**		**Cytochrome *c***
Band	**Haem *aa*$_3$**	**Haem *b***	**Haem *c*$_1$**	**Haem *c***
α	605	562	553	550
β	520	532	520	521
γ	445	430	418	416

5.3.9 Yeast studies

Yeast studies were performed by Dr Brigitte Meunier (Centre de Génétique Moléculaire, UPR3404, CNRS, Avenue de la Terrasse, 91198, Gif-sur-Yvette, France). The mutant yeast Δcox10 and the centromeric plasmid carrying the human COX10 gene were kindly received from Professor A. Tzagoloff and are previously described (Glerum and Tzagoloff, 1994; Valnot et al., 2000). The mutations were introduced using the Quikchange site-directed mutagenesis procedure (Stratagene) according to the manufacturer's recommendation. The plasmids, carrying the control or mutated human *COX10* gene, were used to transform the mutant yeast *Δcox10*. Transformants, after growth on selective medium, were inoculated on nonfermentable medium, containing glycerol and ethanol as carbon source.

5.3.10 Modelling of COX10 protein from predicted contacts

Since the crystal structure for the COX10 protein is undetermined, the here reported novel Arg339Trp, in addition to the previously reported COX10 amino acid substitutions Thr196Lys, Asp204Lys, Pro225Leu, Asp336Gly, and Asp336Val (Antonicka et al., 2003; Valnot et al., 2000), were mapped to a hypothetical COX10 protein model predicted using computational analysis by Dr Michael Sadowski, MRC National Institute for Medical Research (NIMR). The resulting structural

consequences were subsequently analysed to generate hypotheses for potential mechanisms underlying the pathogenicity of these mutations. The full-length COX10 sequence was used as a query to search the Uniref100 database with 3 iterations of JackHammer from the HMMer3 package (Eddy, 2011). The resulting alignment was used to predict contacts between residues using covariance matrix inversion as previously described (Jones et al., 2012; Taylor et al., 2012). Predicted contacts were then used to provide restraints for *ab initio* modelling of the transmembrane bundle. Several transmembrane prediction packages were run (MEMSAT3, MEMSAT-SVM, OCTOPUS) and found to disagree on the transmembrane topology and locations of the transmembrane helices. It was therefore decided to use the curated Uniprot transmembrane annotations as the basis for the model. Predicted contacts were implemented as harmonic restraints between alpha carbons with mean distance 8 Å and standard deviation of 3 Å. Restraints within a single element of secondary structure were removed to prevent distortion of the transmembrane helices owing to noise in the predictions. The model was built using MODELLER 9v3 (Sali and Blundell, 1993) with a custom script defined as follows: first the sequence is built as an extended chain and the normal stereochemical restraints are implemented at this stage. Following this the 'secondarystructure.alpha' routine was used to define the 9 transmembrane segments as detailed in the UNIPROT entry. The bundle was then folded sequentially by adding one restraint at a time and refining with 100 steps of conjugate gradient minimisation using the 'refine.slow()' protocol. Restraints were added in order of sequence distance starting with the closest. Restraints involving coil residues were added after restraints between elements of secondary structure. The process was repeated several times with varying numbers of restraints from 1000 to 5000 and the model which was most compact, with the most nearly parallel bundle and with the most hydrophobic surface was chosen. Figures were rendered in PyMOL (DeLano, 2002).

5.4 Results

5.4.1 Whole exome sequencing bioinformatic analysis

A total of 138,006 SNVs were identified (Table 5.2). Of these 9,456 were predicted to be functional and 404 of these were novel. When these variants were filtered under a recessive model, searching for two mutations within genes predicted to play a role in COX biogenesis, no candidate genes were detected. However, when the filtering stringency was relaxed to include variants reported to dbSNP132 and 1000 Genomes under a recessive model, three missense SNVs in *COX10* were identified: one reported pathogenic mutation (c.1007A>T; p.Asp336Val); one novel mutation (c.1015C>T; p.Arg339Trp); and one SNP (c.476G>A; p.Arg159Gln, dbSNP132 rs8077302). The SNP was subsequently discounted from further analysis. No other compound heterozygous (or homozygous) variants were detected in any other genes predicted to play a role in COX biogenesis.

5.4.2 Automated Sanger sequencing of *COX10*

COX10 Sanger sequencing of gDNA from Patient 5.1 confirmed the presence of c.1007A>T and c.1015C>T (Figure 5.3A). The unaffected parents both carried one mutation (Figure 5.3B), thus confirming the compound heterozygous nature of the mutations in Patient 5.1. Evolutionary conservation studies demonstrated invariance of Asp336 and p.Arg339 across species.

Table 5.2: Identification of candidate genes for cytochrome *c* oxidase deficiency in Patient 5.1 using exome resequencing

Filter	**SNVs**	**Genes**
Total	138,006	13,268
SC	9,465	5,825
NSC/LOF	9,456	5,445
Novel NS/LOF	404	376
Novel homozygous NSC/LOF	24	21
Novel heterozygous NSC/LOF	380	358
Novel compound heterozygous NSC/LOF	39	17
With predicted mitochondrial localisation	0	0
With predicted role in COX biogenesis	0	0
Homozygous NSC/LOF	3749	2,597
Heterozygous NSC/LOF	5,707	3,596
Compound heterozygous NSC/LOF	3,211	1,100
With predicted mitochondrial localisation	104	43
With predicted role in COX biogenesis	3	**1 (*COX10*)**

Among the identified SNVs, non-synonymous coding and loss of function variants were subsequently filtered for a predicted role in cytochrome *c* oxidase biogenesis under a recessive model. Variants were considered novel when not present in dbSNP132 or 1000 Genomes databases. Abbreviations: COX = cytochrome *c* oxidase; SNVs = single nucleotide variants; SC = synonymous coding; NSC = non-synonymous coding; LOF = loss of function (frame-shift coding/stop gained/splice site).

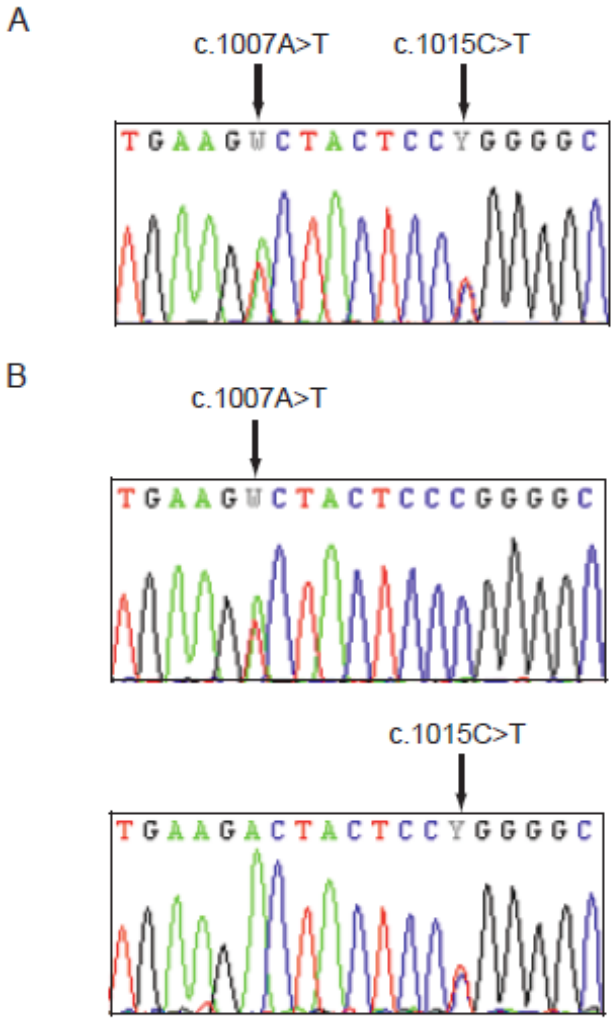

Figure 5.3: *COX10* sequencing data for Patient 5.1 and amino acid alignment of the human COX10 protein reference sequence versus sequences of various species. *COX10* Sanger sequencing of gDNA from the patient confirmed the presence of c.1007A>T and c.1015C>T (A). *COX10* Sanger sequencing of gDNA from the unaffected parents confirmed the compound heterozygous nature of the mutations in the patient (B).

5.4.3 Western blot analysis of SDS denaturing polyacrylamide gels and immunocytochemistry

Western blot analysis of SDS-denaturing polyacrylamide (Figure 5.4) gels and immunocytochemistry (Figure 5.5) demonstrated that steady state levels of MTCO1 were significantly reduced in muscle and fibroblasts, respectively. However, COX10 protein levels were normal in muscle (Figure 5.4).

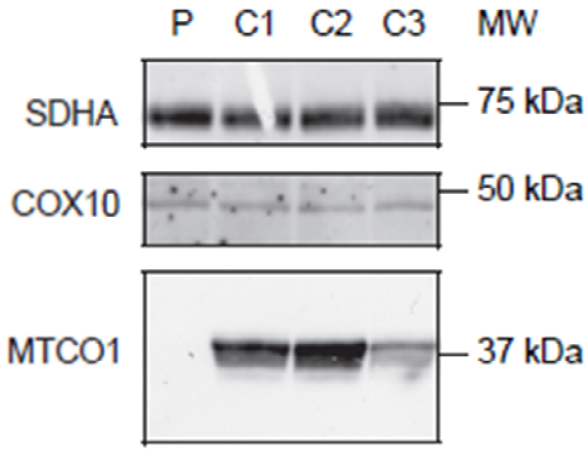

Figure 5.4: Immunoblot analysis of an SDS denaturing polyacrylamide gel loaded with mitochondrial membrane proteins extracted from muscle of Patient 5.1. COX10 protein steady-state levels were normal in Patient 5.1 (P) compared with controls (C1-3), indicating that the *COX10* missense mutations do not impair COX10 protein stability, whilst MTCO1 was undetectable in P, unlike C1-3.

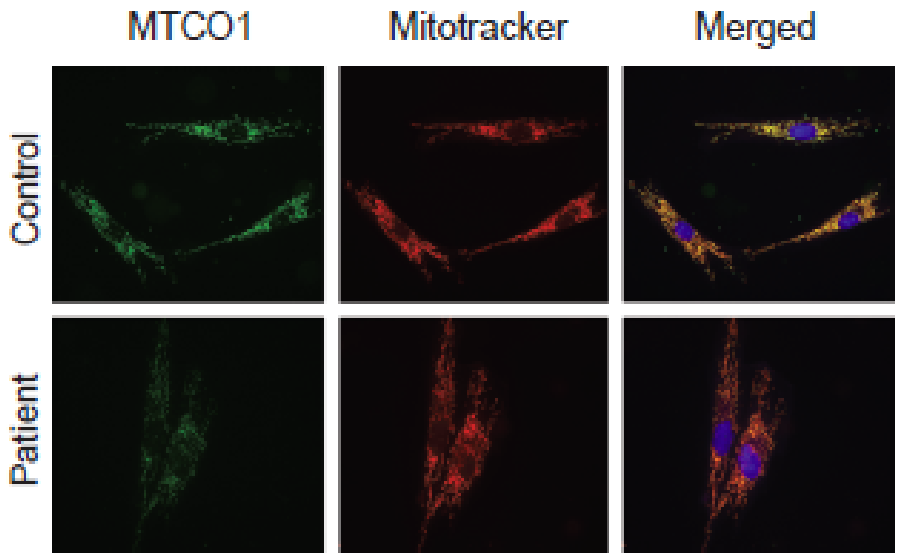

Figure 5.5: Micrographs of control and Patient 5.1 fibroblasts immunocytochemically stained for MTCO1 (green fluorescence) and MitoTracker Red (red fluorescence), and counterstained with the DNA fluorochrome 4',6-diamidino-2-phenylindole (blue fluorescence). The cells of Patient 5.1 show a general decrease in MTCO1 levels compared to control cells.

5.4.4 Western blot analysis of one-dimensional blue-native polyacrylamide gels

Analysis of western blots of blue-native polyacrylamide gels revealed undetectable COX holoenzyme with no abnormal subassemblies (Figure 5.6).

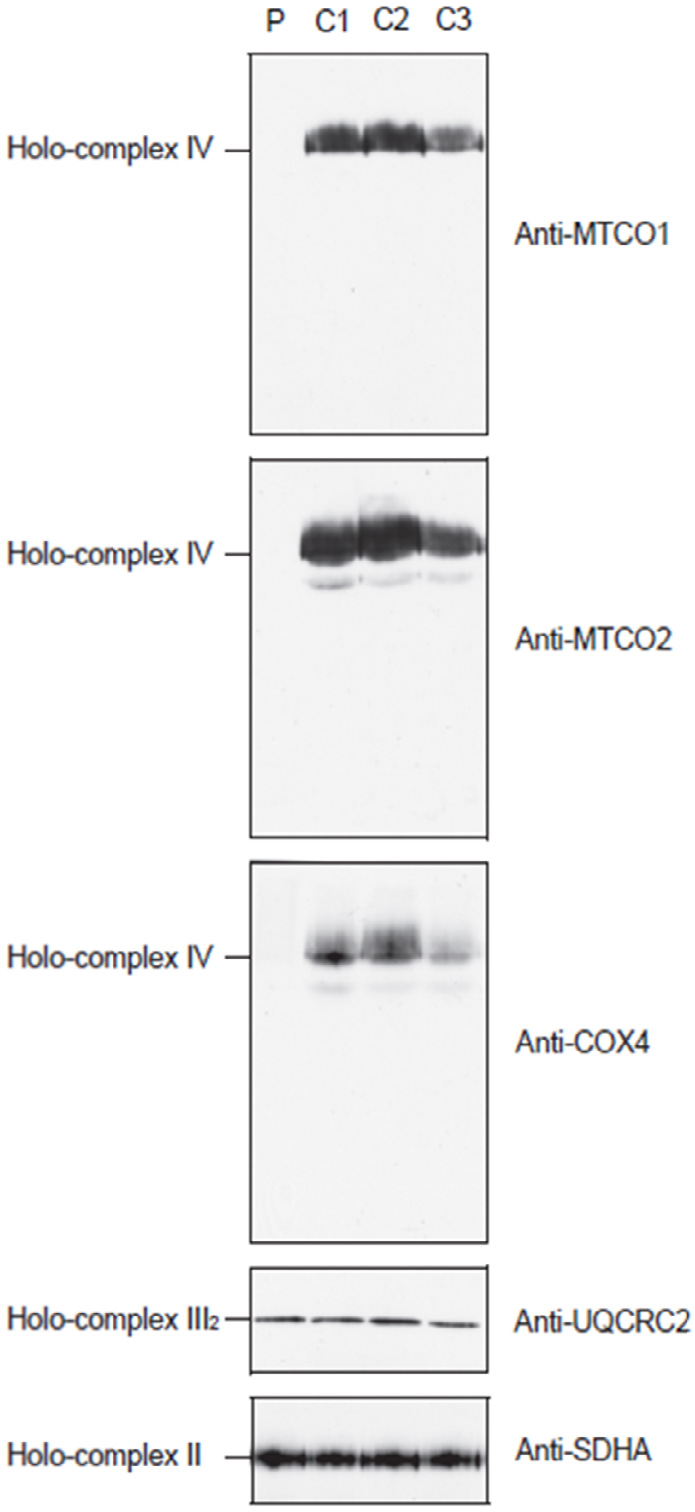

Figure 5.6: Immunoblot analysis of a blue-native polyacrylamide gel loaded with mitochondrial membrane proteins extracted from muscle of Patient 5.1. Compared to controls (C1-3), COX holoenzyme was undetectable in the muscle tissue of Patient 5.1 (P).

5.4.5 Haem spectrophotometry

Muscle haem absorption spectra confirmed reduction in haem aa_3 levels with loss of the haem aa_3 γ band at 445 nm (Figure 5.7). The haem aa_3 α (605 nm) and β (520 nm) bands were masked by contaminating haemoglobin.

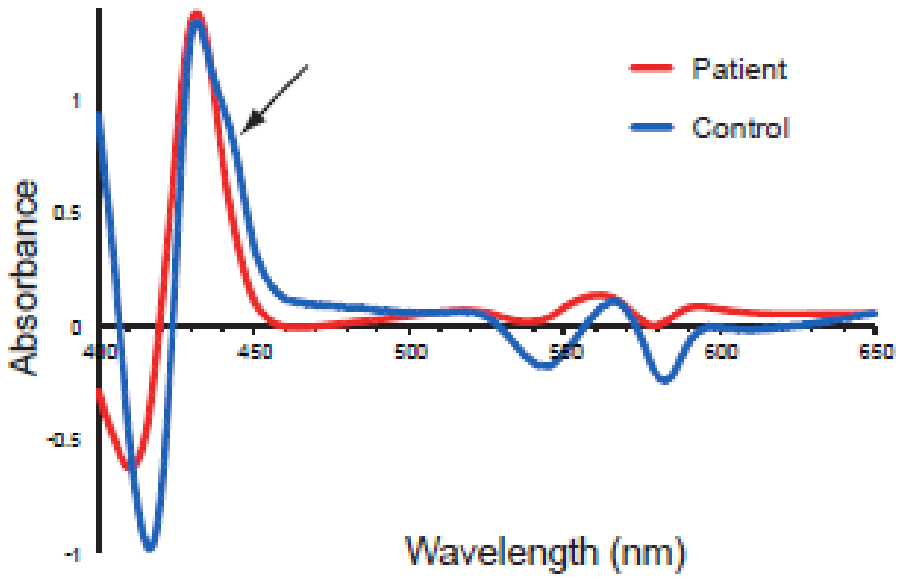

Figure 5.7: Air-oxidised versus sodium dithionite-reduced haem spectra of the muscle mitochondrial proteins of Patient 5.1. There is loss of the haem aa_3 γ band at 445 nm (arrow) in Patient 5.1 compared with the control.

5.4.6 Yeast studies

The functional significance of the mutations was demonstrated by introducing p.Asp336Val and p.Arg339Trp into the yeast *Saccharomyces cerevisiae.* Growth on a nonfermentable carbon source confirmed that each mutation caused respiratory deficiency individually, which was even more prominent when the mutations co-existed (Figure 5.8A, B).

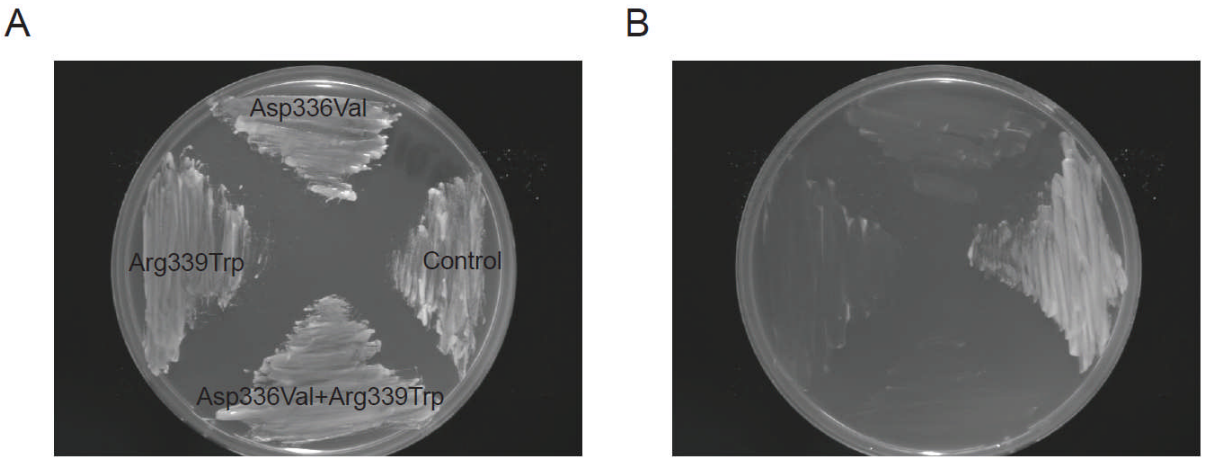

Figure 5.8: Growth of control and *COX10* p.Asp336Val, *COX10* p.Arg339Trp and *COX10* Asp336Val + Arg339Trp yeast strains on glucose (A) and glycerol+ethanol (B) as carbon source. Both *COX10* mutations cause respiratory deficiency as demonstrated by impaired growth on the nonfermentable carbon source glycerol+ethanol. When both mutations co-existed, the respiratory deficiency appeared to be even more pronounced (A and B).

5.4.7 Modelling of COX10 protein from predicted contacts

The protein model (Figure 5.9) indicates that helices 7 and 9 of COX10 contain two highly conserved histidine residues (360 and 418) in close proximity, suggesting that the haem-binding site might be located in this C-terminal region. Substitutions Thr196Lys and Asp204Lys, implicated in severe infantile mitochondrial disease, affect hydrophilic residues in helix 2 which interact with other helices in the bundle. The larger lysine side chain would disrupt these interactions and destabilize the overall protein structure, thereby explaining the deleterious effects of both these variants. The reported Pro225Leu substitution is in a long loop region predicted to localize to the mitochondrial matrix between helices 2 and 3. Thus, this mutation may cause dynamic changes by increasing local flexibility and disrupting interactions with partner proteins. Residues 336 (Asp to Gly and Val) and 339 (Arg to Trp) are found in a loop region which, based on the positive-inside rule of von Heijne (von Heijne and Gavel, 1988), would be expected to be intra-organellar. These residues may therefore participate in functional interactions taking place within the mitochondrial matrix.

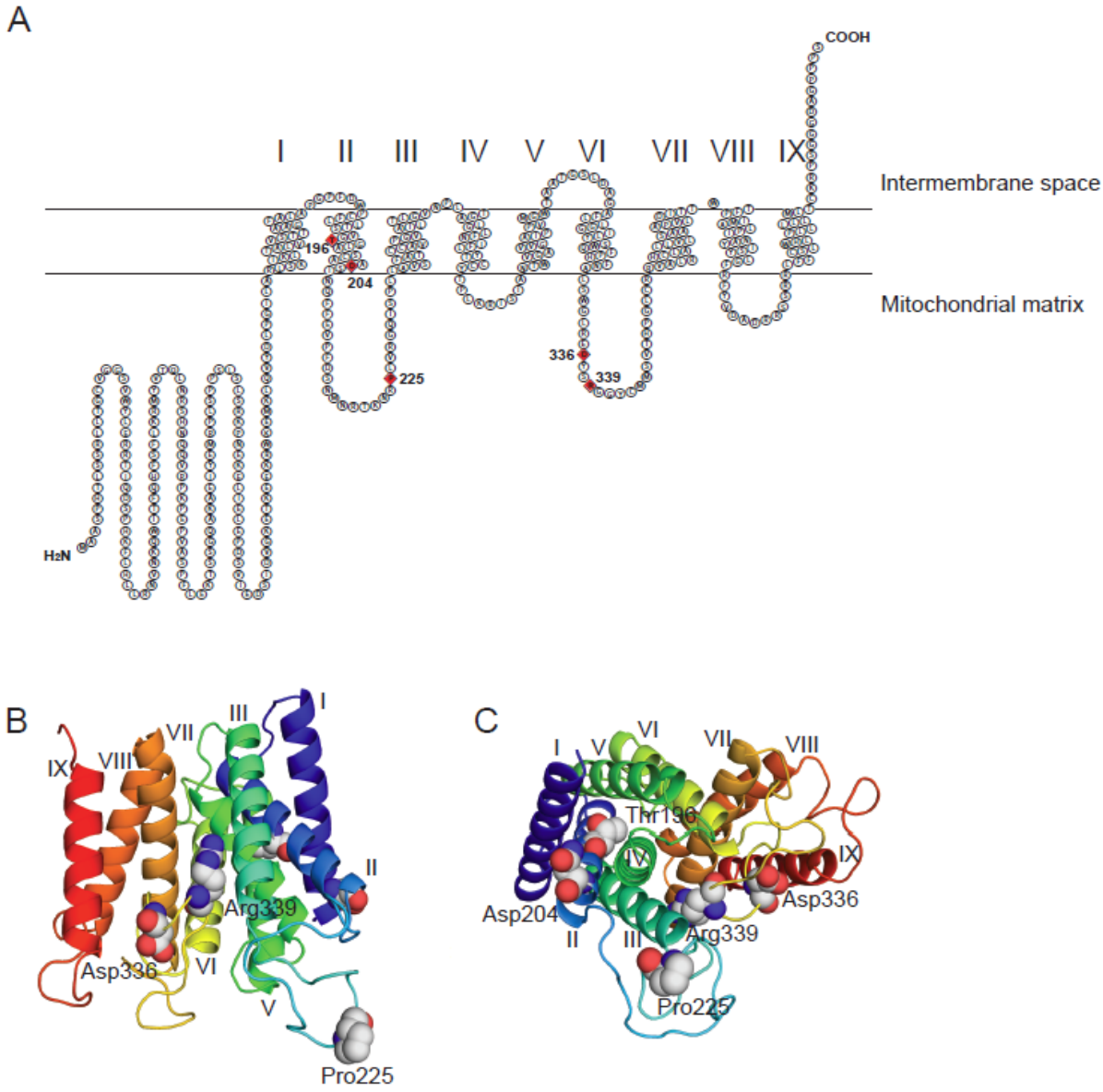

Figure 5.9: Topology diagram and structural model of the COX10 protein. Locations of known and here reported mutated residues highlighted in red, with transmembrane segments labelled with Roman numerals (I-IX) (A). Structural model of the COX10 protein showing locations of residues 336, 339, and 225 (B) and residues 196, 204, 225, 336, and 339 looking up from the mitochondrial matrix at the putative face of the bundle (C).

5.5 Discussion

The structural and functional data presented, including biochemical and protein analysis, yeast studies, and *in silico* protein modelling, confirm the pathogenic nature of both mutations detected, and provide mechanistic insight for variability in phenotypic presentation associated with COX deficiency.

To study the effect of both mutations on COX assembly BN-PAGE was used. This showed undetectable COX holoenzyme and subassemblies in muscle. Lack of COX assembly intermediates is consistent with previous reports of infantile COX10 dysfunction and reflects the requirement for COX10 at an early stage of COX assembly (Antonicka et al., 2003). Insertion of haem A is thought to occur prior to folding of MTCO1 during its association with subunits COX4 and COX5A. Consequently, *COX10* mutations do not cause accumulation of COX subassemblies typical of *SCO1* and *SURF1* defects (Williams et al., 2004d). The absence of assembly intermediates is probably related to impaired stability and downregulation of MTCO1, which requires association with COX4 and COX5A and insertion of haem A to prevent its rapid degradation by mitochondrial proteases (Arnold and Langer, 2002; Williams et al., 2004d). The yeast studies provide further support for pathogenicity of each mutation; both variants caused respiratory deficiency in isolation, and this was exaggerated further when the mutations co-existed.

Despite the limitations of this computational COX10 protein model, it is tempting to hypothesise that the Asp336Gly substitution (previously reported as co-existing with Asp336Val in a paediatric case with death at 4 months) generates more significant structural changes within the COX10 protein than the novel Arg339Trp substitution reported here. As such, the potentially less deleterious combination of Asp336Val and Arg339Trp might contribute towards the milder clinical phenotype observed in Patient 5.1.

CHAPTER 6

NDUFA4 mutations underlie human cytochrome *c* oxidase-deficient Leigh syndrome

CHAPTER 6

6. *NDUFA4* mutations underlie human cytochrome *c* oxidase-deficient Leigh syndrome

6.1 Introduction

This chapter investigates the genetic basis of neurological disease in a large consanguineous Pakistani family in whom four affected relatives had isolated COX deficiency. The natural history was of an initial presentation with congenital lactic acidosis and subsequent evolution into a Leigh syndrome phenotype with bulbar dysfunction, dystonia and intermittent encephalopathy. A combined homozygosity mapping and whole exome sequencing approach identified a homozygous splice donor site mutation in *NDUFA4*, a gene previously considered to encode an accessory subunit of complex I.

6.2 Case histories

6.2.1 Patient 6.1 (III-4)

The proband, Patient 6.1 (III-4, Figure 6.1, Tables 6.1 and 6.2), was the fourth child of healthy first cousin Pakistani parents. He presented with lactic acidosis at birth following a normal pregnancy and full-term delivery. Birth weight was 2.7 kg. There was initial normal motor development but gait was later considered 'stiff' and at 24 months he was diagnosed with a spastic diplegia. Speech was delayed and there were moderate learning difficulties. Aged 13 years he suffered his first generalised tonic-clonic seizure and subsequently developed treatment-resistant myoclonus. An electroencephalogram indicated a right temporal focus with inter ictal discharges over the right anterior temporal and frontocentral regions. At 17 years plasma lactate was 2.4 mmol/L and CSF lactate 3.2 mmol/L. CSF protein was also elevated at 0.54 g/L, as was CSF alanine at 45 µg/L (reference 16-36). Brain CT (13 years) and MRI (17 years) were both normal. However, a brain MRI aged 25 years demonstrated T2 hyperintensities in the deep white matter. NCS indicated there was a sensory axonal peripheral neuropathy. Muscle biopsy aged 17 years showed non-specific changes, including increased fibre size variation and intense peripheral staining of some fibres on modified Gomori trichrome, although no true RRF. COX histochemistry was surprisingly normal, and might reflect the existence of residual COX activity measured by an endpoint (rather than kinetic) enzyme assay. EM revealed lipid droplets in some fibres. Spectrophotometric assay of muscle confirmed significant COX deficiency (COX/CS ratio 0.008; controls 0.014-0.034). Cultured skin fibroblasts grown on glucose medium has normal COX activity (COX/CS ratio 2.2; controls >1). Pyruvate dehydrogenase activity was normal in cultured skin fibroblasts, and mutations in *SURF1*, *POLG*, *C10orf2*, and the entire mitochondrial genome were excluded.

Most recent clinical examination aged 32 years showed short stature (5 ft 4 in) and a spastic gait. Cranial nerves were normal. Upper and lower limb examination revealed dystonic posturing and increased tone with pyramidal weakness (MRC grade 4/5). Tendon reflexes were pathologically brisk in arms and legs and plantar responses extensor.

6.2.2 Patient 6.2 (III-3)

Patient 6.2 (III-3, Figures 6.1 and 6.2, Tables 6.1 and 6.2) was an older sibling of Patient 6.1. She was born at term following a normal delivery. Birth weight was 2.3 kg. Growth was poor in the neonatal period but no underlying cause was identified. She had a systolic murmur and mild pulmonary stenosis was found on cardiac catheterisation. At 6 months lactic acidosis was noted, with plasma lactate levels ranging from 3.5-6.6 mmol/L and elevated plasma alanine. There was also evidence of proximal renal tubular acidosis. This was treated with oral sodium bicarbonate. At 10 months she had mild motor delay and she was later diagnosed with speech delay and moderate learning difficulties. There is no history of seizures.

Neurophysiology showed evidence of a predominantly sensory axonal peripheral neuropathy mainly affecting lower limbs, with no evidence of myopathy. Brain MRI (Figure 6.2) showed multiple scattered foci of T2 hyperintensities within the deep white matter of both cerebral hemispheres, medial thalami, at the level of the superior cerebellar peduncles, corticospinal tracts of the pons, right middle cerebellar peduncles, cerebellar hemispheres and descending tracts at the levels of the medulla oblongata. She has not had a muscle biopsy.

Most recent clinical examination aged 34 years showed limited speech and understanding. There was mild upper limb and gait dystonia, but neurological assessment was otherwise normal.

6.2.3 Patient 6.3 (III-6)

Patient 6.3 (III-6, Figure 6.1, Tables 6.1 and 6.2) was a younger sibling of Patients 6.1 and 6.2. She presented at birth following an uneventful pregnancy with lactic acidosis, which resolved with sodium bicarbonate, and intrauterine growth retardation (birth weight was 1.9 kg). She was discharged one month later and continued on oral sodium bicarbonate until aged 7 years. She was subsequently diagnosed with mild learning difficulties, but was otherwise medically stable until the age of 25 years when she developed hypertension and suffered a respiratory arrest requiring tracheal intubation and admission to intensive care. Brain MRI demonstrated T2 hyperintensities in the anterior lateral medulla, posterior pons, and

the thalami, parietal white matter and basal ganglia. Muscle histology demonstrated a mild increase in lipid but was otherwise normal, including COX histochemistry. Spectrophotometric assay of muscle confirmed COX deficiency (COX/CS ratio 0.004; controls 0.014-0.034). She was eventually extubated and established on nocturnal non-invasive ventilation. She required a protracted period of rehabilitation and was discharged 8 months following her initial admission when she was alert and conversing, although was dependent for most care needs. Unfortunately, she later died aged 26 years of a second respiratory arrest caused by presumed extension of her existing or new brainstem lesions.

6.2.4 Patient 6.4 (III-13)

Patient 6.4 (III-13, Figure 6.1, Tables 6.1 and 6.2) was the seventh child of healthy Pakistani parents who are second cousins, and is probably a cousin of Patients 6.1, 6.2 and 6.3. His six siblings are all well. He was a second twin and was born by forceps delivery for breech presentation at 37 weeks' gestation. At birth he was floppy and bradycardic and required cardiopulmonary resuscitation. Apgar scores were 3 at 1 minute and 9 at 5 minutes. He had a mixed respiratory and metabolic acidosis (pH 6.99, pCO2 8.74, bicarbonate 14 mmol/L, base deficit 14.8 mmol/L) and was admitted briefly to the neonatal unit for headbox oxygen treatment, but his respiratory symptoms had settled by 24 hours of age. At 4 months poor growth and mild motor developmental delay were noted. At 2 years he was referred to the metabolic unit because of poor growth, developmental delay and lactic acidosis. At 3 years he developed dystonic posturing of the left arm and respiratory distress due to lactic acidosis, which responded to sodium bicarbonate (1 mmol/kg/day). He had frequent upper respiratory infections during the first 5 years of life. Neurological regression occurred from 4 years, with gradual but progressive loss of skills (walking, speech, cognition) over the next four years until his death at 8 years and 9 months of age.

Examination at 4 years revealed bilateral horizonatal nystagmus, optic atrophy, gait ataxia, tremor, thin musculature and brisk tendon reflexes. At 8 years he also had a four-limb dystonia. He never had seizures or myoclonus.

Plasma lactate ranged from 2.1-8.5 mmol/L and CSF lactate was elevated at 6.4 mmol/L with a paired blood lactate of 5.8 mmol/L. ECHO was normal, and there was no evidence of renal tubulopathy or hearing impairment. MRI brain at 2 years demonstrated abnormal signal in the parietal white matter with no convincing involvement of the basal ganglia or brainstem, whilst magnetic resonance spectroscopy showed an increased lactate peak in the basal ganglia. Muscle histology at 2 years revealed reduced histochemical staining of COX in all muscle fibres and increased lipid in type I fibres. Respiratory chain enzyme activities were not formally determined in muscle, but fibroblast COX activity was normal at 43 nmole/mg protein/min (reference range 30-90) with a normal COX/CS ratio of 1.7 (normal >1).

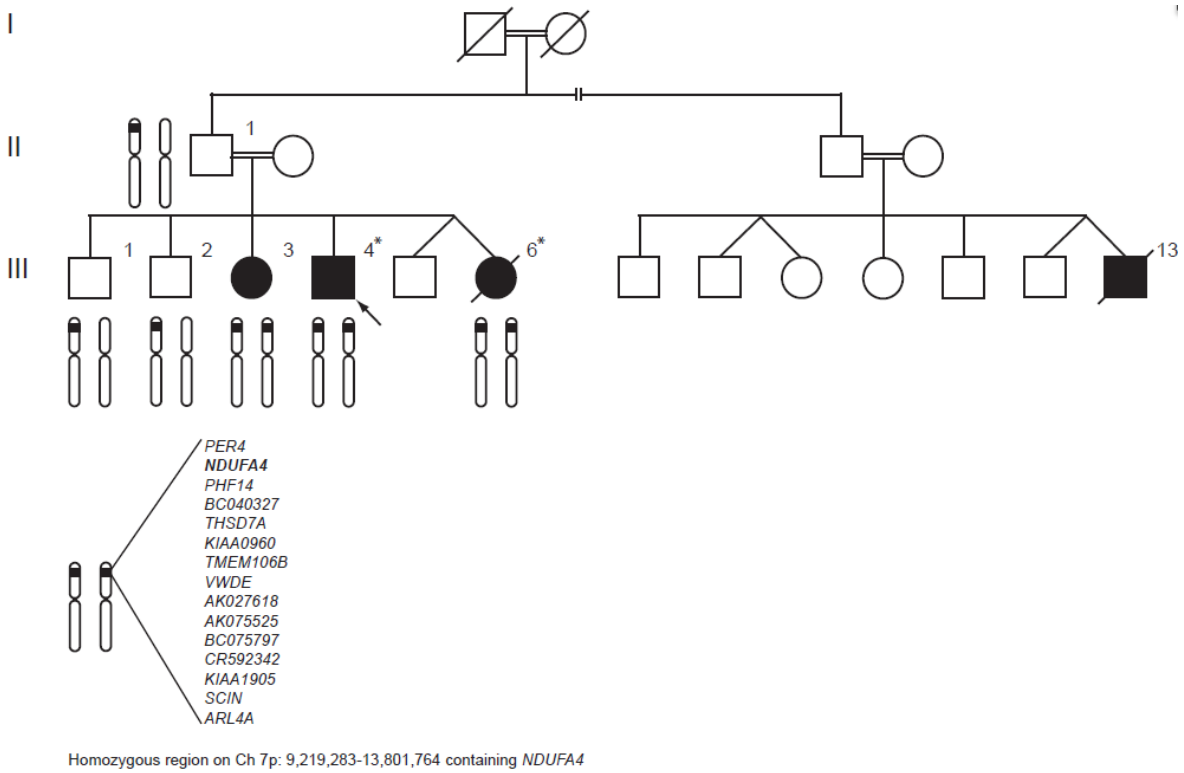

Figure 6.1: Pedigree of consanguineous family harbouring the c.42+1G>C mutation in *NDUFA4*. Arrow indicates proband. Members of the family whose genotype data were used in homozygosity mapping analyses are illustrated by chromosome 7 schematic. Those whose exomes were sequenced are marked with an asterisk (*). Filled symbols indicate affected individuals. Square symbols indicate male gender. Round symbols indicate female gender. Symbols with diagonal strikethrough indicate deceased. Broken line (┤├) indicates the possibility that III-13 is a more distant cousin.

Figure 6.2: Brain MRI of Patient 6.2 characteristic of Leigh syndrome. MR T2-weighted coronal image demonstrates multiple scattered T2 hyperintensities in deep white matter of both cerebral hemispheres (arrow, 1), medial thalami (arrow, 2) and at the level of the superior cerebellar peduncles (arrow, 3). Hyperintensities were also evident in the corticospinal tracts of the pons, right middle cerebellar peduncles, cerebellar hemispheres, and descending tracts at the level of the medulla oblongata (not shown). Similar appearances were evident on the brain MRI of the other affected patients.

Table 6.1: Clinical characteristics of Patients 6.1, 6.2, 6.3 and 6.4 with homozygous c.42+1G>C splice donor site mutation in *NDUFA4*

PATIENT	AGE (years)	CLINICAL PHENOTYPE	CLINICAL MANIFESTATIONS							
			DD	FTT	LD	Dystonia	Myoclonus	Ataxia	UMN signs	Seizures
6.1 (III-4)	34	CLA, LS	L, M	-	+	+	+	+	+	+
6.2 (III-3)	32	CLA, LS	L	+	+	+	-	-	-	-
6.3 (III-6)	Died 26	CLA, LS	L	-	+	-	-	-	-	-
6.4 (III-13)	Died 8	CLA, LS	L, M	+	+	+	-	+	+	-

Abbreviations: CLA = congenital lactic acidosis; DD = developmental delay; FTT = failure to thrive; L = language; LD = learning difficulties; LS = Leigh syndrome; M = motor; UMN = upper motor neuron. Positive symbol (+) = present; Negative symbol (-) = absent.

Table 6.2: Laboratory, neurophysiological, imaging, histopathological and biochemical characteristics of Patients 6.1, 6.2, 6.3 and 6.4 with homozygous c.42+1G>C splice donor site mutations in *NDUFA4*

PATIENT	PLASMA LACTATE	CSF LACTATE	NCS	BRAIN MRI	BRAIN MRS	MUSCLE PATHOLOGY	COX/CS		COX (k/mg/min)
							Muscle (0.014-0.034)	**Fibroblasts (glucose)** (>1)	**Fibroblasts (galactose)** (3.35-3.88)
6.1 (III-4)	1.6-2.4	3.2	Sensory axonal neuropathy	Aged 17: Normal Aged 25: ↑T2 signal deep WM	-	↑lipid	0.008	2.2	1.07
6.2 (III-3)	3.5-6.6	-	Sensory axonal neuropathy	Aged 32: ↑T2 signal deep WM, thalami, brainstem, cerebellum	-	-	-	-	-
6.3 (III-6)	2.5-4.7	-	-	Aged 25: ↑T2 signal parietal WM, BG, thalami, brainstem	-	↑lipid	0.004	-	-
6.4 (III-13)	2.1-8.5	6.4	-	Aged 2 yrs: ↑T2 signal parietal WM	↑Lactate peak in BG	Global ↓COX, ↑lipid	-	1.7	-

Abbreviations: BG = basal ganglia; COX = cytochrome *c* oxidase; CS = citrate synthase; CSF = cerebrospinal fluid; NCS = nerve conduction studies; MRI = magnetic resonance imaging; MRS = magnetic resonance spectroscopy; WM = white matter. Reference ranges: plasma lactate 0.7-2.1 mmol/L; CSF lactate <2 mmol/L; COX/CS in muscle 0.014-0.034; COX/CS in glucose-grown fibroblasts >1; COX/protein in galactose-grown fibroblasts 3.35-3.88 k/min/mg. Hyphen (-) = test not performed.

6.3 Methods

6.3.1 Galactose-containing cell culture medium

For spectrophotometric analysis of respiratory chain enzyme activities and immunocytochemistry of cultured skin fibroblasts, the glucose in the cell culture medium was replaced with 4.5g/L of D-(+)-galactose for 6 days prior to harvesting. See section 2.2 for cell culture methods.

6.3.2 Spectrophotometric analysis

Complex I, complex II+III and complex IV activities were measured in the muscle tissue of Patient 6.1 and 6.3 in the UCLH NHNN NCG Neurometabolic diagnostic laboratory by Dr Iain Hargreaves. Complex IV activity was measured using the glucose-grown cultured skin fibroblasts of Patient 6.1 in the Oxford NCG biochemistry laboratory by Dr Garry Brown. Complex I and IV activities of the galactose-grown cultured skin fibroblasts of Patient 6.1 were measured as described in section 2.3.2.

6.3.3 Homozygosity mapping

Homozygosity is defined as having two identical copies of the same allele. In an outbred population, homozygosity at any particular locus occurs by chance alone. However, the offspring of related parents, as occurs in consanguineous partnerships, usually contain large regions in which multiple, consecutive polymorphic loci are homozygous. In such circumstances, homozygosity is not by chance but by descent. The more closely related the child is to their parents, the greater proportion of the child's genome is likely to be homozygous (parent/child or sibling parents will have offspring with 25% of their genome homozygous-by-descent compared with first cousin parents whose children have 6.25% of their genome homozygous-by-descent), and therefore the higher probability of the child harbouring a rare homozygous disease-causing mutation. Homozygosity mapping is a powerful tool when searching for homozygous mutations in small, closed populations with a limited gene pool. It was first described by Eric Lander in 1987 as a strategy for mapping human genes caused by recessive traits using mapped restriction fragment length

polymorphisms (RFLPs) and the DNA of affected children from consanguineous marriages, with detection of the disease locus by virtue of the fact that the adjacent region will preferentially be homozygous by descent in such inbred children (Lander and Botstein, 1987). Modern techniques utilise microsatellite markers or SNP microarrays rather than RFLPs. Panels of ~300-400 microsatellite markers spaced at ~5 megabase intervals or microarrays that can genotype over one million SNPs (the affymetrix Genome-Wide Human SNP Array 6.0 features 1.8 million genetic markers, including more than 906,600 SNPs and more than 946,000 probes for the detection of copy number variation) are used to identify regions of homozygosity. Despite a mean heterozygosity for individual SNPs of approximately 50% of microsatellites, much smaller regions of homozygosity can be detected with SNP microarrays.

In this particular study, total gDNA was extracted from peripheral blood leucocytes in the UCLH NHNN NCG Neurogenetics diagnostic laboratory as previously described (see section 2.4.1). Subjects II-2, III-1, III-2, III-3, III-4, and III-6 were genotyped using the Illumina 740K OmniExpress SNP array according to the manufacturer's instructions and previous publications (Paisan-Ruiz et al., 2009). All files were visually examined by Dr Anna Sailer using GenomeViewer tool within BeadStudio v3.1 Genotyping module (Illumina Inc., San Diego, CA), where two metrics were assessed: log *R* ratio and B allele frequency. The log *R* ratio gives an indirect measure of copy number of each SNP by plotting the ratio of observed to expected hybridisation intensity. B allele frequency plots the proportion of times an allele is called B at each SNP locus: thus the expected values are 1.0 (B/B), 0.5 (A/B) and 0.0 (A/A). These two statistics allow visualisation of copy number changes and homozygosity mapping. After quality control, the first analysis was visual inspection to determine whether any large insertions/deletions were present, and whether any extended regions of homozygosity were shared by affected individuals and absent in unaffected family members. Subsequent, more detailed analysis used PennCNV to collate the CNV data into Excel tables and to examine the CNV data to look for unique smaller insertions/deletions. The genotyping data with AA, AB and BB were then saved as excel files for affected and unaffected individuals so that shared regions could be easily analysed.

6.3.4 Whole exome sequencing

Genomic DNA (1-3 µg) was sheared to 100–400 bp using a Covaris E210 or LE220 (Covaris, Woburn, MA, USA). Sheared DNA was subjected to Illumina paired-end DNA library preparation and enriched for target sequences (Agilent Technologies; Human All Exon 50 Mb - ELID S02972011) according to manufacturer's recommendations (Agilent Technologies; SureSelectXT Automated Target Enrichment for Illumina Paired-End Multiplexed Sequencing). Enriched libraries were sequenced using the HiSeq platform (IIIumina, Inc., San Diego, CA, USA) as paired-end 75 base reads according to the manufacturer's protocol (see section 2.4.5).

6.3.5 Whole exome sequencing bioinformatic analysis

Autosomal recessive inheritance was assumed in view of the consanguineous lineage, because parents were unaffected, and because all reports of COX deficiency result from loss-of-function genetic defects. The filtering pathway searched for novel (not reported to dbSNP132 and/or 1000 Genomes), homozygous (in view of parental consanguinity), functional SNVs and/or coding indels shared by both affected siblings. Genes predicted to play a role in COX biogenesis were initially searched. However, using this strategy no candidate genes were identified across the entire exome. The stringency of the filtering strategy was subsequently relaxed to include all known nuclear-encoded mitochondrial genes, still assuming recessive inheritance (Pagliarini et al., 2008b).

6.3.6 Automated Sanger sequence analysis of *NDUFA4*

Confirmation and segregation of the c.42+1G>C mutation and screening of 20 additional COX-deficient probands for mutations in *NDUFA4* was assessed using standard dideoxynucleotide chain termination. Amplitaq Gold 360 Mastermix (Applied Biosystems) was used for all PCRs. Oligonucleotides for *NDUFA4* PCR amplification and sequence analysis in gDNA are listed in Table 6.3 below. M13 universal sequences to prime sequencing reactions were added to the 5' end of the primers (5'-tgtaaaacgacggccagt to forward primers and 5'-ccagtatcgacaaaggac to reverse primers) in order to simplify the sequencing reaction setup. Amplification of *NDUFA4* fragments for sequencing of complementary DNA (cDNA) was performed using a forward primer annealing in exon 1 (5'-GTCAGGCCAAGAAGCATCC-3') and

a reverse primer annealing in exon 4 (5-ACACCTAATGTCGTTCGACTT-3'). Primers were designed using Primer3 (http://frodo.wi.mit.edu/primer3/), and Sanger sequencing was performed using M13 primers and BigDye Terminator v.1.1 cycle sequencing kit (Applied Biosystems). The samples were run on a 3730xl DNA Analyzer, assembled and analysed using Seqscape v2.5 software (Applied Biosystems).

Table 6.3: Oligonucleotides for *NDUFA4* PCR amplification and sequence analysis in genomic DNA

	Forward primers (5' to 3')	**Reverse primers (5' to 3')**
Exon 1	GACCAGGTCAGGACGAACAT	GGTGAATGGCAGGCAGTCTG
Exon 2	ATCTCTCGTTGGCCAGTGTT	ACCAAGAGCCGTGTACATTT
Exon 3	AAAGGTTTTGTGAAAGCCAGA	AAGTCGGAATAGGGGTCTCT
Exon 4	CATTGAAGGCTGGAATTTTAGG	CGTATGTATTGTTGACCTTGACCT

6.3.7 RNA extraction

RNA was extracted from whole blood using the Qiagen/PreAnalytix blood RNA system and from cultured cells using the Qiagen/RNeasy Mini Kit following the manufacturer's instructions.

6.3.8 RNA to complementary DNA conversion

Complementary DNA was synthesised from ~1 μg RNA in a 20 μl reaction using the Applied Biosystems high capacity cDNA reverse transcription kit, following the manufacturer's instructions.

6.3.9 Polyacrylamide-gel electrophoresis of amplified complementary DNA

Amplified cDNA fragments were resolved on a denaturing 7% polyacrylamide gel and stained with silver as previously described (Sambrook and Russell, 2001).

	7% gel
40% acrylamide/bis (37.5:1)	5.25 ml
5x TBE (54 g Tris, 27.5 g boric acid, 20 ml 0.5 M EDTA [pH 8.0] per litre)	6 ml
Urea	12.6 g
10% ammonium persulphate	100 μl
TEMED	40 μl
ddH_2O (to a final volume of 30 ml)	

The mixture, except for ammonium persulphate and TEMED, was placed on a roller until the urea had dissolved and then ddH_2O was added to a final volume of 30 ml. Whilst shaking, the plates were cleaned with ddH_2O, ethanol, and with ddH_2O again. The gel casting apparatus (Model AE-6210, Atto Corporation) was then assembled, but not sealed, until ready to add the last two reagents. Once the urea had dissolved the gel mix was filtered into a small beaker. Once ready to pour between the plates 10% APS and TEMED were added whilst on a stirrer. The gel was poured and the comb inserted at an angle to avoid trapping bubbles and left to set for 20-30 min. Sufficient TBE buffer was poured into the gel tank to cover the 'feet' at the bottom. Once the gel had set it was removed from the casting apparatus along with the rubber spacer and placed in the tank with the bevelled plate facing towards the back. TBE was subsequently poured into the rear of the tank almost to the top of the plates. The comb was removed and the wells flushed with a syringe containing buffer using a loading tip to remove any acrylamide. In order to heat the gel it was run for two hours prior to loading at a constant 50 mA (the voltage was set to ~600 V to ensure the amps remained constant). The products were initially run on an agarose gel to determine the optimum loading concentration which was found to be 1 μl along with 2 μl of the denaturing loading buffer (98% formamide, 0.05% xylene cyanol [2%], 0.05% bromophenol blue [2%]). Prior to loading each sample was denatured briefly

at 95°C and each lane was flushed to remove any urea. In order to visualise the PCR products of ~250 bp the gel was run for approximately 2 h 30 min.

6.3.10 Silver staining of polyacrylamide gel

The following solutions were made up to 300 ml using clean bottles rinsed with nitric acid (one part nitric acid to three parts ddH_2O):

Solution 1 (5-10 min, Fix)	**Solution 2 (5 min)**	**Solution 3 (until bands visible on light box)**	**Solution 4 (10-15 min, Stop)**
10% ethanol (30 ml) 0.5% acetic acid (1.5 ml)	0.5 g silver nitrate	4.5 g sodium hydroxide 450 μl formaldehyde (added after solution 2 was used)	2.25 g sodium carbonate

The gel was taken out of the tank and the non-bevelled plate was removed by lifting the plate and teasing the gel off using a clean Gilson tip. The gel was then submerged in solution 1 in a large plastic tray (also washed and rinsed with nitric acid). The gel was then washed in each of the solutions in order for the times specified above using a shaker, rinsing with ddH_2O between each solution. The gel was scanned on an Epson Perfection V700 Photo scanner and subsequently wrapped in Clingfilm and stored at -4°C.

6.3.11 Fluorescent polymerase chain reaction

Fluorescent PCR of cDNA was performed, in order to quantify the wild-type versus mutant cDNA, using a forward primer annealing in exon 1 (5'-GTCAGGCCAAGAAGCATCC-3') and a 6-FAM-labelled reverse primer annealing in exon 4 (5'-ACACCTAATGTCGTTCGACTT-3'), in order to measure the relative quantities of wild-type and mutant transcripts. PCR products were electrophoresed on an Applied Biosystems 3730xl capillary analyzer with a LIZ500 internal size-standard (Applied Biosystems). Data was analysed using GeneMapper v3.7 software (Applied Biosystems).

6.3.12 Western blot analysis of SDS denaturing polyacrylamide gels

Protein steady-state levels were evaluated using western blot analysis of SDS-denaturing polyacrylamide gels probed with antibodies directed against NDUFA4 (1:1,000, Stratech Scientific Ltd, AssaybioTech cat. no. C16821) and MTCO2 (clone 12C4F12, Abcam).

6.3.13 Immunocytochemistry

Immunocytochemistry of the NDUFA4/MTCO1 and NDUFA4/MitoTracker Red CM-H_2XRos (Life Technologies) stained cells was carried as described in Chapter 2. Anti-MTCO1 (clone 1D6E11A8, Abcam) was detected with goat anti-mouse IgG Alexa Fluor 488 (Life Technologies), anti-NDUFA4 (1:300, Stratech Scientific Ltd, AssaybioTech cat. no. C16821) with goat anti rabbit-IgG Alexa 594 or 488 (Life Technologies) and nuclei were counterstained with 1 μg of 4',6-diamidino-2-phenylindole (Sigma) per ml of Citifluor-glycerol-PBS solution (Agar Scientific).

6.3.14 In-gel activity and western blot analysis of one- and two-dimensional blue-native polyacrylamide gels

To establish the optimal concentration of DDM required to analyse NDUFA4 as part of the COX holoenzyme, western blot analysis of 8-16% polyacrylamide gradient blue-native gels loaded with 10 μg of mitochondrial protein extracted from control muscle tissue using serial dilutions of DDM (0.01%, 0.02%, 0.04%, 0.08%, 0.16%, and 0.32%) for mitochondrial membrane protein extraction was performed (Schägger, 1995; Williams et al., 2004d). Blots were developed with antibodies directed against NDUFA4 and MTCO1. Mitochondrial membrane proteins (10 μg), extracted using 0.08% DDM in order to verify co-localisation of the NDUFA4 protein with complex IV, were subsequently applied and run on 3-12% polyacrylamide gradient blue-native gels. For two-dimensional analysis, a single lane was excised from the gel, denatured with 1% SDS and 2% β-mecaptoethanol and resolved by denaturing electrophoresis in the second dimension on an SDS 15% polyacrylamide gel, prior to immunoblotting. Blots were probed with specific antibodies against complex I (anti-NDUFA9; clone 20C11B11B11, Abcam), complex III (anti-UQCRC2; clone 13G12AF12BB11, Abcam), complex IV (anti-MTCO1, anti-MTCO2) and NDUFA4.

Native markers were obtained by reprobing one-dimensional blots for SDHA (anti-SDHA clone 2E3GC1FB2AE2, Abcam) to detect complex II (~125 kDa) and ATP5A1 (anti-ATP5A1 clone 7H10BD4F9, Abcam) to detect holo-complex V (~600 kDa), the F_1 portion of complex V (~400 kDa) and the free subunit (55 kDa).

6.4 Results

6.4.1 Spectrophotometric analysis

Despite the normal COX activity measured using glucose-grown cultured skin fibroblasts, a repeat assay using whole cell lysate of cultured skin fibroblasts grown on galactose-containing medium did demonstrate reduced COX activity (1.07 k/min/mg; control mean±standard deviation [*n*=5]: 3.60±0.24 k/min/mg) (Table 6.2). Complex I activity in fibroblasts grown under the same conditions was normal (37.3 nmol/min/mg; control mean±standard deviation [*n*=5]: 19.4±7.2 nmol/min/mg).

6.4.2 Homozygosity mapping and whole exome sequencing bioinformatic analysis

To identify areas of shared homozygosity amongst affected relatives, six family members were genotyped (three affected and three unaffected, Figure 6.1A). Two large regions of shared homozygosity mapped to chromosome 7p (nucleotides 9,219,283-13,801,764, containing 15 protein-coding genes; and nucleotides 19,034,191-29,250,335, containing 92 protein-coding genes, Table 6.4). As no candidate genes for COX deficiency were present in either region, it was initially concluded that a small area of homozygosity had been overlooked. Whole exome sequencing was therefore subsequently performed in two affected family members: Patient 6.1 (III-4); and Patient 6.3 (III-6).

A total of 78,004 shared variants were identified (Table 6.5). Of these, 19,389 were shared homozygous SNVs and indels and 190 of these were novel variants. Thirteen of these homozygous variants were predicted to be functional. The only gene within this group predicted to encode a protein product known to localise to the mitochondrion was *NDUFA4*, which contained a homozygous splice donor site mutation (c.42+1G>C). *NDUFA4* was also a gene within one of the previously identified regions of homozygosity.

Table 6.4: Two large regions of homozygosity shared by Patients 6.1 (III-4), 6.2 (III-3) and 6.3 (III-6)

Region 1 (Ch 7p: 9,219,283-13,801,764) containing genes (15)
*PER4, **NDUFA4**, PHF14, BC040327,THSD7A, KIAA0960, TMEM106B, VWDE, AK027618, AK075525, BC075797, CR592342, KIAA1905, SCIN, ARL4A*
Region 2 (Ch 7p: 19,034,191-29,250,335) containing genes (92)
CR623750, TWIST1, BC043576, FERD3L, TWISTNB, TMEM196, ABCB5, SP8, ITGB8, MACC1, RPL23P8, SP4, DNAH11, CDCA7L, RAPGEF5, MGC87042, AK123961, LOC541472, IL6, C7orf30, TOMM7, SNORD93, KLHL7, NUPL2, AK057873, GPNMB, BC065766, IGF2BP3, IMP-3, TRA2A, hAWMS1, CLK2P, CCDC126, C7orf46, STK31, FAM126A, DRCTNNB1A, AK054880, RPS2P32, DKFZp434E052, DFNA5, NPY, MPP6, CYCS, ICERE-1, OSBPL3, C7orf31, NPVF, SNX10, MIR148A, NFE2L3, HNRNPA2B1, CBX3, hp1-gamma, SNX10, LOC441204, KIAA0087, C7orf71, LOC285941, SKAP2, HOXA2, HOXA3, AK311383, BC035889, HOXA5, HOXA6, AX747263, DQ655986, AK096334, HOXA7, HOXA9, MIR196B, HOXA10, HOXA11, HOXA11AS, HOXA13, AK093987, HIBADH, EVX1, TSL-A, TAX1BP1, BC034444, NS5ATP1, JAZF1, LOC402644, CREB5, BC087859, KIAA0644, DQ601810, CPVL, AK124888, CHN2

Table 6.5: Identification of shared candidate genes for cytochrome *c* oxidase deficiency in Patient 6.1 (III-4) and 6.3 (III-6) using exome resequencing

Filter	**III-4**	**III-6**	**Shared variants**
Total number of variants	140456	140859	78004
Total number of homozygous variants	50868	50832	28320
Number of homozygous PASS SNVs and indels	26379	25289	19389
Novel homozygous PASS SNVs and indels	442	412	190
Functional novel homozygous PASS SNVs and indels	46	40	13
Functional novel homozygous PASS SNVs and indels with predicted mitochondrial localisation	2	2	1
	IARS	*FTSJ2*	
	NDUFA4	*NDUFA4*	***NDUFA4***

Abbreviations: indel = insertion/deletion; PASS = variants that have passed the Genome Analysis Toolkit (GATK) filter criteria; SNV(s) = single nucleotide variant(s).

6.4.3 Automated Sanger sequence analysis of *NDUFA4*

Sanger sequencing demonstrated that all four affected individuals were homozygous for the mutation (Figure 6.3A, Patient 6.2 shown), whilst three unaffected family members (II-2, III-1, and III-2) were heterozygous (Figure 6.1A). A further 20 probands with isolated COX deficiency were screened for mutations in *NDUFA4* but no further variants were identified.

6.4.4 Transcriptional analysis of c.42+1G>C mutation

To study the effect the c.42+1G>C mutation had on mRNA splicing, *NDUFA4* cDNA fragments were amplified, after generation from reverse transcription of mRNA extracted from whole blood and cultured skin fibroblasts. The PCR products were resolved on a denaturing 7% polyacrylamide gel followed by silver staining. This revealed two fragments in blood: (1) a band measuring 241 bp, corresponding to the wild-type transcript, which was present in all samples but at much lower levels in the affected subjects (III-3 and III-4) compared with an unaffected carrier (II-2) and the control; and (2) a band at 245 bp which was absent in the control sample but present at high levels in the affected subjects with lower levels detectable in the unaffected carrier. Cultured skin fibroblasts demonstrated a 245 bp fragment in the patient studied (III-4), with no evidence of wild-type transcript (Figure 6.3B). Low-level wild-type cDNA sequence was observed in the sequencing electropherograms of both affected individuals (Figure 6.3C, Patient 6.2 shown), which was also demonstrated by fluorescent PCR using FAM-labelled primers (Figure 6.4). These data indicate that the c.42+1G>C mutation does not appear to completely abolish correct splicing of *NDUFA4* exon 1 to exon 2 in blood. Sanger sequencing of the PCR products revealed that the first 4 bp of intron 1 are retained following activation of a cryptic splice site 4 bp downstream of the c.42+1G>C mutation (Figure 6.3A, C). This frameshift is predicted to introduce a premature stop codon (TAA) 105 bp downstream in exon 3. If translated, the resultant protein would consist of 14 in-frame amino acids followed by 35 out-of-frame amino acids (compared to the 81 amino acid wild-type protein).

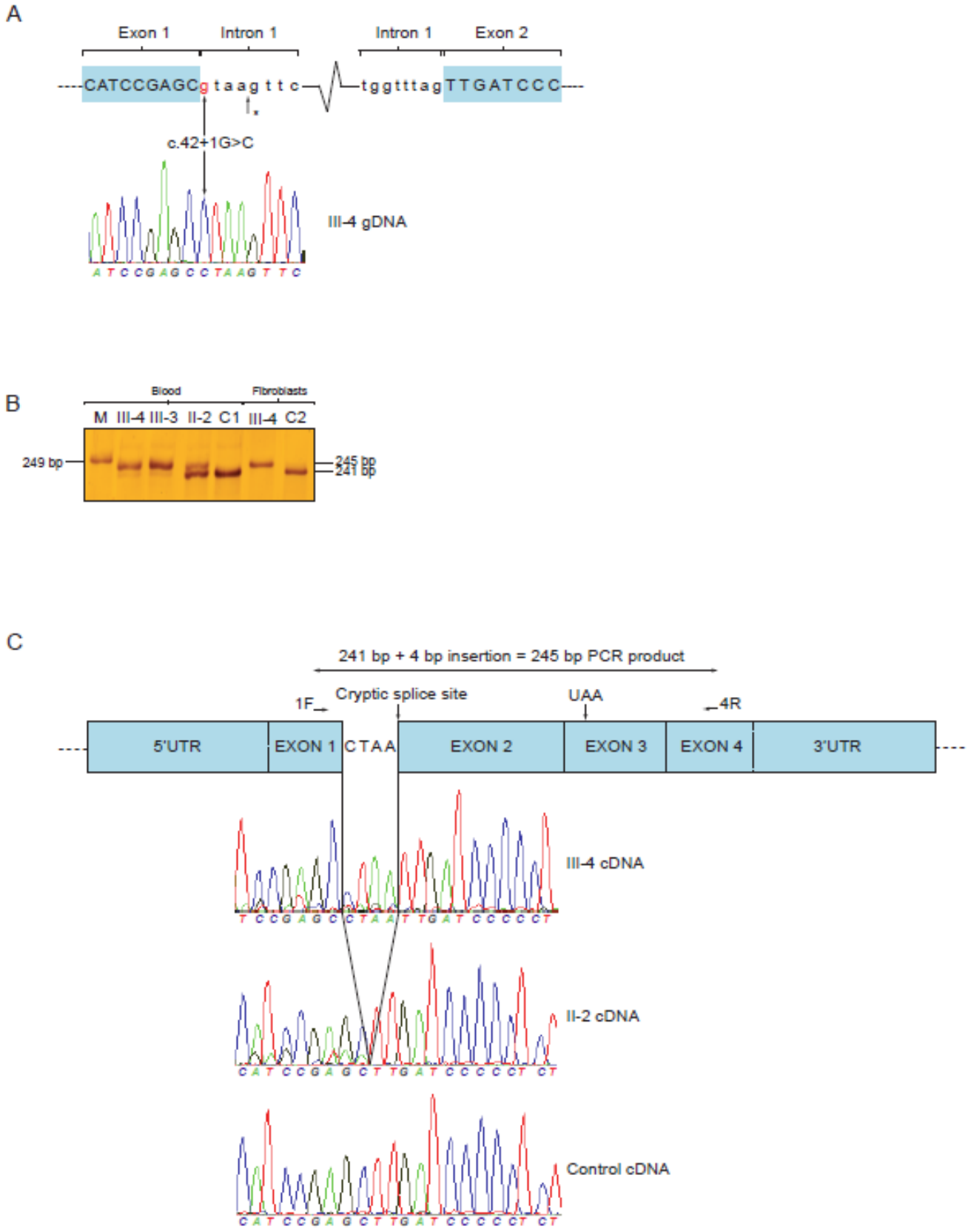
A
Exon 1
Intron 1
Intron 1
Exon 2
CATCCGAGCg t a a g t t c
t g g t t t a g TTGATCCC
c.42+1G>C
III-4 gDNA
B
Blood
Fibroblasts
M III-4 III-3 II-2 C1 III-4 C2
249 bp
245 bp
241 bp
C
241 bp + 4 bp insertion = 245 bp PCR product
1F
Cryptic splice site
UAA
4R
5'UTR
EXON 1
CTAA
EXON 2
EXON 3
EXON 4
3'UTR
III-4 cDNA
II-2 cDNA
Control cDNA

Figure 6.3: Schematic showing activated cryptic splice site downstream to the c.42+1G>C mutation causes a frameshift and introduces a premature stop codon in mRNA, and silver-stained polyacrylamide gel of Patient 6.1 and 6.2 complementary DNA. Schematic demonstrating location of the c.42+1G>C mutation within *NDUFA4* intron 1 and homozygous mutation in forward genomic DNA sequencing of an affected subject (A). Position of cryptic splice site activated adjacent to the next GT dinucleotide 4 base-pairs (bp) downstream of c.42+1G>C is marked with an asterisk (*). Silver-stained polyacrylamide gel of amplified complementary DNA extracted from blood and cultured skin fibroblasts alongside a 249 bp molecular weight marker (M) (B). In blood, Patient 6.2 (III-3) and Patient 6.1 (III-4) (affected siblings) have a strongly staining (mutant) band at 245 bp and a faintly staining (wild-type) band at 241 bp, whilst II-2 (unaffected father) has a strongly staining band at 241 bp and a faintly staining band at 245 bp. In cultured skin fibroblasts, III-4 only has a band at 245 bp. The control blood (C1) and cultured skin fibroblasts (C2) only have a band at 241 bp. Schematic depicting the mutant *NDUFA4* transcript retaining 4 bp of intron 1, with sequencing electropherograms below (reverse sequencing shown) (C). Close inspection of the mixed electropherogram 5' of exon 2 in III-4 confirmed that wild-type sequence was present at low levels (also seen in Patient 6.2, data not shown). Mutant sequence can also be seen in II-2. Abbreviations: 1F and 4R = exonic primer binding sites; UAA = premature stop codon.

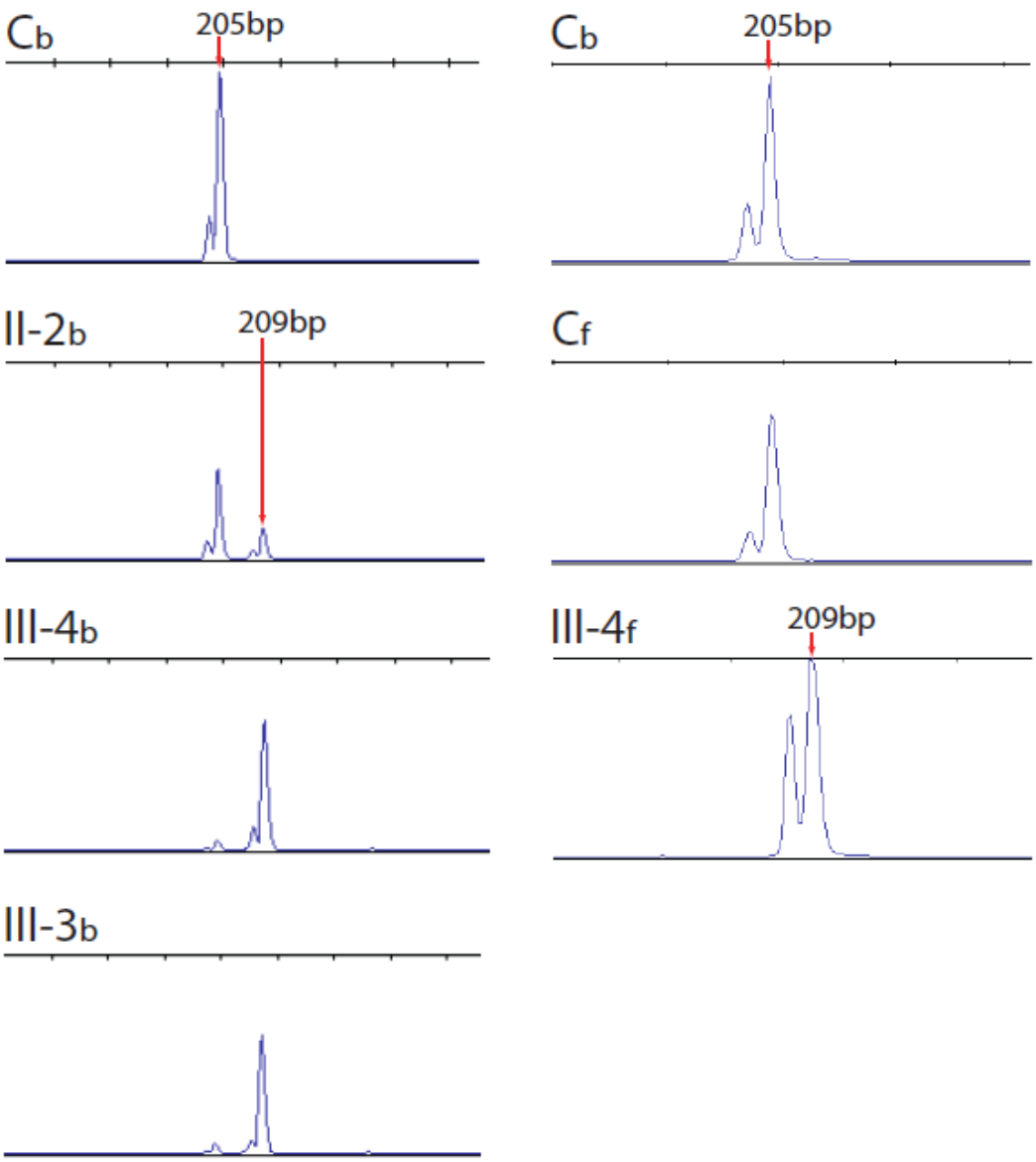

Figure 6.4: Fluorescent PCR of Patient 6.1 and 6.2 complementary DNA using a 6-FAM-labelled reverse primer annealing in exon 4. Patients 6.2 (III-3) and 6.1 (III-4) (affected siblings) have a large peak measuring 209 bp representing mutant PCR product and a small peak measuring 205 bp representing wild-type PCR product in blood. Patient 6.1 (III-4) has only mutant PCR product detectable in fibroblasts. Subject II-2 (unaffected father) has a large wild-type peak (205 bp) and a small mutant peak (209 bp) present. Control (C) shows wild-type peak (205 bp) only. Abbreviations: b = blood; f = fibroblasts.

6.4.5 Western blot of SDS denaturing polyacrylamide gels and immunocytochemistry

NDUFA4 protein was undetectable in all affected subjects examined (muscle tissue of III-4, III-6 and III-13, cultured skin fibroblasts of III-4). Steady-state level of the mitochondrially encoded COX subunit MTCO2 was markedly reduced in the muscle tissue of one patient compared with the mean MTCO2 value of four controls (MTCO2 level in III-6 56% of controls). The steady-state MTCO2 subunit levels in III-6 and III-13 were comparable to the control muscle tissue samples (Figure 6.5A). Immunocytochemistry also showed absent NDUFA4 protein in cultured skin fibroblasts (III-4) with normal mitochondrially encoded COX subunit MTCO1 (Figure 6.5B). MitoTracker confirmed co-localisation of NDUFA4 in control fibroblasts (Figure 6.6).

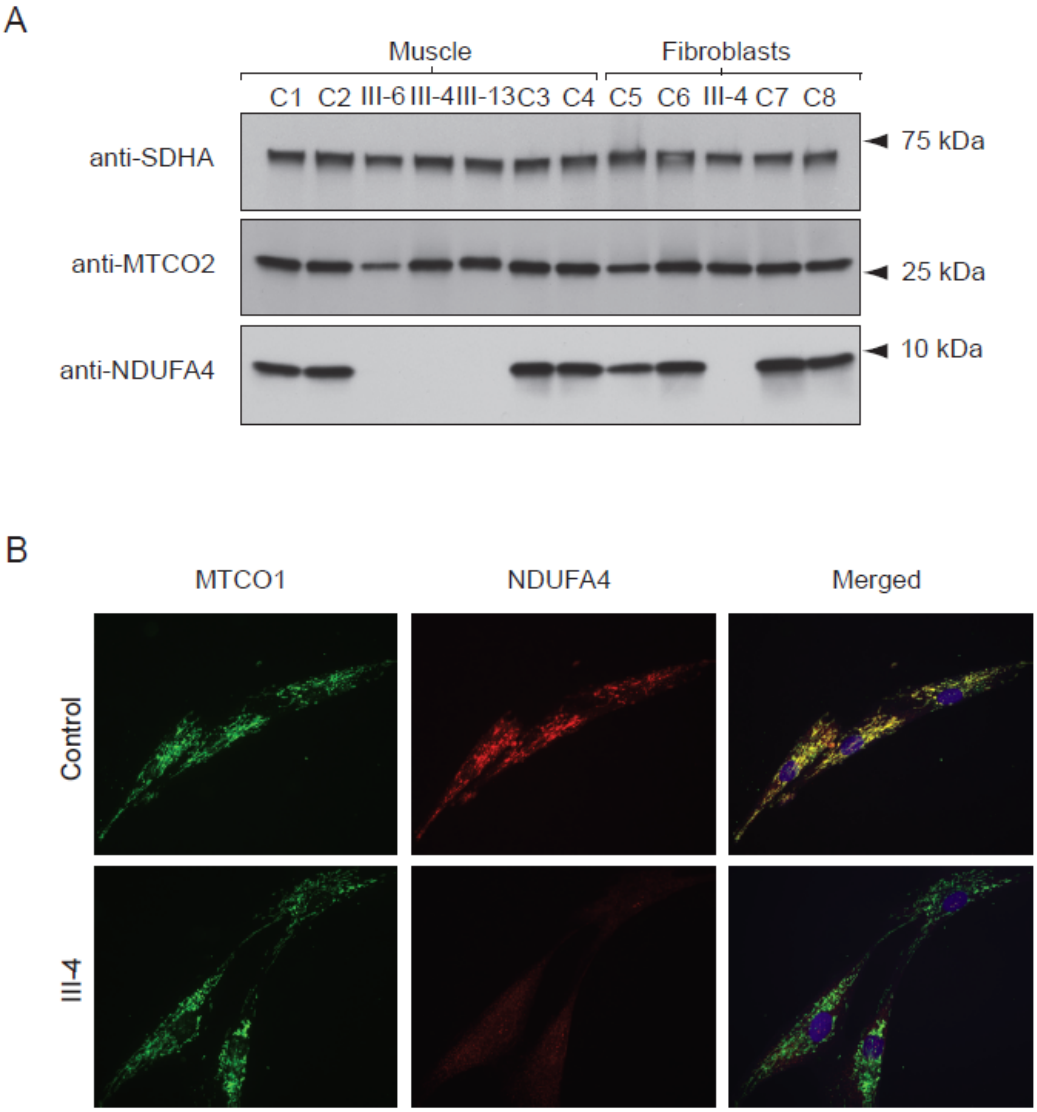

Figure 6.5: Western blot analysis of an SDS polyacrylamide gel and micrographs of control and Patient 6.1 fibroblasts immunocytochemically stained for NDUFA4 and MTCO1. SDS polyacrylamide gel loaded with 10 μg of mitochondrial protein pellets extracted from muscle tissue of Patients 6.1 (III-4), 6.3 (III-6) and 6.4 (III-13), and cultured skin fibroblasts of Patients 6.1 (III-4) compared with controls (C1-8) (A). Blots were developed with antibodies directed against SDHA, MTCO2 and NDUFA4. The antibody to complex II subunit SDHA was used to confirm equal protein loading. Micrographs of control and Patient 6.1 (III-4) fibroblasts immunocytochemically stained for NDUFA4 (red fluorescence) and MTCO1 (green fluorescence) and counterstained with the DNA fluorochrome 4',6-diamidino-2-phenylindole (blue fluorescence) (B). Note that NDUFA4 is absent from patient cells whilst MTCO1 levels are comparable to the control cells.

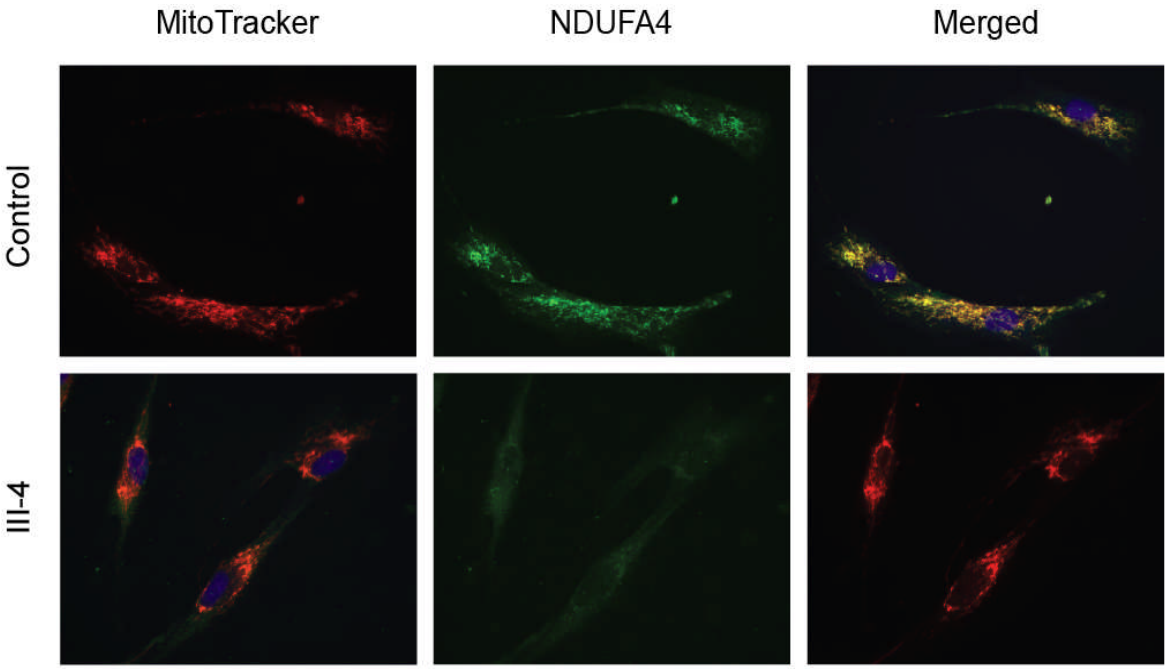

Figure 6.6: Micrographs of control and Patient 6.1 (III-4) fibroblasts immunocytochemically stained for MitoTracker (red fluorescence) and NDUFA4 (green fluorescence) and counterstained with the DNA fluorochrome 4',6-diamidino-2-phenylindole (blue fluorescence). Note that NDUFA4 co-localises with MitoTracker in control cells whist it is absent from patient cells.

6.4.6 In-gel activity and western blot analysis of one- and two-dimensional blue-native polyacrylamide gels

In-gel activity staining of blue-native gels supported spectrophotometric analysis of respiratory chain enzyme with normal complex I and reduced complex IV in the muscle tissue of Patients 6.1 (III-4) and 6.3 (III-6) (Figure 6.7A). Recent work suggests an interaction of NDUFA4 with complex IV which is disrupted when high concentrations (>1.5%) of DDM, the standard detergent used to purify complex IV for crystallisation purposes, are used (Balsa et al., 2012a). To establish the optimal concentration of DDM required to analyse NDUFA4 as part of COX holoenzyme, western blot analysis of blue-native polyacrylamide gels loaded with 10 μg of mitochondrial enriched protein pellets extracted from control muscle tissue using serial dilutions of DDM for mitochondrial membrane protein extraction was performed (Schägger, 1995; Williams et al., 2004d). Blots were developed with antibodies directed against NDUFA4 and MTCO1. This analysis demonstrated that dissociation of NDUFA4 subunit from the COX enzyme complex occurred when >0.08% DDM was used to extract mitochondrial membrane proteins, whilst ≤0.08% DDM allowed detection of NDUFA4 as part of the COX enzyme complex (Figure 6.7B). Western blot analysis of respiratory chain enzymes extracted using 0.08% DDM in order to verify interaction of the NDUFA4 protein with complex IV was subsequently performed (Figure 6.7C). Analysis of one-dimensional blots of blue-native gels showed complex IV holoenzyme was present in the muscle tissue of III-4 with no abnormal subassemblies, whilst one- and two-dimensional blots confirmed association of NDUFA4 with complex IV in the control.

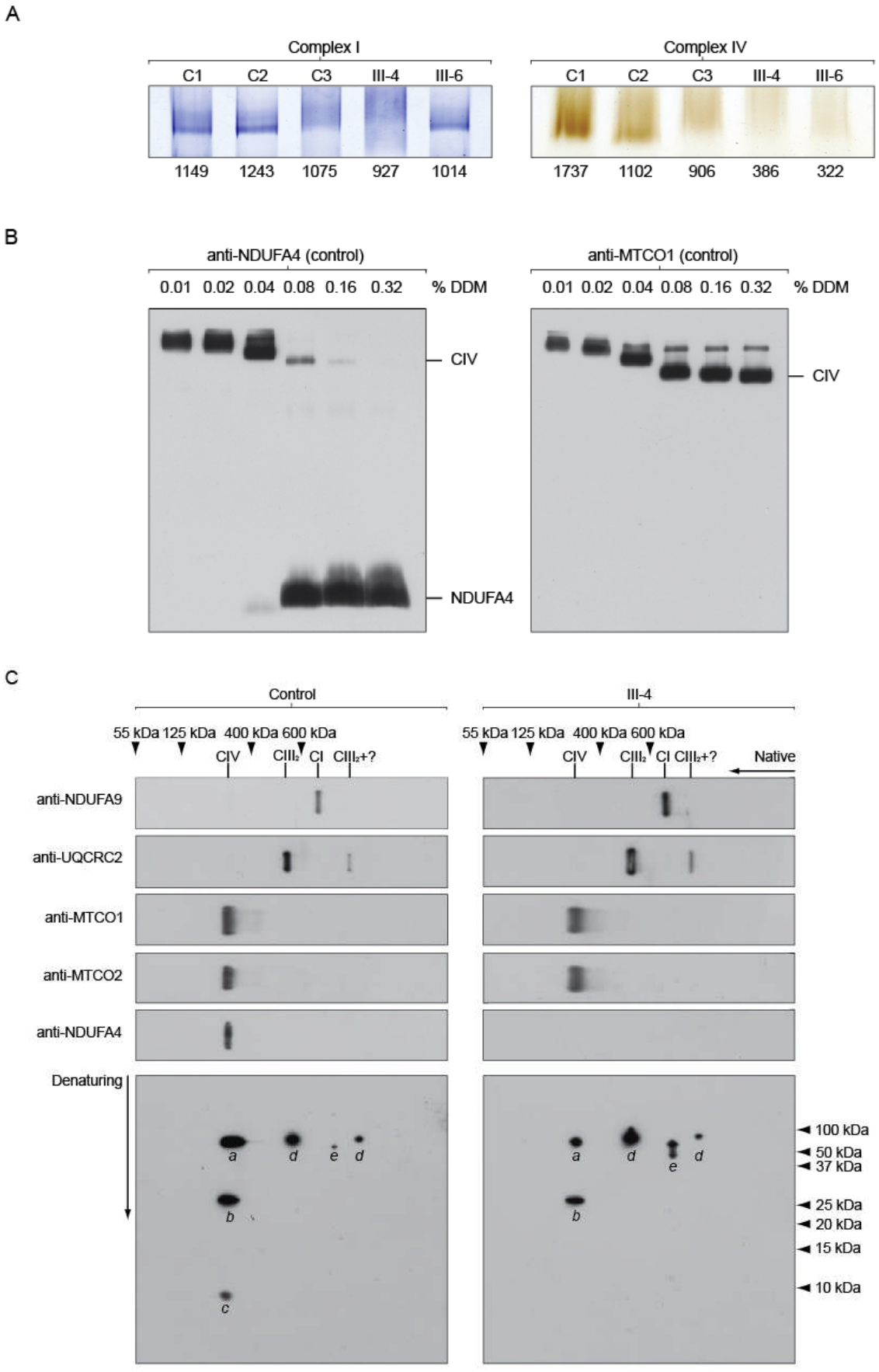
A
Complex I
C1
C2
C3
III-4
III-6
1149
1243
1075
927
1014
Complex IV
C1
C2
C3
III-4
III-6
1737
1102
906
386
322
B
anti-NDUFA4 (control)
0.01 0.02 0.04 0.08 0.16 0.32 % DDM
CIV
NDUFA4
anti-MTCO1 (control)
0.01 0.02 0.04 0.08 0.16 0.32 % DDM
CIV
C
Control
55 kDa 125 kDa 400 kDa 600 kDa
CIV
CIII2
CI
CIII2+?
III-4
55 kDa 125 kDa 400 kDa 600 kDa
CIV
CIII2
CI
CIII2+?
Native
anti-NDUFA9
anti-UQCRC2
anti-MTCO1
anti-MTCO2
anti-NDUFA4
Denaturing
a
d
e
d
b
c
a
d
e
d
b
100 kDa
50 kDa
37 kDa
25 kDa
20 kDa
15 kDa
10 kDa

Figure 6.7: In-gel activity and western blot analysis of one- and two-dimensional blue-native polyacrylamide gels. In-gel activity of complex I and IV in 3-12% polyacrylamide blue-native gels loaded with 70 μg of mitochondrial enriched protein pellets extracted from control (C1-3) and the muscle tissue of Patient 6.1 (III-4) and 6.3 (III-6) (A). Complex I activity is comparable amongst the control and Patient 6.1 and 6.3. However, significant reduction in complex IV activity is demonstrated in patient muscle tissue. Smearing of complex I can be seen in C3 and Patient 6.1 due to high amount of protein loaded. The measured staining intensity is indicated below each lane. Western blot analysis of blue-native polyacrylamide gels loaded with 10 μg of mitochondrial protein pellets extracted from control muscle tissue (B). The following concentrations of n-dodecyl β-D-maltoside (DDM) were used to extract mitochondrial membrane proteins: 0.01%; 0.02%; 0.04%; 0.08%; 0.16%; 0.32%. Proteins were run on 8-16% polyacrylamide gradient blue-native gels to visualize the free NDUFA4 protein subunit (left panel), and were also probed for MTCO1 to examine the complex IV associations (right panel). Mitochondrial membrane proteins (10 μg), extracted using 0.08% DDM in order to verify co-localization of the NDUFA4 protein with complex IV (also see Figure 6.7B), were applied and run on 3-12% polyacrylamide gradient blue-native gels using the muscle tissue of Patient 6.1 and a control (C). For two-dimensional analysis a single lane was excised from the gel, denatured, and resolved by denaturing electrophoresis in the second dimension on an SDS polyacrylamide gel, prior to immunoblotting. One-dimensional native blots are shown above two-dimensional denatured blots to aid identification of protein spots. Blots were probed with specific antibodies against complex I (anti-NDUFA9), complex III (anti-UQCRC2), complex IV (anti-MTCO1, anti-MTCO2) and NDUFA4. Native markers were obtained by reprobing one-dimensional blots for SDHA to detect complex II (~125 kDa) and ATP5A1 to detect holo-complex V (~600 kDa), the F_1 portion of complex V (~400 kDa) and the free subunit (55 kDa). Abbreviations: CI = complex I; $CIII_2$ = complex III dimer; CIV = complex IV; *a* = MTCO1; *b* = MTCO2; *c* = NDUFA4; *d* = UQCRC2; *e* = NDUFA9.

6.5 Discussion

The work presented in this chapter focuses on a large consanguineous Pakistani family with COX-deficient Leigh Syndrome of unknown genetic aetiology. Through a combined homozygosity mapping and whole exome sequencing approach, a homozygous splice donor site mutation was identified in *NDUFA4*, a gene previously considered to encode a subunit of respiratory chain complex I. Transcriptional studies demonstrated the c.42+1G>C transversion significantly reduces wild-type *NDUFA4* mRNA and produces an aberrant transcript which predicts a translated protein comprising 14 in-frame amino acids followed by 35 out-of-frame amino acids. Western blot analysis of denaturing gels and immunocytochemistry revealed undetectable steady-state NDUFA4 protein levels indicating that this mutation causes a loss-of-function effect in the homozygous state.

The existence of some very low level wild-type *NDUFA4* transcripts in patients harbouring the c.42+1G>C mutation might explain the slower natural history and the comparatively milder clinical phenotype observed; most previously reported patients with nuclear-encoded COX deficiency exhibit severe phenotypes resulting in early childhood death. Interestingly, only mutant transcript alone was detected in cultured skin fibroblasts, despite apparently normal fibroblast COX activity observed in patient III-4 using a glucose-containing culture medium. Cells cultured with galactose as a carbon source are not able to produce ATP through glycolysis and are entirely dependent on OXPHOS for their ATP synthesis (Petrova-Benedict et al., 1992). Biochemical assays were therefore repeated with cells grown in galactose-containing medium for 6 days in order to accentuate the underlying defect in OXPHOS. In contrast to III-4 fibroblasts grown in glucose containing medium, III-4 fibroblasts grown in galactose-containing medium showed a clear COX deficiency. These observations indicate that current diagnostic procedures which typically use glucose as a carbon source in the culture medium may not detect a reduction in COX activity.

Balsa and colleagues (2012) found that >1.5% of DDM disrupted the binding of NDUFA4 with complex IV in HeLa cell mitochondria, whilst in the experiments reported here >0.08% of DDM disrupted the binding in human muscle mitochondrial preparations. The discrepancy in the concentration of DDM required to dissociate

NDUFA4 from the COX enzyme complex may be explained by differences in the buffer conditions or tissue-types used. DDM extractions were performed in 1 M ε-amino-n-caproic acid, 50 mM bistris (pH 7.0) (Schägger, 1995). The buffer conditions used by Balsa and colleagues were not specified.

These data confirm that NDUFA4 is not required for assembly of the other COX subunits since COX enzyme complex with no abnormal subassemblies were detected on native gels of patient mitochondrial membrane proteins. In addition, the observation that COX activity is retained following its purification using concentrations of DDM known to disrupt NDUFA4 (Sinjorgo et al., 1987) implies that NDUFA4 is not directly required for catalysis per se. However, deficiency of NDUFA4 clearly impairs COX activity in muscle tissue and cultured skin fibroblasts in patients harbouring homozygous loss-of-function *NDUFA4* mutations. NDUFA4 is probably a subunit of COX rather than an assembly factor because blots of two-dimensional blue-native polyacrylamide gels demonstrated a clear association between NDUFA4 and the COX enzyme complex. It is likely that NDUFA4 is required during the biogenesis of COX to become an active enzyme and remains loosely associated with the enzyme complex. In addition, a critical interaction must occur between NDUFA4 and the remaining COX subunits during biogenesis of the enzyme complex which is essential for overall COX activity. For example, it is possible that NDUFA4 facilitates folding of MTCO1 or is involved in addition or modification of prosthetic groups that affects downstream catalysis but not assembly of the enzyme. The precise nature of this interaction requires further study.

CHAPTER 7

Discussion

CHAPTER 7

7. Discussion

The aims of this thesis were to characterise new clinical phenotypes and to identify the underlying causative pathogenic mutations in both known and novel nuclear genes in adult patients with clinically and/or biochemically suspected mitochondrial disease. To investigate the latter, three main experimental strategies were adopted: 1) in patients where long PCR and/or Southern blotting genetic analysis had demonstrated impaired mtDNA maintenance, as evidenced by multiple mtDNA deletions, the candidate nuclear gene *RRM2B* was sequenced, after *POLG* and *C10orf2* mutations were excluded; 2) in a non-consanguineous pedigree where spectrophotometric analysis of the RC enzymes indicated complex IV deficiency, and mutations in mtDNA and a number of candidate nuclear genes had been excluded, a whole-exome sequencing approach in the affected individual was utilised; 3) in a consanguineous kinship with biochemical evidence of isolated complex IV deficiency, in whom mutations in mtDNA and other candidate nuclear genes were excluded, a combined homozygosity mapping and whole-exome sequencing approach was applied.

This work contributes to current understanding of both the phenotypic presentation and molecular basis of mitochondrial disease. Firstly, the characterisation of new disease phenotypes associated with mutations in both mitochondrial *(MT-ATP6)* and nuclear (*POLG* and *COX10*) genes expands the clinical spectrum of mitochondrial dysfunction and should increase the probability that a genetic diagnosis is achieved in such patients; *MT-ATP6/8* sequencing is now routinely performed in the UCLH NHNN NCG Neurogenetics diagnostic laboratory in patients with CMT2 following the findings reported in Chapter 3 that mutations in these genes can cause an isolated axonal neuropathy. Secondly, the finding that *COX10* mutations link to adult COX deficiency highlights the remarkable variability in clinical severity associated with human COX deficiency. It also raises important questions concerning the precise biological mechanisms underpinning the relatively mild clinical phenotype exhibited by the patient despite harbouring a severe biochemical defect. Understanding these cellular compensatory processes could potentially facilitate future treatment

strategies for human COX deficiency. Thirdly, the discovery that dysfunction of the NDUFA4 protein, previously assigned to be a complex I subunit, causes human COX deficiency confirms its essential role in COX function and builds upon existing published work using cell lines which suggests NDUFA4 is actually a component of complex IV.

7.1 Novel adult mitochondrial clinical phenotypes

7.1.1 m.9185T>C in *MT-ATP6* causes axonal Charcot-Marie-Tooth disease

One of the major unresolved challenges in neuromuscular disease is the determination of the genetic basis of inherited axonal neuropathy (CMT2). Although a genetic diagnosis is achieved in the majority of inherited demyelinating neuropathies (CMT1), this is not the case in inherited axonal neuropathies (Reilly and Shy, 2009; Reilly et al., 2011). Molecular defects are only detected in ~35% of patients with CMT2 and 15% of patients with dHMN (Saporta et al., 2011; Dierick et al., 2008). There is overlap both clinically and genetically between CMT2 and dHMN, and mutations in *HSPB1*, *HSPB8*, *TRPV4*, *BSCL2* and *GARS* are all reported to cause either phenotype (Tang et al., 2005; Irobi et al., 2004; Evgrafov et al., 2004; Auer-Grumbach et al., 2005; Antonellis et al., 2003; Zimoń et al., 2010), but are only identified in a small minority of cases.

In Chapter 3, four unrelated families with CMT2 caused by the known pathogenic m.9185T>C mutation in the mitochondrial-encoded *MT-ATP6* gene are described. It is notable that all of the patients presented had previously been assessed by experienced clinicians, and based on detailed clinical and electrophysiological evaluation were considered to have CMT2. All but one of these cases was homoplasmic for the m.9185T>C mutation. However, despite three of the four pedigrees exhibiting a matrilineal pattern of inheritance, an underlying mitochondrial basis for disease had not previously been considered due to the relatively peripheral nerve-specific disease phenotype. The patients presented could be broadly divided into four clinical severity-related groups according to their m.9185T>C mutant load: (Group 1) unaffected individuals (<64% mutant load); (Group 2) individuals without

symptoms or signs of peripheral neuropathy but with UMN signs (64-79% mutant load); (Group 3) individuals with signs and symptoms of an UMN axonopathy (80-91% mutant load); (Group 4) affected individuals with motor-predominant CMT2 with or without UMN signs (92-100% mutant load).

The m.9185T>C variant was originally reported in a seven year-old patient who developed sudden onset ptosis, ophthalmoparesis and fatigue having previously been well (Moslemi et al., 2005). Although isolated axonal neuropathy is documented at 85% m.9185T>C heteroplasmy, higher mutant loads have been reported to cause a more severe neurological phenotype, including NARP and early and late-onset LS (Castagna et al., 2007; Childs et al., 2007; Moslemi et al., 2005; Saneto and Singh, 2010). Families 3.2, 3.3 and 3.4 exhibited surprising tissue-specificity of disease expression considering they had homoplasmic m.9185T>C mutant levels detected in blood, urine, skin and muscle. Unlike previous reports that suggest disease expression requires more than 85% mutant load (Moslemi et al., 2005; Castagna et al., 2007), we found the threshold for disease manifestation to be lower in our cohort; for example, one asymptomatic individual (Figure 3.3, Family 3.2, Patient III-5) displayed pyramidal tract signs with a mutant load of 73%.

It is unclear why some patients harbouring homoplasmic levels of m.9185T>C should develop a tissue-specific peripheral neuropathic phenotype, whilst other reported patients and families with similar mutant loads develop a multi-system neurological syndrome such as LS. Variable clinical severity in patients with similar mutant loads has been reported with a number of known pathogenic mtDNA mutations. It is possible this variability relates to subtle differences in tissue heteroplasmy; however, no correlation has been shown between the presence of neuropathy and muscle m.3243A>G mutant levels despite the disease phenotype being more severe in the patients with neuropathy (Kärppä et al., 2003). This finding suggests there may be additional factors that increase the susceptibility of certain patients to neuropathy, such as activation of nuclear encoded genes that enhance pathways which partially compensate for aberrant complex V function or reduced ATP production. This hypothesis requires further study. The precise molecular mechanisms linking respiratory chain dysfunction to axonal degeneration are not determined. One

possibility is that axonal degeneration relates to loss of the axon membrane potential as a consequence of failure of the energy-dependent Na^+/K^+ ATPase pump, comparable to ischaemia. However, a recent study did not show detectable changes in nerve excitability in patients with mitochondrial disease, as would be expected if there was significant axonal depolarisation due to failure of energy-dependent systems (Ng et al., 2010a).

The data presented adds to the increasing evidence that mitochondrial dysfunction is an important cause of CMT2. *MT-ATP6* mutations should be considered early in the diagnostic evaluation of patients with inherited axonal neuropathies.

7.1.2 Distal myopathy associated with novel *POLG* mutations

POLG mutations account for up to 25% of mitochondrial disease (Chinnery and Zeviani, 2008) and more than 150 different pathogenic mutations are reported (http://tools.niehs.nih.gov/polg/). They are a heterogeneous group which frequently affect multiple organ systems and exhibit variable clinical severity and age of onset. Patients with identical molecular defects can be almost as diverse as patients with different *POLG* mutations (Neeve et al., 2012). Genetic, environmental and epigenetic factors are thought to modify the disease course and contribute to the broad phenotypic spectrum. Despite this clinical heterogeneity, however, age at presentation and overlapping clinical symptoms allow the major clinical syndromes to be divided into distinct groups (Table 7.1).

Skeletal limb myopathy is common (79%) in adult patients with *POLG* mutations but invariably occurs with PEO and affects proximal musculature (Horvath et al., 2006).

The distal myopathic phenotype seen in both Patient 4.1 and 4.2 discussed in Chapter 4 was striking and has not previously been described in association with *POLG*-related multiple mtDNA deletions. Patient 4.1 presented with isolated upper limb distal myopathy during adolescence before developing PEO when the differential diagnosis would have included the distal-predominant hereditary myopathies, particularly those with upper limb onset. Welander distal myopathy can present with early wrist and finger extensor weakness. However, the early age of onset would be highly unusual for this condition (Chinnery, 2010). Isolated finger and wrist extensor weakness has also been reported in an adult with compound heterozygous *POLG* mutations (c.1156C>T; p.Arg386Cys and c.2794C>T; p.His932Tyr) associated with mtDNA depletion but no detectable mtDNA deletions (Giordano et al., 2010).

POLG mutations should be considered prior to muscle biopsy in patients presenting with distal muscle weakness, even when more classical clinical features of mitochondrial disease are absent.

Table 7.1: Major clinical syndromes associated with *POLG* mutations

Age of onset	Syndrome	Reference
Neonate/infancy	Hepatocerebral	(Ferrari et al., 2005; de Vries et al., 2007)
Infancy/childhood	Alpers-Huttenlocher (AHS)	(Naviaux and Nguyen, 2004)
Adolescence/adulthood	Ataxia neuropathy syndrome (ANS[a])	(Hakonen et al., 2005)
	Myoclonus, epilepsy, myopathy, sensory ataxia (MEMSA)	(Van Goethem et al., 2004)
	Progressive external ophthalmoplegia (PEO)[b,c]	(Van Goethem et al., 2001b)

Table adapted from (Stumpf et al., 2013). [a]ANS previously termed mitochondrial recessive ataxia syndrome (MIRAS), sensory ataxic neuropathy with dysarthria and ophthalmoplegia (SANDO), and spinocerebellar ataxia epilepsy syndrome (SCAE). [b]PEO labelled PEO+ when associated with additional symptoms including: peripheral neuropathy, ataxia, hearing loss, depression, premature menopause, hypogonadism, Parkinsonism, cataracts, or gastrointestinal dysmotility. [c]Dominant and recessive mutations in *POLG* have been associated with PEO.

7.1.3 *RRM2B*-related Kearns-Sayre syndrome

KSS is a multisystem disorder defined clinically by the triad of PEO and pigmentary retinopathy with onset before the age of 20 years plus at least one of: cardiac conduction block; CSF protein concentration greater than 1 g/L; cerebellar ataxia (Berenberg et al., 1977; Kearns, 1965; Kearns and Sayre, 1958; Rowland, 1975; Rowland et al., 1983). Frequent additional signs include sensorineural hearing loss, renal tubular acidosis, dementia, seizures, short stature and endocrine disturbance (diabetes mellitus, hypoparathyroidism and growth hormone deficiency). A progressive skeletal myopathy is also frequently seen. The most common MRI appearances are cerebral and cerebellar atrophy with bilateral, often symmetrical, hyperintense lesions in the subcortical white matter, thalamus, basal ganglia and brainstem (Lerman-Sagie et al., 2005; Wray et al., 1995; Saneto et al., 2008). Interestingly, there appears to be little correlation between neurological deficits and the severity of the MRI features (Chu et al., 1999). KSS is most commonly associated with single large-scale deletions of mtDNA (Yamashita et al., 2008).

In Chapter 4, Patient 4.3 had a clinical phenotype compatible with KSS. This finding expanded the clinical spectrum of *RRM2B*-related adult mitochondrial disease beyond that of PEO and 'PEO plus' syndromes. Additional cases of *RRM2B*-related KSS have since been reported (Pitceathly et al., 2012), thus providing support for this important association, although the majority of cases remain sporadic.

It is now estimated that *RRM2B* mutations represent the third most common cause of Mendelian PEO and multiple mtDNA deletions in adults (13%), following mutations in *POLG* (27%) and *C10orf2* (14%) (Pitceathly et al., 2012). The first reported human diseases linked to mutations in *RRM2B* were associated with mtDNA depletion (Acham-Roschitz et al., 2009; Bornstein et al., 2008; Bourdon et al., 2007a; Kollberg et al., 2009; Spinazzola et al., 2009b) and caused severe, early-onset, multisystem disease with infant mortality. *RRM2B* mutations have since been recognised to cause adult-onset syndromes. This was first demonstrated in a patient with MNGIE and mtDNA depletion (Shaibani et al., 2009). Tyynsimaa *et al*. later published a large adPEO family with multiple mtDNA deletions whose disease was not explained by mutations in any of the known adPEO genes (Tyynismaa et al., 2009). A

heterozygous nonsense mutation in exon 9 or *RRM2B* was detected resulting in a truncated protein that was postulated to cause a dominant-negative or gain-of-function effect on the heterotetrameric structure of the RNR enzyme. The mechanistic importance of truncating exon 9 mutations was further expanded by Fratter *et al*. where three further novel pathogenic variants in exon 9 were shown to cause familial adPEO in seven unrelated probands. In addition, clinically more severe, recessively-inherited, compound heterozygous mutations were demonstrated (Fratter et al., 2011). More recently, a clear relationship between phenotypic severity and genotype in patients harbouring pathogenic *RRM2B* mutations has been established (Pitceathly et al., 2012). Individuals harbouring recessively-inherited compound heterozygous *RRM2B* mutations, as with Patient 4.3 in Chapter 4, present at an earlier age (mean age 7 years) with a more severe and multisystem disorder, whilst patients with single heterozygous mutations, implying autosomal dominant transmission, have a later age of disease onset (mean age 46 years) and develop a predominantly myopathic phenotype comprising PEO, ptosis, proximal muscle weakness and bulbar dysfunction. The distinction between recessively- and dominantly-inherited mutations is also evident on histochemical analysis of skeletal muscle tissue, in which COX-deficient fibres are more widespread in patients with recessively-inherited compound heterozygous mutations.

In conclusion, the work presented in Chapter 4 confirms *RRM2B* mutations as one of the leading causes of adult-onset mitochondrial disease associated with disruption of mtDNA maintenance and reported the first case of KSS associated with nuclear genomic dysfunction.

7.1.4 *COX10* linked adult cytochrome *c* oxidase deficiency

In Chapter 5, an adult with severe COX deficiency caused by compound heterozygous *COX10* mutations, detected using whole exome sequencing, is described.

To date, four infants with early-onset COX-deficient mitochondrial disease caused by *COX10* mutations have been reported (Valnot et al., 2000; Antonicka et al., 2003; Coenen et al., 2004) (Table 7.2). Presentation was with progressive neurological decline from the neonatal period up to six months of age. Clinical findings included a combination of seizures, ataxia, hypotonia, pyramidal signs, renal tubulopathy, hypertrophic cardiomyopathy, SNHL and anaemia. None survived beyond two years. Although some clinical features exhibited by these children are shared with the adult presented in Chapter 5, specifically renal tubulopathy and SNHL, the adult phenotype is considerably milder, and might be considered a 'slow motion' multisystem version of the more severe fatal infantile disease.

The protein modelling data presented in Chapter 5 suggests there are milder structural consequences to the adult patient's mutations as compared with previously reported amino acid substitutions. The difference in clinical severity might also relate to a nuclear modifier or epigenetic phenomenon which partially compensates for the underlying biochemical defect. It is also possible that our patient has never been exposed to a physiological stress sufficient to trigger a severe metabolic decompensation.

The normality of the patient's oxygen polarographic studies, a technique which has not previously been reported in patients with *COX10* mutations, was surprising given the severe histochemical and spectrophotometric reduction in COX activity and might provide some evidence for the patient's ability to tolerate her biochemical defect. This finding could reflect the capacity of any residual assembled COX to partially compensate for the underlying biochemical defect. Polarography measures RC function at physiological levels when electron flux through complex IV is at a controlled/low rate. This scenario mimics the cellular environment in which only suboptimal substrate concentrations are usually available. In contrast,

spectrophotometric assay of RC function records the optimal enzyme activity under conditions where there is maximum electron flux. The residual COX activity in the patient could be sufficient to maintain electron transport and proton translocation activities under non-strenuous conditions, explaining the normal polarographic results. However, during times of physiological stress it is not possible to upregulate COX activity to meet the higher energy demands required due to impaired COX10 function. This is reflected by the reduced COX activity on spectrophotometric assay.

In conclusion, research presented in this thesis has provided some evidence to explain the variable clinical severity seen with *COX10* mutations. Furthermore, *COX10* genetic analysis should be added to the diagnostic armamentarium for adult mitochondrial disease associated with COX deficiency. It remains essential that additional unrelated adult cases with *COX10* mutations are identified to help fully understand the extreme variation in clinical severity associated with COX10 dysfunction.

Table 7.2: Clinical and molecular data of published cases with genetically confirmed *COX10* mutations

Source	Clinical Phenotype	Brain MRI	Age of Onset (months)	Age of Death (months)	Genotype
(Valnot et al., 2000)	Ataxia, muscle weakness, hypotonia, ptosis, UMN signs, seizures, proximal renal tubulopathy	-	18	24	Homozygous: c.612C>A; p.Asp204Lys
(Antonicka et al., 2003)	Hypoglycaemia, lactic acidosis, hypotonia, poor feeding, SNHL, macrocytic anemia, HCM	-	0.25	5	Compound heterozygous: c.791C>A; p.Thr196Lys and c.878C>T; p.Pro225Leu
(Antonicka et al., 2003)	Leigh syndrome: anemia, splenomegaly, hypotonia, lactic acidosis, central respiratory failure	Symmetrical BG lesions	1.5	4	Compound heterozygous: c.1007A>T; p.Asp336Val and c.1007A>G; p.Asp336Gly
(Coenen et al., 2004)	Leigh syndrome: FTT, hypotonia, ataxia, UMN signs, lactic acidosis	Thalamic lesions	5	9	Homozygous: T>C transition in start codon (ATG)

Abbreviations: BG = basal ganglia; MRI = magnetic resonance imaging; UMN = upper motor neuron; FTT = failure to thrive; HCM = hypertrophic cardiomyopathy; SNHL = sensorineural hearing loss.

7.2 NDUFA4 is a new complex IV subunit

The association of *NDUFA4* mutations and human COX deficiency presented in Chapter 6 indicates an important role of the NDUFA4 protein in COX function, and confirms that NDUFA4 is a COX polypeptide subunit despite its previously accepted role as an accessory component of complex I (Carroll et al., 2002). It is likely that NDUFA4 is necessary during biogenesis of COX in order to generate the active enzyme, and subsequently remains loosely associated with the COX enzyme complex. This interaction is clearly essential for overall COX activity, as evidenced by the severe isolated COX deficiency exhibited by individuals harbouring loss-of-function *NDUFA4* mutations, and requires further study. The findings presented are supported by mouse and human cell line evidence that the NDUFA4 protein is an additional COX subunit (Balsa et al., 2012b).

These findings have important implications for understanding the precise biological function of the NDUFA4 protein and its interaction with the other COX polypeptide subunits and assembly factors. Analysis of the *NDUFA4* gene should therefore be considered in all patients with unexplained COX deficiency.

Finally, it is important to emphasise that careful clinical observation and biochemical stratification were central to this discovery, thus highlighting the importance of patients in unravelling fundamental aspects of normal cellular biology, so called ‘back-translation.’

7.3 Future research

Over the next decade, NGS is likely to unravel the molecular basis of all the remaining genetically undefined Mendelian disorders. However, it is essential that physicians continue to clinically characterise novel and unusual phenotypes related to known disease-causing genes, as highlighted by work described in Chapters 3 (CMT2/*MT-ATP6*), 4 (distal myopathy/*POLG* and KSS/*RRM2B*), and 5 (adult COX deficiency/*COX10*), in order to facilitate rapid recognition of patients with genetic disorders and improve upon current knowledge concerning the natural history of their disease.

Understanding the biological mechanisms underpinning the phenotypic diversity associated with dysfunction of identical protein products is likely to contribute towards the development of new treatment strategies for the benefit of patients. One example of this phenomenon is the remarkable variability in clinical severity associated with COX deficiency, as evidenced by the adult described in Chapter 5 harbouring *COX10* mutations.

This work raises a number of potential areas that require further study. Firstly, it is important an attempt is made to identify additional unrelated cases harbouring the here reported novel mutation to unequivocally prove its pathogenicity. Identification of adult patients would also help determine whether the phenotype is related to specific combinations of mutations or the location of a mutation within a specific COX10 protein domain, and if there are other genetic, epigenetic and/or environmental factors which influence the variability in clinical severity. Secondly, determination of the COX10 crystal structure would greatly improve the predicted structural implications different mutations confer on the COX10 protein structure. Thirdly, genetic analysis of both the mitochondrial genome and other components of COX, specifically those acting in concert with COX10 such as MT-CO1, might reveal genetic modifiers of the clinical phenotype. In addition, establishing chromosomal haplotype and mtDNA haplogroup would help establish whether there is a protective or deleterious influence from these factors, as is seen with mtDNA haplogroups U and Parkinson's disease in the Russian Tatar population (Khusnutdinova et al., 2008). An obvious challenge to this work concerns the limited number of patients with *COX10* mutations available for further study. However, it remains possible a shared common mechanism underlies the variability in clinical severity associated with COX deficiency caused by other molecular defects. Collation of the data from all of these patients might therefore be informative. Mitochondrial cybrid studies could then be utilised to further investigate these factors. Finally, it is important to consider whether variable tissue-specific requirements for COX10 (and COX) might explain why certain clinical characteristics are shared by patients harbouring *COX10* mutations (see Table 7.2). This phenomenon is exemplified by the normal COX activity frequently observed in the cultured skin fibroblasts of patients harbouring mutations in many of the complex IV assembly factors (excluding *SURF1*), despite

patients exhibiting severe biochemical defects in muscle tissue (Williams et al., 2004b). One explanation for this might be that fibroblasts require less of certain assembly factors to produce functional COX than muscle tissue, or that fibroblasts are less reliant on OXPHOS to maintain cellular function. Alternatively, the laboratory conditions under which fibroblasts are cultured might influence their COX activity when measured using spectrophotometric analysis. This was demonstrated in Chapter 6 when fibroblasts grown on galactose-containing medium expressed a biochemical defect which was not present in cells grown on glucose-containing medium.

The work presented in Chapter 6 highlights the importance of comprehensively reappraising previously published and accepted research data. The original attribution of NDUFA4 to complex I was made with the caveat that it was inconsistently detected in preparations of complex I, and its presence correlated with COXVIB. There was also existing work from yeast that the number of COX subunits isolated using different purification methods varied as a result of their dissociation from the COX enzyme complex depending on the strength of detergent used (Taanman and Capaldi, 1992). Data presented in this thesis supports recent evidence gained from mouse and human cell lines that NDUFA4 is an important component of COX, and confirms that *NDUFA4* mutations cause human disease. However, the precise function of NDUFA4 remains unclear. In the first instance, the crystal structure of COX requires redefinition. X-ray crystallography should be performed using concentrations of DDM $\leq$0.08% in order to visualise the NDUFA4 subunit as part of the enzyme complex. This would provide insight into the interaction formed between NDUFA4 and the other polypeptide subunits, from which functional implications could then be inferred. There are significant challenges to using this approach; particularly the potential risk of contamination with unrelated protein products when such low concentrations of detergent are used during the crystallisation process. It is also essential that additional families harbouring *NDUFA4* mutations are identified to further understand the function of NDUFA4, fully characterise the phenotypic spectrum of *NDUFA4*-related disease, and establish any genotype/phenotype correlations.

In conclusion, this thesis expands the clinical phenotypic spectrum associated with mutations in both the mitochondrial and nuclear genome and provides evidence that *NDUFA4* mutations link to human disease, thus confirming the essential role of the NDUFA4 protein as a complex IV subunit.

References

Acham-Roschitz, B., Plecko, B., Lindbichler, F., Bittner, R., Mache, C.J., Sperl, W., and Mayr, J.A. (2009). A novel mutation of the RRM2B gene in an infant with early fatal encephalomyopathy, central hypomyelination, and tubulopathy. Mol. Genet. Metab *98*, 300–304.

Adzhubei, I.A., Schmidt, S., Peshkin, L., Ramensky, V.E., Gerasimova, A., Bork, P., Kondrashov, A.S., and Sunyaev, S.R. (2010). A method and server for predicting damaging missense mutations. Nat. Methods *7*, 248–249.

Altmann, R. (1890). Die Elementarorganismen und ihre Beziehungen zu den Zellen. (Leipzig).

Anderson, S., Bankier, A.T., Barrell, B.G., de Bruijn, M.H., Coulson, A.R., Drouin, J., Eperon, I.C., Nierlich, D.P., Roe, B.A., Sanger, F., et al. (1981). Sequence and organization of the human mitochondrial genome. Nature *290*, 457–465.

Antonicka, H., Leary, S.C., Guercin, G.-H., Agar, J.N., Horvath, R., Kennaway, N.G., Harding, C.O., Jaksch, M., and Shoubridge, E.A. (2003). Mutations in COX10 result in a defect in mitochondrial heme A biosynthesis and account for multiple, early-onset clinical phenotypes associated with isolated COX deficiency. Hum. Mol. Genet *12*, 2693–2702.

Arnberg, A., van Bruggen, E.F., and Borst, P. (1971). The presence of DNA molecules with a displacement loop in standard mitochondrial DNA preparations. Biochim. Biophys. Acta *246*, 353–357.

Arnér, E.S., and Eriksson, S. (1995). Mammalian deoxyribonucleoside kinases. Pharmacol. Ther *67*, 155–186.

Arnold, I., and Langer, T. (2002). Membrane protein degradation by AAA proteases in mitochondria. Biochim. Biophys. Acta *1592*, 89–96.

Bai, R.-K., and Wong, L.-J.C. (2005). Simultaneous detection and quantification of mitochondrial DNA deletion(s), depletion, and over-replication in patients with mitochondrial disease. J Mol Diagn *7*, 613–622.

Balsa, E., Marco, R., Perales-Clemente, E., Szklarczyk, R., Calvo, E., Landázuri, M.O., and Enríquez, J.A. (2012a). NDUFA4 Is a Subunit of Complex IV of the Mammalian Electron Transport Chain. Cell Metab.

Balsa, E., Marco, R., Perales-Clemente, E., Szklarczyk, R., Calvo, E., Landázuri, M.O., and Enríquez, J.A. (2012b). NDUFA4 is a subunit of complex IV of the mammalian electron transport chain. Cell Metab. *16*, 378–386.

Bamshad, M.J., Ng, S.B., Bigham, A.W., Tabor, H.K., Emond, M.J., Nickerson, D.A., and Shendure, J. (2011). Exome sequencing as a tool for Mendelian disease gene discovery. Nat. Rev. Genet. *12*, 745–755.

Baxter, R.V., Ben Othmane, K., Rochelle, J.M., Stajich, J.E., Hulette, C., Dew-Knight, S., Hentati, F., Ben Hamida, M., Bel, S., Stenger, J.E., et al. (2002). Ganglioside-induced differentiation-associated protein-1 is mutant in Charcot-Marie-Tooth disease type 4A/8q21. Nat. Genet. *30*, 21–22.

Benda, C. (1898). Ueber die Spermatogenese der Vertebraten und höherer Evertebraten, II. Theil: Die Histiogenese der Spermien. Arch. Anat. Physiol. *73*, 393–398.

Bereiter-Hahn, J., and Jendrach, M. (2010). Mitochondrial dynamics. Int Rev Cell Mol Biol *284*, 1–65.

Berenberg, R.A., Pellock, J.M., DiMauro, S., Schotland, D.L., Bonilla, E., Eastwood, A., Hays, A., Vicale, C.T., Behrens, M., Chutorian, A., et al. (1977). Lumping or splitting? “Ophthalmoplegia-plus” or Kearns-Sayre syndrome? Ann. Neurol *1*, 37–54.

Bestwick, R.K., and Mathews, C.K. (1982). Unusual compartmentation of precursors for nuclear and mitochondrial DNA in mouse L cells. J. Biol. Chem *257*, 9305–9308.

Bochkarev, A., Pfuetzner, R.A., Edwards, A.M., and Frappier, L. (1997). Structure of the single-stranded-DNA-binding domain of replication protein A bound to DNA. Nature *385*, 176–181.

Bogenhagen, D., and Clayton, D.A. (1976). Thymidylate nucleotide supply for mitochondrial DNA synthesis in mouse L-cells. Effect of 5-fluorodeoxyuridine and

methotrexate in thymidine kinase plus and thymidine kinase minus cells. J. Biol. Chem *251*, 2938–2944.

Bogenhagen, D.F., and Clayton, D.A. (2003a). The mitochondrial DNA replication bubble has not burst. Trends Biochem. Sci *28*, 357–360.

Bogenhagen, D.F., and Clayton, D.A. (2003b). Concluding remarks: The mitochondrial DNA replication bubble has not burst. Trends Biochem. Sci *28*, 404–405.

Bogenhagen, D., Gillum, A.M., Martens, P.A., and Clayton, D.A. (1979). Replication of mouse L-cell mitochondrial DNA. Cold Spring Harb. Symp. Quant. Biol *43 Pt 1*, 253–262.

Bornstein, B., Area, E., Flanigan, K.M., Ganesh, J., Jayakar, P., Swoboda, K.J., Coku, J., Naini, A., Shanske, S., Tanji, K., et al. (2008). Mitochondrial DNA depletion syndrome due to mutations in the RRM2B gene. Neuromuscul. Disord *18*, 453–459.

Bouillot, S., Martin-Négrier, M.L., Vital, A., Ferrer, X., Lagueny, A., Vincent, D., Coquet, M., Orgogozo, J.M., Bloch, B., and Vita, C. (2002). Peripheral neuropathy associated with mitochondrial disorders: 8 cases and review of the literature. J. Peripher. Nerv. Syst *7*, 213–220.

Bourdon, A., Minai, L., Serre, V., Jais, J.-P., Sarzi, E., Aubert, S., Chrétien, D., de Lonlay, P., Paquis-Flucklinger, V., Arakawa, H., et al. (2007a). Mutation of RRM2B, encoding p53-controlled ribonucleotide reductase (p53R2), causes severe mitochondrial DNA depletion. Nat. Genet *39*, 776–780.

Bourdon, A., Minai, L., Serre, V., Jais, J.-P., Sarzi, E., Aubert, S., Chrétien, D., de Lonlay, P., Paquis-Flucklinger, V., Arakawa, H., et al. (2007b). Mutation of RRM2B, encoding p53-controlled ribonucleotide reductase (p53R2), causes severe mitochondrial DNA depletion. Nat Genet *39*, 776–780.

Bowmaker, M., Yang, M.Y., Yasukawa, T., Reyes, A., Jacobs, H.T., Huberman, J.A., and Holt, I.J. (2003). Mammalian mitochondrial DNA replicates bidirectionally from an initiation zone. J. Biol. Chem *278*, 50961–50969.

Bravo, R., Vicencio, J.M., Parra, V., Troncoso, R., Munoz, J.P., Bui, M., Quiroga, C., Rodriguez, A.E., Verdejo, H.E., Ferreira, J., et al. (2011). Increased ER-mitochondrial coupling promotes mitochondrial respiration and bioenergetics during early phases of ER stress. J. Cell. Sci. *124*, 2143–2152.

Brewer, B.J., and Fangman, W.L. (1987). The localization of replication origins on ARS plasmids in S. cerevisiae. Cell *51*, 463–471.

Calhoun, M.W., Thomas, J.W., and Gennis, R.B. (1994). The cytochrome oxidase superfamily of redox-driven proton pumps. Trends Biochem. Sci. *19*, 325–330.

Calvo, S.E., and Mootha, V.K. (2010). The mitochondrial proteome and human disease. Annu Rev Genomics Hum Genet *11*, 25–44.

Calvo, S., Jain, M., Xie, X., Sheth, S.A., Chang, B., Goldberger, O.A., Spinazzola, A., Zeviani, M., Carr, S.A., and Mootha, V.K. (2006). Systematic identification of human mitochondrial disease genes through integrative genomics. Nat. Genet *38*, 576–582.

Capaldi, R.A. (1990). Structure and assembly of cytochrome c oxidase. Arch. Biochem. Biophys. *280*, 252–262.

Capaldi, R.A., Aggeler, R., Turina, P., and Wilkens, S. (1994). Coupling between catalytic sites and the proton channel in F1F0-type ATPases. Trends Biochem. Sci. *19*, 284–289.

Capaldi, R.A., Marusich, M.F., and Taanman, J.W. (1995). Mammalian cytochrome-c oxidase: characterization of enzyme and immunological detection of subunits in tissue extracts and whole cells. Meth. Enzymol. *260*, 117–132.

Carrodeguas, J.A., Kobayashi, R., Lim, S.E., Copeland, W.C., and Bogenhagen, D.F. (1999). The accessory subunit of Xenopus laevis mitochondrial DNA polymerase gamma increases processivity of the catalytic subunit of human DNA polymerase gamma and is related to class II aminoacyl-tRNA synthetases. Mol. Cell. Biol *19*, 4039–4046.

Carroll, J., Shannon, R.J., Fearnley, I.M., Walker, J.E., and Hirst, J. (2002). Definition of the nuclear encoded protein composition of bovine heart mitochondrial complex I. Identification of two new subunits. J. Biol. Chem. *277*, 50311–50317.

Castagna, A.E., Addis, J., McInnes, R.R., Clarke, J.T.R., Ashby, P., Blaser, S., and Robinson, B.H. (2007). Late onset Leigh syndrome and ataxia due to a T to C mutation at bp 9,185 of mitochondrial DNA. Am. J. Med. Genet. A *143A*, 808–816.

Chan, S.S.L., and Copeland, W.C. (2009). DNA polymerase gamma and mitochondrial disease: understanding the consequence of POLG mutations. Biochim. Biophys. Acta *1787*, 312–319.

Chan, S.S.L., Longley, M.J., and Copeland, W.C. (2005). The common A467T mutation in the human mitochondrial DNA polymerase (POLG) compromises catalytic efficiency and interaction with the accessory subunit. J. Biol. Chem *280*, 31341–31346.

Chang, D.D., and Clayton, D.A. (1985). Priming of human mitochondrial DNA replication occurs at the light-strand promoter. Proc. Natl. Acad. Sci. U.S.A *82*, 351–355.

Chang, D.D., Hauswirth, W.W., and Clayton, D.A. (1985). Replication priming and transcription initiate from precisely the same site in mouse mitochondrial DNA. EMBO J *4*, 1559–1567.

Chang, L., Zhou, B., Hu, S., Guo, R., Liu, X., Jones, S.N., and Yen, Y. (2008). ATM-mediated serine 72 phosphorylation stabilizes ribonucleotide reductase small subunit p53R2 protein against MDM2 to DNA damage. Proc. Natl. Acad. Sci. U.S.A *105*, 18519–18524.

Chen, X.J., and Butow, R.A. (2005). The organization and inheritance of the mitochondrial genome. Nat. Rev. Genet *6*, 815–825.

Childs, A.-M., Hutchin, T., Pysden, K., Highet, L., Bamford, J., Livingston, J., and Crow, Y.J. (2007). Variable phenotype including Leigh syndrome with a 9185T>C mutation in the MTATP6 gene. Neuropediatrics *38*, 313–316.

Chinnery, P.F. (2010). The age of single-gene neurological disorders is not dead. Brain *133*, 1865–1868.

Chinnery, P.F., and Zeviani, M. (2008). 155th ENMC workshop: polymerase gamma and disorders of mitochondrial DNA synthesis, 21-23 September 2007, Naarden, The Netherlands. Neuromuscul. Disord. *18*, 259–267.

Chu, B.C., Terae, S., Takahashi, C., Kikuchi, Y., Miyasaka, K., Abe, S., Minowa, K., and Sawamura, T. (1999). MRI of the brain in the Kearns-Sayre syndrome: report of four cases and a review. Neuroradiology *41*, 759–764.

Chung, K.W., Kim, S.B., Park, K.D., Choi, K.G., Lee, J.H., Eun, H.W., Suh, J.S., Hwang, J.H., Kim, W.K., Seo, B.C., et al. (2006). Early onset severe and late-onset mild Charcot-Marie-Tooth disease with mitofusin 2 (MFN2) mutations. Brain *129*, 2103–2118.

Cízková, A., Stránecký, V., Mayr, J.A., Tesarová, M., Havlícková, V., Paul, J., Ivánek, R., Kuss, A.W., Hansíková, H., Kaplanová, V., et al. (2008). TMEM70 mutations cause isolated ATP synthase deficiency and neonatal mitochondrial encephalocardiomyopathy. Nat. Genet. *40*, 1288–1290.

Clayton, D.A. (1982). Replication of animal mitochondrial DNA. Cell *28*, 693–705.

Clayton, D.A. (2003). Mitochondrial DNA replication: what we know. IUBMB Life *55*, 213–217.

Coenen, M.J.H., van den Heuvel, L.P., Ugalde, C., Ten Brinke, M., Nijtmans, L.G.J., Trijbels, F.J.M., Beblo, S., Maier, E.M., Muntau, A.C., and Smeitink, J.A.M. (2004). Cytochrome c oxidase biogenesis in a patient with a mutation in COX10 gene. Ann. Neurol *56*, 560–564.

Cohen, B., Chinery, P., and Copeland, W. (1993). POLG-related disorders [GeneReviews^{TM}] (Seattle (WA): University of Washington, Seattle).

Cooper, G.M., Goode, D.L., Ng, S.B., Sidow, A., Bamshad, M.J., Shendure, J., and Nickerson, D.A. (2010). Single-nucleotide evolutionary constraint scores highlight disease-causing mutations. Nat. Methods *7*, 250–251.

Cooper, J.M., Mann, V.M., and Schapira, A.H. (1992). Analyses of mitochondrial respiratory chain function and mitochondrial DNA deletion in human skeletal muscle: effect of ageing. J. Neurol. Sci. *113*, 91–98.

Coore, H.G., Denton, R.M., Martin, B.R., and Randle, P.J. (1971). Regulation of adipose tissue pyruvate dehydrogenase by insulin and other hormones. Biochem. J. *125*, 115–127.

Crews, S., Ojala, D., Posakony, J., Nishiguchi, J., and Attardi, G. (1979). Nucleotide sequence of a region of human mitochondrial DNA containing the precisely identified origin of replication. Nature *277*, 192–198.

Croft, P.B., Cutting, J.C., Jewesbury, E.C., Blackwood, W., and Mair, W.G. (1977). Ocular myopathy (progressive external ophthalmoplegia) with neuropathic complications. Acta Neurol. Scand *55*, 169–197.

DeLano, W.L. (2002). The PyMOL Molecular Graphics System. (DeLano Scientific LLC, San Carlos, CA, USA.).

DePristo, M.A., Banks, E., Poplin, R., Garimella, K.V., Maguire, J.R., Hartl, C., Philippakis, A.A., del Angel, G., Rivas, M.A., Hanna, M., et al. (2011). A framework for variation discovery and genotyping using next-generation DNA sequencing data. Nat. Genet. *43*, 491–498.

Dierick, I., Baets, J., Irobi, J., Jacobs, A., De Vriendt, E., Deconinck, T., Merlini, L., Van den Bergh, P., Rasic, V.M., Robberecht, W., et al. (2008). Relative contribution of mutations in genes for autosomal dominant distal hereditary motor neuropathies: a genotype-phenotype correlation study. Brain *131*, 1217–1227.

Doda, J.N., Wright, C.T., and Clayton, D.A. (1981). Elongation of displacement-loop strands in human and mouse mitochondrial DNA is arrested near specific template sequences. Proc. Natl. Acad. Sci. U.S.A *78*, 6116–6120.

Dohm, J.C., Lottaz, C., Borodina, T., and Himmelbauer, H. (2008). Substantial biases in ultra-short read data sets from high-throughput DNA sequencing. Nucleic Acids Res. *36*, e105.

Dolce, V., Fiermonte, G., Runswick, M.J., Palmieri, F., and Walker, J.E. (2001). The human mitochondrial deoxynucleotide carrier and its role in the toxicity of nucleoside antivirals. Proc. Natl. Acad. Sci. U.S.A *98*, 2284–2288.

Duncan, A.J., Knight, J.A., Costello, H., Conway, G.S., and Rahman, S. (2012). POLG mutations and age at menopause. Hum. Reprod. *27*, 2243–2244.

Eddy, S.R. (2011). Accelerated Profile HMM Searches. PLoS Comput. Biol. *7*, e1002195.

Emelyanov, V.V. (2003). Mitochondrial connection to the origin of the eukaryotic cell. Eur. J. Biochem. *270*, 1599–1618.

Eriksson, S., Munch-Petersen, B., Johansson, K., and Eklund, H. (2002). Structure and function of cellular deoxyribonucleoside kinases. Cell. Mol. Life Sci *59*, 1327–1346.

Ernster, L., Ikkos, D., and Luft, R. (1959). Enzymic activities of human skeletal muscle mitochondria: a tool in clinical metabolic research. Nature *184*, 1851–1854.

Farr, C.L., Wang, Y., and Kaguni, L.S. (1999). Functional interactions of mitochondrial DNA polymerase and single-stranded DNA-binding protein. Template-primer DNA binding and initiation and elongation of DNA strand synthesis. J. Biol. Chem *274*, 14779–14785.

Ferrari, G., Lamantea, E., Donati, A., Filosto, M., Briem, E., Carrara, F., Parini, R., Simonati, A., Santer, R., and Zeviani, M. (2005). Infantile hepatocerebral syndromes associated with mutations in the mitochondrial DNA polymerase-gammaA. Brain *128*, 723–731.

Fish, J., Raule, N., and Attardi, G. (2004). Discovery of a major D-loop replication origin reveals two modes of human mtDNA synthesis. Science *306*, 2098–2101.

Fratter, C., Raman, P., Alston, C.L., Blakely, E.L., Craig, K., Smith, C., Evans, J., Seller, A., Czermin, B., Hanna, M.G., et al. (2011). RRM2B mutations are frequent in familial PEO with multiple mtDNA deletions. Neurology *76*, 2032–2034.

Fusté, J.M., Wanrooij, S., Jemt, E., Granycome, C.E., Cluett, T.J., Shi, Y., Atanassova, N., Holt, I.J., Gustafsson, C.M., and Falkenberg, M. (2010). Mitochondrial RNA polymerase is needed for activation of the origin of light-strand DNA replication. Mol. Cell *37*, 67–78.

Futuyma, D.J. (2005). On Darwin's Shoulders. Natural History *114*, 64–68.

Gallinaro, L., Crovatto, K., Rampazzo, C., Pontarin, G., Ferraro, P., Milanesi, E., Reichard, P., and Bianchi, V. (2002). Human mitochondrial 5'-deoxyribonucleotidase. Overproduction in cultured cells and functional aspects. J. Biol. Chem *277*, 35080–35087.

Garrido, N., Griparic, L., Jokitalo, E., Wartiovaara, J., van der Bliek, A.M., and Spelbrink, J.N. (2003). Composition and dynamics of human mitochondrial nucleoids. Mol. Biol. Cell *14*, 1583–1596.

Gemignani, F., Juvarra, G., Marbini, A., Calzetti, S., Bragaglia, M.M., and Govoni, E. (1982). Polyneuropathy in progressive external ophthalmoplegia. Eur. Neurol *21*, 181–188.

Gillum, A.M., and Clayton, D.A. (1978). Displacement-loop replication initiation sequence in animal mitochondrial DNA exists as a family of discrete lengths. Proc. Natl. Acad. Sci. U.S.A *75*, 677–681.

Giordano, C., Pichiorri, F., Blakely, E.L., Perli, E., Orlandi, M., Gallo, P., Taylor, R.W., Inghilleri, M., and d' Amati, G. (2010). Isolated distal myopathy of the upper limbs associated with mitochondrial DNA depletion and polymerase gamma mutations. Arch. Neurol *67*, 1144–1146.

Giorgio, V., von Stockum, S., Antoniel, M., Fabbro, A., Fogolari, F., Forte, M., Glick, G.D., Petronilli, V., Zoratti, M., Szabó, I., et al. (2013). Dimers of mitochondrial ATP synthase form the permeability transition pore. Proc. Natl. Acad. Sci. U.S.A. *110*, 5887–5892.

Glerum, D.M., and Tzagoloff, A. (1994). Isolation of a human cDNA for heme A:farnesyltransferase by functional complementation of a yeast cox10 mutant. Proc. Natl. Acad. Sci. U.S.A. *91*, 8452–8456.

Van Goethem, G., Dermaut, B., Löfgren, A., Martin, J.J., and Van Broeckhoven, C. (2001a). Mutation of POLG is associated with progressive external ophthalmoplegia characterized by mtDNA deletions. Nat. Genet *28*, 211–212.

Van Goethem, G., Dermaut, B., Löfgren, A., Martin, J.J., and Van Broeckhoven, C. (2001b). Mutation of POLG is associated with progressive external ophthalmoplegia characterized by mtDNA deletions. Nat. Genet. *28*, 211–212.

Van Goethem, G., Luoma, P., Rantamäki, M., Al Memar, A., Kaakkola, S., Hackman, P., Krahe, R., Löfgren, A., Martin, J.J., De Jonghe, P., et al. (2004). POLG mutations in neurodegenerative disorders with ataxia but no muscle involvement. Neurology *63*, 1251–1257.

Graziewicz, M.A., Longley, M.J., and Copeland, W.C. (2006). DNA polymerase gamma in mitochondrial DNA replication and repair. Chem. Rev. *106*, 383–405.

Greenleaf, A.L., Kelly, J.L., and Lehman, I.R. (1986). Yeast RPO41 gene product is required for transcription and maintenance of the mitochondrial genome. Proc. Natl. Acad. Sci. U.S.A *83*, 3391–3394.

Grivell, L.A. (1983). Mitochondrial DNA. Sci. Am. *248*, 78–89.

Håkansson, P., Hofer, A., and Thelander, L. (2006). Regulation of mammalian ribonucleotide reduction and dNTP pools after DNA damage and in resting cells. J. Biol. Chem *281*, 7834–7841.

Hakonen, A.H., Heiskanen, S., Juvonen, V., Lappalainen, I., Luoma, P.T., Rantamaki, M., Goethem, G.V., Lofgren, A., Hackman, P., Paetau, A., et al. (2005). Mitochondrial DNA polymerase W748S mutation: a common cause of autosomal recessive ataxia with ancient European origin. Am. J. Hum. Genet. *77*, 430–441.

Hanna, M.G., Nelson, I.P., Rahman, S., Lane, R.J., Land, J., Heales, S., Cooper, M.J., Schapira, A.H., Morgan-Hughes, J.A., and Wood, N.W. (1998). Cytochrome c oxidase deficiency associated with the first stop-codon point mutation in human mtDNA. Am. J. Hum. Genet. *63*, 29–36.

Hargreaves, P., Rahman, S., Guthrie, P., Taanman, J.W., Leonard, J.V., Land, J.M., and Heales, S.J.R. (2002). Diagnostic value of succinate ubiquinone reductase activity in the identification of patients with mitochondrial DNA depletion. J. Inherit. Metab. Dis. *25*, 7–16.

Harismendy, O., Ng, P.C., Strausberg, R.L., Wang, X., Stockwell, T.B., Beeson, K.Y., Schork, N.J., Murray, S.S., Topol, E.J., Levy, S., et al. (2009). Evaluation of next generation sequencing platforms for population targeted sequencing studies. Genome Biol. *10*, R32.

He, J., Mao, C.-C., Reyes, A., Sembongi, H., Di Re, M., Granycome, C., Clippingdale, A.B., Fearnley, I.M., Harbour, M., Robinson, A.J., et al. (2007). The AAA+ protein ATAD3 has displacement loop binding properties and is involved in mitochondrial nucleoid organization. J. Cell Biol *176*, 141–146.

Von Heijne, G., and Gavel, Y. (1988). Topogenic signals in integral membrane proteins. Eur. J. Biochem. *174*, 671–678.

Henle, J. (1841). Allgemeine Anatomie: Lehre von den Mischungs- und Formbestandtheilen des menschlichen Körpers [= Sömmering, Samuel Thomas von. Vom Baue des menschlichen Körpers, Vol. 6] (Leipzig: Voss).

Hillier, L.W., Marth, G.T., Quinlan, A.R., Dooling, D., Fewell, G., Barnett, D., Fox, P., Glasscock, J.I., Hickenbotham, M., Huang, W., et al. (2008). Whole-genome sequencing and variant discovery in C. elegans. Nat. Methods *5*, 183–188.

Hirst, J., Carroll, J., Fearnley, I.M., Shannon, R.J., and Walker, J.E. (2003). The nuclear encoded subunits of complex I from bovine heart mitochondria. Biochim. Biophys. Acta *1604*, 135–150.

Holt, I.J., and Jacobs, H.T. (2003). Response: The mitochondrial DNA replication bubble has not burst. Trends Biochem. Sci *28*, 355–356.

Holt, I.J., Harding, A.E., Petty, R.K., and Morgan-Hughes, J.A. (1990). A new mitochondrial disease associated with mitochondrial DNA heteroplasmy. Am. J. Hum. Genet. *46*, 428–433.

Holt, I.J., Lorimer, H.E., and Jacobs, H.T. (2000). Coupled leading- and lagging-strand synthesis of mammalian mitochondrial DNA. Cell *100*, 515–524.

Holt, I.J., He, J., Mao, C.-C., Boyd-Kirkup, J.D., Martinsson, P., Sembongi, H., Reyes, A., and Spelbrink, J.N. (2007). Mammalian mitochondrial nucleoids: organizing an independently minded genome. Mitochondrion *7*, 311–321.

Horvath, R., Hudson, G., Ferrari, G., Fütterer, N., Ahola, S., Lamantea, E., Prokisch, H., Lochmüller, H., McFarland, R., Ramesh, V., et al. (2006). Phenotypic spectrum associated with mutations of the mitochondrial polymerase gamma gene. Brain *129*, 1674–1684.

Iborra, F.J., Kimura, H., and Cook, P.R. (2004). The functional organization of mitochondrial genomes in human cells. BMC Biol *2*, 9.

Indrieri, A., van Rahden, V.A., Tiranti, V., Morleo, M., Iaconis, D., Tammaro, R., D'Amato, I., Conte, I., Maystadt, I., Demuth, S., et al. (2012). Mutations in COX7B Cause Microphthalmia with Linear Skin Lesions, an Unconventional Mitochondrial Disease. Am. J. Hum. Genet. *91*, 942–949.

Jacobs, J.M., and Love, S. (1985). Qualitative and quantitative morphology of human sural nerve at different ages. Brain *108 (Pt 4)*, 897–924.

Jonckheere, A.I., Hogeveen, M., Nijtmans, L.G.J., van den Brand, M.A.M., Janssen, A.J.M., Diepstra, J.H.S., van den Brandt, F.C.A., van den Heuvel, L.P., Hol, F.A., Hofste, T.G.J., et al. (2008). A novel mitochondrial ATP8 gene mutation in a patient with apical hypertrophic cardiomyopathy and neuropathy. J. Med. Genet. *45*, 129–133.

Jones, M.E. (1980). Pyrimidine nucleotide biosynthesis in animals: genes, enzymes, and regulation of UMP biosynthesis. Annu. Rev. Biochem *49*, 253–279.

Jones, D.T., Buchan, D.W.A., Cozzetto, D., and Pontil, M. (2012). PSICOV: precise structural contact prediction using sparse inverse covariance estimation on large multiple sequence alignments. Bioinformatics *28*, 184–190.

Kadenbach, B., Hartmann, R., Glanville, R., and Buse, G. (1982). Tissue-specific genes code for polypeptide VIa of bovine liver and heart cytochrome c oxidase. FEBS Lett. *138*, 236–238.

Kadenbach, B., Jarausch, J., Hartmann, R., and Merle, P. (1983). Separation of mammalian cytochrome c oxidase into 13 polypeptides by a sodium dodecyl sulfate-gel electrophoretic procedure. Anal. Biochem. *129*, 517–521.

Kadenbach, B., Hüttemann, M., Arnold, S., Lee, I., and Bender, E. (2000). Mitochondrial energy metabolism is regulated via nuclear-coded subunits of cytochrome c oxidase. Free Radic. Biol. Med. *29*, 211–221.

Kang, D., Miyako, K., Kai, Y., Irie, T., and Takeshige, K. (1997). In vivo determination of replication origins of human mitochondrial DNA by ligation-mediated polymerase chain reaction. J. Biol. Chem *272*, 15275–15279.

Kärppä, M., Syrjälä, P., Tolonen, U., and Majamaa, K. (2003). Peripheral neuropathy in patients with the 3243A>G mutation in mitochondrial DNA. J. Neurol *250*, 216–221.

Kaukonen, J., Juselius, J.K., Tiranti, V., Kyttälä, A., Zeviani, M., Comi, G.P., Keränen, S., Peltonen, L., and Suomalainen, A. (2000). Role of adenine nucleotide translocator 1 in mtDNA maintenance. Science *289*, 782–785.

Kearns, T.P. (1965). External Ophthalmoplegia, Pigmentary Degeneration of the Retina, and Cardiomyopathy: A Newly Recognized Syndrome. Trans Am Ophthalmol Soc *63*, 559–625.

Kearns, T.P., and Sayre, G.P. (1958). Retinitis pigmentosa, external ophthalmophegia, and complete heart block: unusual syndrome with histologic study in one of two cases. AMA Arch Ophthalmol *60*, 280–289.

Kelly, J.L., Greenleaf, A.L., and Lehman, I.R. (1986). Isolation of the nuclear gene encoding a subunit of the yeast mitochondrial RNA polymerase. J. Biol. Chem *261*, 10348–10351.

Kennedy, E.P., and Lehninger, A.L. (1949). Oxidation of fatty acids and tricarboxylic acid cycle intermediates by isolated rat liver mitochondria. J. Biol. Chem. *179*, 957–972.

Khusnutdinova, E., Gilyazova, I., Ruiz-Pesini, E., Derbeneva, O., Khusainova, R., Khidiyatova, I., Magzhanov, R., and Wallace, D.C. (2008). A mitochondrial etiology of neurodegenerative diseases: evidence from Parkinson's disease. Ann. N. Y. Acad. Sci. *1147*, 1–20.

Kimura, T., Takeda, S., Sagiya, Y., Gotoh, M., Nakamura, Y., and Arakawa, H. (2003). Impaired function of p53R2 in Rrm2b-null mice causes severe renal failure through attenuation of dNTP pools. Nat. Genet *34*, 440–445.

King, T.E. (1967). [40] Preparations of succinate—cytochrome c reductase and the cytochrome b-c1 particle, and reconstitution of succinate-cytochrome c reductase. In Methods in Enzymology, M.E.P. Ronald W. Estabrook, ed. (Academic Press), pp. 216–225.

Kollberg, G., Darin, N., Benan, K., Moslemi, A.-R., Lindal, S., Tulinius, M., Oldfors, A., and Holme, E. (2009). A novel homozygous RRM2B missense mutation in association with severe mtDNA depletion. Neuromuscul. Disord *19*, 147–150.

Korhonen, J.A., Pham, X.H., Pellegrini, M., and Falkenberg, M. (2004). Reconstitution of a minimal mtDNA replisome in vitro. EMBO J *23*, 2423–2429.

Kornberg, R.D. (1974). Chromatin structure: a repeating unit of histones and DNA. Science *184*, 868–871.

Krishnan, K.J., Reeve, A.K., Samuels, D.C., Chinnery, P.F., Blackwood, J.K., Taylor, R.W., Wanrooij, S., Spelbrink, J.N., Lightowlers, R.N., and Turnbull, D.M. (2008). What causes mitochondrial DNA deletions in human cells? Nat. Genet *40*, 275–279.

Kucharczyk, R., Zick, M., Bietenhader, M., Rak, M., Couplan, E., Blondel, M., Caubet, S., and Dirago, J. (2009a). Mitochondrial ATP synthase disorders: Molecular mechanisms and the quest for curative therapeutic approaches. Biochimica et Biophysica Acta (BBA) - Molecular Cell Research *1793*, 186–199.

Kucharczyk, R., Salin, B., and di Rago, J.-P. (2009b). Introducing the human Leigh syndrome mutation T9176G into Saccharomyces cerevisiae mitochondrial DNA leads to severe defects in the incorporation of Atp6p into the ATP synthase and in the mitochondrial morphology. Human Molecular Genetics *18*, 2889–2898.

Kucharczyk, R., Rak, M., and di Rago, J.-P. (2009c). Biochemical consequences in yeast of the human mitochondrial DNA 8993T>C mutation in the ATPase6 gene found in NARP/MILS patients. Biochimica et Biophysica Acta (BBA) - Molecular Cell Research *1793*, 817–824.

Kucharczyk, R., Ezkurdia, N., Couplan, E., Procaccio, V., Ackerman, S.H., Blondel, M., and di Rago, J.-P. (2010). Consequences of the pathogenic T9176C mutation of human mitochondrial DNA on yeast mitochondrial ATP synthase. Biochimica et Biophysica Acta (BBA) - Bioenergetics *1797*, 1105–1112.

Kucharczyk, R., Giraud, M.-F., Brèthes, D., Wysocka-Kapcinska, M., Ezkurdia, N., Salin, B., Velours, J., Camougrand, N., Haraux, F., and di Rago, J.-P. (2013). Defining the pathogenesis of human mtDNA mutations using a yeast model: The case of T8851C. The International Journal of Biochemistry & Cell Biology *45*, 130–140.

Kukat, C., Wurm, C.A., Spåhr, H., Falkenberg, M., Larsson, N.-G., and Jakobs, S. (2011). Super-resolution microscopy reveals that mammalian mitochondrial nucleoids have a uniform size and frequently contain a single copy of mtDNA. Proc. Natl. Acad. Sci. U.S.A. *108*, 13534–13539.

Kumar, P., Henikoff, S., and Ng, P.C. (2009). Predicting the effects of coding non-synonymous variants on protein function using the SIFT algorithm. Nat Protoc *4*, 1073–1081.

Kunji, E.R.S., and Crichton, P.G. (2010). Mitochondrial carriers function as monomers. Biochim. Biophys. Acta *1797*, 817–831.

Kunz, B.A., Kohalmi, S.E., Kunkel, T.A., Mathews, C.K., McIntosh, E.M., and Reidy, J.A. (1994). International Commission for Protection Against Environmental

Mutagens and Carcinogens. Deoxyribonucleoside triphosphate levels: a critical factor in the maintenance of genetic stability. Mutat. Res *318*, 1–64.

Lander, E.S., and Botstein, D. (1987). Homozygosity mapping: a way to map human recessive traits with the DNA of inbred children. Science *236*, 1567–1570.

Lee, Y.-S., Kennedy, W.D., and Yin, Y.W. (2009). Structural insight into processive human mitochondrial DNA synthesis and disease-related polymerase mutations. Cell *139*, 312–324.

Lee, Y.-S., Lee, S., Demeler, B., Molineux, I.J., Johnson, K.A., and Yin, Y.W. (2010). Each monomer of the dimeric accessory protein for human mitochondrial DNA polymerase has a distinct role in conferring processivity. J. Biol. Chem *285*, 1490–1499.

Legros, F., Malka, F., Frachon, P., Lombes, A., and Rojo, M. (2004). Organization and dynamics of human mitochondrial DNA. Journal of Cell Science *117*, 2653.

Lerman-Sagie, T., Leshinsky-Silver, E., Watemberg, N., Luckman, Y., and Lev, D. (2005). White matter involvement in mitochondrial diseases. Mol. Genet. Metab *84*, 127–136.

Li, H., and Durbin, R. (2009). Fast and accurate short read alignment with Burrows-Wheeler transform. Bioinformatics *25*, 1754–1760.

Li, K., and Williams, R.S. (1997). Tetramerization and single-stranded DNA binding properties of native and mutated forms of murine mitochondrial single-stranded DNA-binding proteins. J. Biol. Chem *272*, 8686–8694.

Li, F.Y., Tariq, M., Croxen, R., Morten, K., Squier, W., Newsom-Davis, J., Beeson, D., and Larsson, C. (1999). Mapping of autosomal dominant progressive external ophthalmoplegia to a 7-cM critical region on 10q24. Neurology *53*, 1265–1271.

Li, H., Handsaker, B., Wysoker, A., Fennell, T., Ruan, J., Homer, N., Marth, G., Abecasis, G., and Durbin, R. (2009). The Sequence Alignment/Map format and SAMtools. Bioinformatics *25*, 2078–2079.

Lim, S.E., Longley, M.J., and Copeland, W.C. (1999). The mitochondrial p55 accessory subunit of human DNA polymerase gamma enhances DNA binding, promotes processive DNA synthesis, and confers N-ethylmaleimide resistance. J. Biol. Chem *274*, 38197–38203.

Litonin, D., Sologub, M., Shi, Y., Savkina, M., Anikin, M., Falkenberg, M., Gustafsson, C.M., and Temiakov, D. (2010). Human mitochondrial transcription revisited: only TFAM and TFB2M are required for transcription of the mitochondrial genes in vitro. J. Biol. Chem. *285*, 18129–18133.

Longley, M.J., Graziewicz, M.A., Bienstock, R.J., and Copeland, W.C. (2005). Consequences of mutations in human DNA polymerase gamma. Gene *354*, 125–131.

Longley, M.J., Clark, S., Yu Wai Man, C., Hudson, G., Durham, S.E., Taylor, R.W., Nightingale, S., Turnbull, D.M., Copeland, W.C., and Chinnery, P.F. (2006). Mutant POLG2 disrupts DNA polymerase gamma subunits and causes progressive external ophthalmoplegia. Am. J. Hum. Genet *78*, 1026–1034.

Low, P.A., McLeod, J.G., and Prineas, J.W. (1978). Hypertrophic Charcot-Marie-Tooth disease. Light and electron microscope studies of the sural nerve. J. Neurol. Sci. *35*, 93–115.

Luft, R., Ikkos, D., Palmieri, G., Ernster, L., and Afzelius, B. (1962). A case of severe hypermetabolism of nonthyroid origin with a defect in the maintenance of mitochondrial respiratory control: a correlated clinical, biochemical, and morphological study. J. Clin. Invest *41*, 1776–1804.

Luo, N., and Kaguni, L.S. (2005). Mutations in the spacer region of Drosophila mitochondrial DNA polymerase affect DNA binding, processivity, and the balance between Pol and Exo function. J. Biol. Chem *280*, 2491–2497.

Lynch, M., Koskella, B., and Schaack, S. (2006). Mutation pressure and the evolution of organelle genomic architecture. Science *311*, 1727–1730.

Malka, F., Lombès, A., and Rojo, M. (2006). Organization, dynamics and transmission of mitochondrial DNA: focus on vertebrate nucleoids. Biochim. Biophys. Acta *1763*, 463–472.

Mandel, H., Szargel, R., Labay, V., Elpeleg, O., Saada, A., Shalata, A., Anbinder, Y., Berkowitz, D., Hartman, C., Barak, M., et al. (2001). The deoxyguanosine kinase gene is mutated in individuals with depleted hepatocerebral mitochondrial DNA. Nat. Genet *29*, 337–341.

Mao, C.-C., and Holt, I.J. (2009). Clinical and molecular aspects of diseases of mitochondrial DNA instability. Chang Gung Med J *32*, 354–369.

Martens, P.A., and Clayton, D.A. (1979). Mechanism of mitochondrial DNA replication in mouse L-cells: localization and sequence of the light-strand origin of replication. J. Mol. Biol *135*, 327–351.

Martomo, S.A., and Mathews, C.K. (2002). Effects of biological DNA precursor pool asymmetry upon accuracy of DNA replication in vitro. Mutat. Res *499*, 197–211.

Massa, V., Fernandez-Vizarra, E., Alshahwan, S., Bakhsh, E., Goffrini, P., Ferrero, I., Mereghetti, P., D'Adamo, P., Gasparini, P., and Zeviani, M. (2008). Severe infantile encephalomyopathy caused by a mutation in COX6B1, a nucleus-encoded subunit of cytochrome c oxidase. Am. J. Hum. Genet. *82*, 1281–1289.

Matsushima, Y., Farr, C.L., Fan, L., and Kaguni, L.S. (2008). Physiological and biochemical defects in carboxyl-terminal mutants of mitochondrial DNA helicase. J. Biol. Chem *283*, 23964–23971.

Mayr, J.A., Havlícková, V., Zimmermann, F., Magler, I., Kaplanová, V., Jesina, P., Pecinová, A., Nusková, H., Koch, J., Sperl, W., et al. (2010). Mitochondrial ATP synthase deficiency due to a mutation in the ATP5E gene for the F1 epsilon subunit. Hum. Mol. Genet. *19*, 3430–3439.

McEwen, J.E., Ko, C., Kloeckner-Gruissem, B., and Poyton, R.O. (1986). Nuclear functions required for cytochrome c oxidase biogenesis in Saccharomyces cerevisiae. Characterization of mutants in 34 complementation groups. J. Biol. Chem. *261*, 11872–11879.

McKenna, A., Hanna, M., Banks, E., Sivachenko, A., Cibulskis, K., Kernytsky, A., Garimella, K., Altshuler, D., Gabriel, S., Daly, M., et al. (2010). The Genome Analysis Toolkit: a MapReduce framework for analyzing next-generation DNA sequencing data. Genome Res. *20*, 1297–1303.

De Meirleir, L., Seneca, S., Lissens, W., De Clercq, I., Eyskens, F., Gerlo, E., Smet, J., and Van Coster, R. (2004). Respiratory chain complex V deficiency due to a mutation in the assembly gene ATP12. J. Med. Genet. *41*, 120–124.

Metzker, M.L. (2005). Emerging technologies in DNA sequencing. Genome Res *15*, 1767–1776.

Metzker, M.L. (2010). Sequencing technologies - the next generation. Nat. Rev. Genet *11*, 31–46.

Misko, A., Jiang, S., Wegorzewska, I., Milbrandt, J., and Baloh, R.H. (2010). Mitofusin 2 is necessary for transport of axonal mitochondria and interacts with the Miro/Milton complex. J. Neurosci *30*, 4232–4240.

Mizusawa, H., Ohkoshi, N., Watanabe, M., and Kanazawa, I. (1991). Peripheral neuropathy of mitochondrial myopathies. Rev. Neurol. (Paris) *147*, 501–507.

Moraes, C.T., DiMauro, S., Zeviani, M., Lombes, A., Shanske, S., Miranda, A.F., Nakase, H., Bonilla, E., Werneck, L.C., and Servidei, S. (1989). Mitochondrial DNA deletions in progressive external ophthalmoplegia and Kearns-Sayre syndrome. N. Engl. J. Med *320*, 1293–1299.

Moraes, C.T., Diaz, F., and Barrientos, A. (2004). Defects in the biosynthesis of mitochondrial heme c and heme a in yeast and mammals. Biochim. Biophys. Acta *1659*, 153–159.

Moslemi, A.-R., Darin, N., Tulinius, M., Oldfors, A., and Holme, E. (2005). Two new mutations in the MTATP6 gene associated with Leigh syndrome. Neuropediatrics *36*, 314–318.

Mullis, K., Faloona, F., Scharf, S., Saiki, R., Horn, G., and Erlich, H. (1986). Specific enzymatic amplification of DNA in vitro: the polymerase chain reaction. Cold Spring Harb. Symp. Quant. Biol. *51 Pt 1*, 263–273.

Murphy, S.M., Herrmann, D.N., McDermott, M.P., Scherer, S.S., Shy, M.E., Reilly, M.M., and Pareyson, D. (2011). Reliability of the CMT neuropathy score (second version) in Charcot-Marie-Tooth disease. J. Peripher. Nerv. Syst. *16*, 191–198.

Nakano, K., Bálint, E., Ashcroft, M., and Vousden, K.H. (2000). A ribonucleotide reductase gene is a transcriptional target of p53 and p73. Oncogene *19*, 4283–4289.

Naviaux, R.K., and Nguyen, K.V. (2004). POLG mutations associated with Alpers' syndrome and mitochondrial DNA depletion. Ann. Neurol. *55*, 706–712.

Neeve, V.C.M., Samuels, D.C., Bindoff, L.A., van den Bosch, B., Van Goethem, G., Smeets, H., Lombès, A., Jardel, C., Hirano, M., Dimauro, S., et al. (2012). What is influencing the phenotype of the common homozygous polymerase-γ mutation p.Ala467Thr? Brain *135*, 3614–3626.

Ng, K., Winter, S., Sue, C., and Burke, D. (2010a). Preserved motor axonal membrane potential in mitochondrial disease. J. Neurol. Neurosurg. Psychiatr *81*, 844–846.

Ng, S.B., Buckingham, K.J., Lee, C., Bigham, A.W., Tabor, H.K., Dent, K.M., Huff, C.D., Shannon, P.T., Jabs, E.W., Nickerson, D.A., et al. (2010b). Exome sequencing identifies the cause of a mendelian disorder. Nat. Genet. *42*, 30–35.

Nijtmans, L.G., Taanman, J.W., Muijsers, A.O., Speijer, D., and Van den Bogert, C. (1998). Assembly of cytochrome-c oxidase in cultured human cells. Eur. J. Biochem. *254*, 389–394.

Nijtmans, L.G., Henderson, N.S., Attardi, G., and Holt, I.J. (2001). Impaired ATP synthase assembly associated with a mutation in the human ATP synthase subunit 6 gene. J. Biol. Chem. *276*, 6755–6762.

Nishino, I., Spinazzola, A., and Hirano, M. (1999). Thymidine phosphorylase gene mutations in MNGIE, a human mitochondrial disorder. Science *283*, 689–692.

Nordlund, P., and Reichard, P. (2006). Ribonucleotide reductases. Annu. Rev. Biochem *75*, 681–706.

Olins, A.L., and Olins, D.E. (1974). Spheroid chromatin units (v bodies). Science *183*, 330–332.

Ostergaard, E., Christensen, E., Kristensen, E., Mogensen, B., Duno, M., Shoubridge, E.A., and Wibrand, F. (2007). Deficiency of the alpha subunit of succinate-coenzyme A ligase causes fatal infantile lactic acidosis with mitochondrial DNA depletion. Am. J. Hum. Genet *81*, 383–387.

Pagliarini, D.J., Calvo, S.E., Chang, B., Sheth, S.A., Vafai, S.B., Ong, S.-E., Walford, G.A., Sugiana, C., Boneh, A., Chen, W.K., et al. (2008a). A mitochondrial protein compendium elucidates complex I disease biology. Cell *134*, 112–123.

Pagliarini, D.J., Calvo, S.E., Chang, B., Sheth, S.A., Vafai, S.B., Ong, S.-E., Walford, G.A., Sugiana, C., Boneh, A., Chen, W.K., et al. (2008b). A mitochondrial protein compendium elucidates complex I disease biology. Cell *134*, 112–123.

Pagnamenta, A.T., Taanman, J.-W., Wilson, C.J., Anderson, N.E., Marotta, R., Duncan, A.J., Bitner-Glindzicz, M., Taylor, R.W., Laskowski, A., Thorburn, D.R., et al. (2006). Dominant inheritance of premature ovarian failure associated with mutant mitochondrial DNA polymerase gamma. Hum. Reprod. *21*, 2467–2473.

Paisan-Ruiz, C., Bhatia, K.P., Li, A., Hernandez, D., Davis, M., Wood, N.W., Hardy, J., Houlden, H., Singleton, A., and Schneider, S.A. (2009). Characterization of PLA2G6 as a locus for dystonia-parkinsonism. Ann. Neurol. *65*, 19–23.

Palade, G.E. (1953). An electron microscope study of the mitochondrial structure. J. Histochem. Cytochem. *1*, 188–211.

Pareek, C.S., Smoczynski, R., and Tretyn, A. (2011). Sequencing technologies and genome sequencing. J. Appl. Genet. *52*, 413–435.

Petrova-Benedict, R., Buncic, J.R., Wallace, D.C., and Robinson, B.H. (1992). Selective killing of cells with oxidative defects in galactose medium: a screening test for affected patient fibroblasts. J. Inherit. Metab. Dis. *15*, 943–944.

Peyronnard, J.M., Charron, L., Bellavance, A., and Marchand, L. (1980). Neuropathy and mitochondrial myopathy. Ann. Neurol *7*, 262–268.

Pham, X.H., Farge, G., Shi, Y., Gaspari, M., Gustafsson, C.M., and Falkenberg, M. (2006). Conserved sequence box II directs transcription termination and primer formation in mitochondria. J. Biol. Chem *281*, 24647–24652.

Pitceathly, R.D.S., Fassone, E., Taanman, J.-W., Sadowski, M., Fratter, C., Mudanohwo, E.E., Woodward, C.E., Sweeney, M.G., Holton, J.L., Hanna, M.G., et al. (2011a). Kearns-Sayre syndrome caused by defective R1/p53R2 assembly. J. Med. Genet. *48*, 610–617.

Pitceathly, R.D.S., Fassone, E., Taanman, J.-W., Sadowski, M., Fratter, C., Mudanohwo, E.E., Woodward, C.E., Sweeney, M.G., Holton, J.L., Hanna, M.G., et al. (2011b). Kearns--Sayre syndrome caused by defective R1/p53R2 assembly. J. Med. Genet. *48*, 610–617.

Pitceathly, R.D.S., Smith, C., Fratter, C., Alston, C.L., He, L., Craig, K., Blakely, E.L., Evans, J.C., Taylor, J., Shabbir, Z., et al. (2012). Adults with RRM2B-related mitochondrial disease have distinct clinical and molecular characteristics. Brain *135*, 3392–3403.

Pontarin, G., Gallinaro, L., Ferraro, P., Reichard, P., and Bianchi, V. (2003). Origins of mitochondrial thymidine triphosphate: dynamic relations to cytosolic pools. Proc. Natl. Acad. Sci. U.S.A *100*, 12159–12164.

Pontarin, G., Fijolek, A., Pizzo, P., Ferraro, P., Rampazzo, C., Pozzan, T., Thelander, L., Reichard, P.A., and Bianchi, V. (2008). Ribonucleotide reduction is a cytosolic process in mammalian cells independently of DNA damage. Proc. Natl. Acad. Sci. U.S.A *105*, 17801–17806.

Rahman, S. (2013). Gastrointestinal and hepatic manifestations of mitochondrial disorders. J. Inherit. Metab. Dis.

Rahman, S., and Hanna, M.G. (2009). Diagnosis and therapy in neuromuscular disorders: diagnosis and new treatments in mitochondrial diseases. J. Neurol. Neurosurg. Psychiatr *80*, 943–953.

Rahman, S., and Poulton, J. (2009). Diagnosis of mitochondrial DNA depletion syndromes. Arch. Dis. Child *94*, 3–5.

Rahman, S., Taanman, J.W., Cooper, J.M., Nelson, I., Hargreaves, I., Meunier, B., Hanna, M.G., García, J.J., Capaldi, R.A., Lake, B.D., et al. (1999). A missense mutation of cytochrome oxidase subunit II causes defective assembly and myopathy. Am. J. Hum. Genet. *65*, 1030–1039.

Rahman, S., Lake, B.D., Taanman, J.W., Hanna, M.G., Cooper, J.M., Schapira, A.H., and Leonard, J.V. (2000). Cytochrome oxidase immunohistochemistry: clues for genetic mechanisms. Brain *123 Pt 3*, 591–600.

Rak, M., Zeng, X., Briere, J., and Tzagoloff, A. (2009). Assembly of F0 in Saccharomyces cerevisiae. Biochimica et Biophysica Acta (BBA) - Molecular Cell Research *1793*, 108–116.

Reichard, P. (1988). Interactions between deoxyribonucleotide and DNA synthesis. Annu. Rev. Biochem *57*, 349–374.

Reilly, M.M., and Shy, M.E. (2009). Diagnosis and new treatments in genetic neuropathies. J. Neurol. Neurosurg. Psychiatr *80*, 1304–1314.

Reilly, M.M., Murphy, S.M., and Laurá, M. (2011). Charcot-Marie-Tooth disease. J. Peripher. Nerv. Syst *16*, 1–14.

Richter, C., Park, J.W., and Ames, B.N. (1988). Normal oxidative damage to mitochondrial and nuclear DNA is extensive. Proc. Natl. Acad. Sci. U.S.A *85*, 6465–6467.

Rickwood, D., Wilson, M.T., and Darley-Usmar, V.M. (1987). Isolation and characteristics of intact mitochondria. In Mitochondria: A Practical Approach, (IRL Press), pp. 1–16.

Rodenburg, R.J.T. (2011). Biochemical diagnosis of mitochondrial disorders. J. Inherit. Metab. Dis. *34*, 283–292.

Van Rompay, A.R., Johansson, M., and Karlsson, A. (2000). Phosphorylation of nucleosides and nucleoside analogs by mammalian nucleoside monophosphate kinases. Pharmacol. Ther *87*, 189–198.

Ropp, P.A., and Copeland, W.C. (1996). Cloning and characterization of the human mitochondrial DNA polymerase, DNA polymerase gamma. Genomics *36*, 449–458.

Rosenberg, M.J., Agarwala, R., Bouffard, G., Davis, J., Fiermonte, G., Hilliard, M.S., Koch, T., Kalikin, L.M., Makalowska, I., Morton, D.H., et al. (2002). Mutant deoxynucleotide carrier is associated with congenital microcephaly. Nat. Genet. *32*, 175–179.

Rouzier, C., Bannwarth, S., Chaussenot, A., Chevrollier, A., Verschueren, A., Bonello-Palot, N., Fragaki, K., Cano, A., Pouget, J., Pellissier, J.-F., et al. (2012). The MFN2 gene is responsible for mitochondrial DNA instability and optic atrophy “plus” phenotype. Brain *135*, 23–34.

Rowland, L.P. (1975). Progressive external ophthalmoplegia. In Handbook of Clinical Neurology. Part II: System Disorders and Atrophies., (New York: American Elsevier Publishing), pp. 177–202.

Rowland, L.P., Hays, A.P., DiMauro, S., DeVivo, D.C., and Behrens, M. (1983). Diverse clinical disorders associated with morphological abnormalities of mitochondria. In Mitochondrial Pathology in Muscle Disease, (Padua: Piccin Medical Books), pp. 141–158.

Saada, A., Shaag, A., Mandel, H., Nevo, Y., Eriksson, S., and Elpeleg, O. (2001). Mutant mitochondrial thymidine kinase in mitochondrial DNA depletion myopathy. Nat. Genet *29*, 342–344.

Saiki, R.K., Gelfand, D.H., Stoffel, S., Scharf, S.J., Higuchi, R., Horn, G.T., Mullis, K.B., and Erlich, H.A. (1988). Primer-directed enzymatic amplification of DNA with a thermostable DNA polymerase. Science *239*, 487–491.

Sali, A., and Blundell, T.L. (1993). Comparative protein modelling by satisfaction of spatial restraints. J. Mol. Biol. *234*, 779–815.

Sambrook, J., and Russell, D.W. (2001). Molecular Cloning: A Laboratory Manual (CSHL Press).

Saneto, R.P., and Singh, K.K. (2010). Illness-induced exacerbation of Leigh syndrome in a patient with the MTATP6 mutation, m. 9185 T>C. Mitochondrion *10*, 567–572.

Saneto, R.P., Friedman, S.D., and Shaw, D.W.W. (2008). Neuroimaging of mitochondrial disease. Mitochondrion *8*, 396–413.

Saporta, A.S.D., Sottile, S.L., Miller, L.J., Feely, S.M.E., Siskind, C.E., and Shy, M.E. (2011). Charcot-Marie-Tooth disease subtypes and genetic testing strategies. Ann. Neurol. *69*, 22–33.

Satoh, M., and Kuroiwa, T. (1991). Organization of multiple nucleoids and DNA molecules in mitochondria of a human cell. Exp. Cell Res. *196*, 137–140.

Schägger, H. (1995). Quantification of oxidative phosphorylation enzymes after blue native electrophoresis and two-dimensional resolution: normal complex I protein amounts in Parkinson's disease conflict with reduced catalytic activities. Electrophoresis *16*, 763–770.

Ter Schegget, J., Flavell, R.A., and Borst, P. (1971). DNA synthesis by isolated mitochondria. 3. Characterization of D-loop DNA, a novel intermediate in mtDNA synthesis. Biochim. Biophys. Acta *254*, 1–14.

Schröder, J.M. (1993). Neuropathy associated with mitochondrial disorders. Brain Pathol *3*, 177–190.

Shaibani, A., Shchelochkov, O.A., Zhang, S., Katsonis, P., Lichtarge, O., Wong, L.-J., and Shinawi, M. (2009). Mitochondrial neurogastrointestinal encephalopathy due to mutations in RRM2B. Arch. Neurol *66*, 1028–1032.

Shoffner, J., and Shoubridge, E. (2001). Oxidative phosphorylation disease of muscle. In Disorders of Voluntary Muscle, G. Karpati, D. Hilton-Jones, and R. Griggs, eds. (Cambridge University Press), pp. 580–603.

Shoffner, J.M., Lott, M.T., Voljavec, A.S., Soueidan, S.A., Costigan, D.A., and Wallace, D.C. (1989). Spontaneous Kearns-Sayre/chronic external ophthalmoplegia plus syndrome associated with a mitochondrial DNA deletion: a slip-replication model and metabolic therapy. Proc. Natl. Acad. Sci. U.S.A *86*, 7952–7956.

Shteyer, E., Saada, A., Shaag, A., Al-Hijawi, F.A., Kidess, R., Revel-Vilk, S., and Elpeleg, O. (2009). Exocrine pancreatic insufficiency, dyserythropoeitic anemia, and calvarial hyperostosis are caused by a mutation in the COX4I2 gene. Am. J. Hum. Genet. *84*, 412–417.

Shutt, T.E., Lodeiro, M.F., Cotney, J., Cameron, C.E., and Shadel, G.S. (2010). Core human mitochondrial transcription apparatus is a regulated two-component system in vitro. Proc. Natl. Acad. Sci. U.S.A. *107*, 12133–12138.

Sinjorgo, K.M., Hakvoort, T.B., Durak, I., Draijer, J.W., Post, J.K., and Muijsers, A.O. (1987). Human cytochrome c oxidase isoenzymes from heart and skeletal muscle; purification and properties. Biochim. Biophys. Acta *890*, 144–150.

Smith, P., Zhou, B., Ho, N., Yuan, Y.-C., Su, L., Tsai, S.-C., and Yen, Y. (2009). 2.6 A X-ray crystal structure of human p53R2, a p53-inducible ribonucleotide reductase. Biochemistry *48*, 11134–11141.

Smits, P., Smeitink, J., and van den Heuvel, L. (2010). Mitochondrial translation and beyond: processes implicated in combined oxidative phosphorylation deficiencies. J. Biomed. Biotechnol *2010*, 737385.

Soto, I.C., Fontanesi, F., Liu, J., and Barrientos, A. (2012a). Biogenesis and assembly of eukaryotic cytochrome c oxidase catalytic core. Biochim. Biophys. Acta *1817*, 883–897.

Soto, I.C., Fontanesi, F., Liu, J., and Barrientos, A. (2012b). Biogenesis and assembly of eukaryotic cytochrome c oxidase catalytic core. Biochim. Biophys. Acta *1817*, 883–897.

Spelbrink, J.N., Li, F.Y., Tiranti, V., Nikali, K., Yuan, Q.P., Tariq, M., Wanrooij, S., Garrido, N., Comi, G., Morandi, L., et al. (2001a). Human mitochondrial DNA

deletions associated with mutations in the gene encoding Twinkle, a phage T7 gene 4-like protein localized in mitochondria. Nat. Genet *28*, 223–231.

Spelbrink, J.N., Li, F.Y., Tiranti, V., Nikali, K., Yuan, Q.P., Tariq, M., Wanrooij, S., Garrido, N., Comi, G., Morandi, L., et al. (2001b). Human mitochondrial DNA deletions associated with mutations in the gene encoding Twinkle, a phage T7 gene 4-like protein localized in mitochondria. Nat. Genet *28*, 223–231.

Spinazzola, A., Invernizzi, F., Carrara, F., Lamantea, E., Donati, A., Dirocco, M., Giordano, I., Meznaric-Petrusa, M., Baruffini, E., Ferrero, I., et al. (2009a). Clinical and molecular features of mitochondrial DNA depletion syndromes. J. Inherit. Metab. Dis *32*, 143–158.

Spinazzola, A., Invernizzi, F., Carrara, F., Lamantea, E., Donati, A., Dirocco, M., Giordano, I., Meznaric-Petrusa, M., Baruffini, E., Ferrero, I., et al. (2009b). Clinical and molecular features of mitochondrial DNA depletion syndromes. J. Inherit. Metab. Dis *32*, 143–158.

Steffens, G., and Buse, G. (1976). [Studies on cytochrome c oxidase, I. Purification and characterization of bovine myocardial enzyme and identification of peptide chains in the complex]. Hoppe-Seyler's Z. Physiol. Chem. *357*, 1125–1137.

Stenson, P.D., Ball, E.V., Howells, K., Phillips, A.D., Mort, M., and Cooper, D.N. (2009). The Human Gene Mutation Database: providing a comprehensive central mutation database for molecular diagnostics and personalized genomics. Hum. Genomics *4*, 69–72.

Stumpf, J.D., Saneto, R.P., and Copeland, W.C. (2013). Clinical and Molecular Features of POLG-Related Mitochondrial Disease. Cold Spring Harb Perspect Biol *5*.

Suomalainen, A., Kaukonen, J., Amati, P., Timonen, R., Haltia, M., Weissenbach, J., Zeviani, M., Somer, H., and Peltonen, L. (1995). An autosomal locus predisposing to deletions of mitochondrial DNA. Nat. Genet *9*, 146–151.

Szklarczyk, R., Wanschers, B.F.J., Nijtmans, L.G., Rodenburg, R.J., Zschocke, J., Dikow, N., van den Brand, M.A.M., Hendriks-Franssen, M.G.M., Gilissen, C., Veltman, J.A., et al. (2013). A mutation in the FAM36A gene, the human ortholog of

COX20, impairs cytochrome c oxidase assembly and is associated with ataxia and muscle hypotonia. Hum. Mol. Genet. *22*, 656–667.

Taanman, J.W. (1997a). Human cytochrome c oxidase: structure, function, and deficiency. J. Bioenerg. Biomembr. *29*, 151–163.

Taanman, J.W. (1997b). Human cytochrome c oxidase: structure, function, and deficiency. J. Bioenerg. Biomembr. *29*, 151–163.

Taanman, J.W. (1999). The mitochondrial genome: structure, transcription, translation and replication. Biochim. Biophys. Acta *1410*, 103–123.

Taanman, J.W., and Capaldi, R.A. (1992). Purification of yeast cytochrome c oxidase with a subunit composition resembling the mammalian enzyme. J. Biol. Chem. *267*, 22481–22485.

Taanman, J.-W., Muddle, J.R., and Muntau, A.C. (2003). Mitochondrial DNA depletion can be prevented by dGMP and dAMP supplementation in a resting culture of deoxyguanosine kinase-deficient fibroblasts. Hum. Mol. Genet. *12*, 1839–1845.

Takata, A., Kato, M., Nakamura, M., Yoshikawa, T., Kanba, S., Sano, A., and Kato, T. (2011). Exome sequencing identifies a novel missense variant in RRM2B associated with autosomal recessive progressive external ophthalmoplegia. Genome Biol. *12*, R92.

Tanaka, H., Arakawa, H., Yamaguchi, T., Shiraishi, K., Fukuda, S., Matsui, K., Takei, Y., and Nakamura, Y. (2000). A ribonucleotide reductase gene involved in a p53-dependent cell-cycle checkpoint for DNA damage. Nature *404*, 42–49.

Tapper, D.P., and Clayton, D.A. (1981). Mechanism of replication of human mitochondrial DNA. Localization of the 5’ ends of nascent daughter strands. J. Biol. Chem *256*, 5109–5115.

Taylor, W.R., Jones, D.T., and Sadowski, M.I. (2012). Protein topology from predicted residue contacts. Protein Sci. *21*, 299–305.

Thömmes, P., Farr, C.L., Marton, R.F., Kaguni, L.S., and Cotterill, S. (1995). Mitochondrial single-stranded DNA-binding protein from Drosophila embryos. Physical and biochemical characterization. J. Biol. Chem *270*, 21137–21143.

Tiranti, V., Savoia, A., Forti, F., D'Apolito, M.F., Centra, M., Rocchi, M., and Zeviani, M. (1997). Identification of the gene encoding the human mitochondrial RNA polymerase (h-mtRPOL) by cyberscreening of the Expressed Sequence Tags database. Hum. Mol. Genet *6*, 615–625.

Tradewell, M.L., Durham, H.D., Mushynski, W.E., and Gentil, B.J. (2009). Mitochondrial and axonal abnormalities precede disruption of the neurofilament network in a model of charcot-marie-tooth disease type 2E and are prevented by heat shock proteins in a mutant-specific fashion. J. Neuropathol. Exp. Neurol *68*, 642–652.

Tsukihara, T., Aoyama, H., Yamashita, E., Tomizaki, T., Yamaguchi, H., Shinzawa-Itoh, K., Nakashima, R., Yaono, R., and Yoshikawa, S. (1995). Structures of metal sites of oxidized bovine heart cytochrome c oxidase at 2.8 A. Science *269*, 1069–1074.

Tsukihara, T., Aoyama, H., Yamashita, E., Tomizaki, T., Yamaguchi, H., Shinzawa-Itoh, K., Nakashima, R., Yaono, R., and Yoshikawa, S. (1996). The whole structure of the 13-subunit oxidized cytochrome c oxidase at 2.8 A. Science *272*, 1136–1144.

Tyynismaa, H., Ylikallio, E., Patel, M., Molnar, M.J., Haller, R.G., and Suomalainen, A. (2009). A heterozygous truncating mutation in RRM2B causes autosomal-dominant progressive external ophthalmoplegia with multiple mtDNA deletions. Am. J. Hum. Genet *85*, 290–295.

Vafai, S.B., and Mootha, V.K. (2012). Mitochondrial disorders as windows into an ancient organelle. Nature *491*, 374–383.

Valnot, I., von Kleist-Retzow, J.C., Barrientos, A., Gorbatyuk, M., Taanman, J.W., Mehaye, B., Rustin, P., Tzagoloff, A., Munnich, A., and Rötig, A. (2000). A mutation in the human heme A:farnesyltransferase gene (COX10) causes cytochrome c oxidase deficiency. Hum. Mol. Genet *9*, 1245–1249.

De Vries, M.C., Rodenburg, R.J., Morava, E., van Kaauwen, E.P.M., ter Laak, H., Mullaart, R.A., Snoeck, I.N., van Hasselt, P.M., Harding, P., van den Heuvel, L.P.W., et al. (2007). Multiple oxidative phosphorylation deficiencies in severe childhood multi-system disorders due to polymerase gamma (POLG1) mutations. Eur. J. Pediatr. *166*, 229–234.

Walker, J.E., and Dickson, V.K. (2006). The peripheral stalk of the mitochondrial ATP synthase. Biochim. Biophys. Acta *1757*, 286–296.

Wang, Y. (2006). Human Mitochondrial DNA Nucleoids Are Linked to Protein Folding Machinery and Metabolic Enzymes at the Mitochondrial Inner Membrane. Journal of Biological Chemistry *281*, 25791–25802.

Wang, L., Munch-Petersen, B., Herrström Sjöberg, A., Hellman, U., Bergman, T., Jörnvall, H., and Eriksson, S. (1999). Human thymidine kinase 2: molecular cloning and characterisation of the enzyme activity with antiviral and cytostatic nucleoside substrates. FEBS Lett *443*, 170–174.

Wanrooij, S., and Falkenberg, M. (2010). The human mitochondrial replication fork in health and disease. Biochim Biophys Acta.

Wanrooij, S., Goffart, S., Pohjoismäki, J.L.O., Yasukawa, T., and Spelbrink, J.N. (2007). Expression of catalytic mutants of the mtDNA helicase Twinkle and polymerase POLG causes distinct replication stalling phenotypes. Nucleic Acids Res *35*, 3238–3251.

Wanrooij, S., Fusté, J.M., Farge, G., Shi, Y., Gustafsson, C.M., and Falkenberg, M. (2008). Human mitochondrial RNA polymerase primes lagging-strand DNA synthesis in vitro. Proc. Natl. Acad. Sci. U.S.A *105*, 11122–11127.

Watt, I.N., Montgomery, M.G., Runswick, M.J., Leslie, A.G.W., and Walker, J.E. (2010). Bioenergetic cost of making an adenosine triphosphate molecule in animal mitochondria. Proc. Natl. Acad. Sci. U.S.A. *107*, 16823–16827.

Wharton, D.C., and Tzagoloff, A. (1967). [45] Cytochrome oxidase from beef heart mitochondria. In Methods in Enzymology, M.E.P. Ronald W. Estabrook, ed. (Academic Press), pp. 245–250.

Wielburski, A., and Nelson, B.D. (1983). Evidence for the sequential assembly of cytochrome oxidase subunits in rat liver mitochondria. Biochem. J. *212*, 829–834.

Williams, S.L., Valnot, I., Rustin, P., and Taanman, J.-W. (2004a). Cytochrome c oxidase subassemblies in fibroblast cultures from patients carrying mutations in COX10, SCO1, or SURF1. J. Biol. Chem. *279*, 7462–7469.

Williams, S.L., Valnot, I., Rustin, P., and Taanman, J.-W. (2004b). Cytochrome c oxidase subassemblies in fibroblast cultures from patients carrying mutations in COX10, SCO1, or SURF1. J. Biol. Chem. *279*, 7462–7469.

Williams, S.L., Valnot, I., Rustin, P., and Taanman, J.-W. (2004c). Cytochrome c oxidase subassemblies in fibroblast cultures from patients carrying mutations in COX10, SCO1, or SURF1. J. Biol. Chem *279*, 7462–7469.

Williams, S.L., Valnot, I., Rustin, P., and Taanman, J.-W. (2004d). Cytochrome c oxidase subassemblies in fibroblast cultures from patients carrying mutations in COX10, SCO1, or SURF1. J. Biol. Chem. *279*, 7462–7469.

Wittig, I., and Schägger, H. (2008). Structural organization of mitochondrial ATP synthase. Biochim. Biophys. Acta *1777*, 592–598.

Wittig, I., Meyer, B., Heide, H., Steger, M., Bleier, L., Wumaier, Z., Karas, M., and Schägger, H. (2010). Assembly and oligomerization of human ATP synthase lacking mitochondrial subunits a and A6L. Biochim. Biophys. Acta *1797*, 1004–1011.

Wray, S.H., Provenzale, J.M., Johns, D.R., and Thulborn, K.R. (1995). MR of the brain in mitochondrial myopathy. AJNR Am J Neuroradiol *16*, 1167–1173.

Yakubovskaya, E., Chen, Z., Carrodeguas, J.A., Kisker, C., and Bogenhagen, D.F. (2006). Functional human mitochondrial DNA polymerase gamma forms a heterotrimer. J. Biol. Chem *281*, 374–382.

Yakubovskaya, E., Lukin, M., Chen, Z., Berriman, J., Wall, J.S., Kobayashi, R., Kisker, C., and Bogenhagen, D.F. (2007). The EM structure of human DNA polymerase gamma reveals a localized contact between the catalytic and accessory subunits. EMBO J *26*, 4283–4291.

Yamaguchi, T., Matsuda, K., Sagiya, Y., Iwadate, M., Fujino, M.A., Nakamura, Y., and Arakawa, H. (2001). p53R2-dependent pathway for DNA synthesis in a p53-regulated cell cycle checkpoint. Cancer Res *61*, 8256–8262.

Yamashita, S., Nishino, I., Nonaka, I., and Goto, Y.-I. (2008). Genotype and phenotype analyses in 136 patients with single large-scale mitochondrial DNA deletions. J. Hum. Genet *53*, 598–606.

Yanamura, W., Zhang, Y.Z., Takamiya, S., and Capaldi, R.A. (1988). Tissue-specific differences between heart and liver cytochrome c oxidase. Biochemistry *27*, 4909–4914.

Yang, C., Curth, U., Urbanke, C., and Kang, C. (1997). Crystal structure of human mitochondrial single-stranded DNA binding protein at 2.4 A resolution. Nat. Struct. Biol *4*, 153–157.

Yasukawa, T., Yang, M.-Y., Jacobs, H.T., and Holt, I.J. (2005). A bidirectional origin of replication maps to the major noncoding region of human mitochondrial DNA. Mol. Cell *18*, 651–662.

Yasukawa, T., Reyes, A., Cluett, T.J., Yang, M.-Y., Bowmaker, M., Jacobs, H.T., and Holt, I.J. (2006). Replication of vertebrate mitochondrial DNA entails transient ribonucleotide incorporation throughout the lagging strand. EMBO J *25*, 5358–5371.

Yiannikas, C., McLeod, J.G., Pollard, J.D., and Baverstock, J. (1986). Peripheral neuropathy associated with mitochondrial myopathy. Ann. Neurol *20*, 249–257.

Zerbetto, E., Vergani, L., and Dabbeni-Sala, F. (1997). Quantification of muscle mitochondrial oxidative phosphorylation enzymes via histochemical staining of blue native polyacrylamide gels. Electrophoresis *18*, 2059–2064.

Zeviani, M., Moraes, C.T., DiMauro, S., Nakase, H., Bonilla, E., Schon, E.A., and Rowland, L.P. (1988). Deletions of mitochondrial DNA in Kearns-Sayre syndrome. Neurology *38*, 1339–1346.

Zhu, C., Johansson, M., Permert, J., and Karlsson, A. (1998). Enhanced cytotoxicity of nucleoside analogs by overexpression of mitochondrial deoxyguanosine kinase in cancer cell lines. J. Biol. Chem *273*, 14707–14711.